CHAPTER 5

ELECTRICAL PROPERTIES

The present chapter describes the electrical properties of prepared gel polymer electrolyte in terms of impedance, DC conductivity, AC conductivity, dielectric and electric modulus at different compositions and temperatures. The ion conduction mechanism is explained as well.

5.1 Introduction

As discussed in Chapter 1, the gel polymer electrolyte (GPE) consists of a polymer matrix in which low molecular weight solvent or plasticizers and a lithium salt are mixed [1]. The lithium salt provides free ionic species that take part in the conduction process. The GPEs have shown enhanced ionic conductivity, better electrochemical stability window (ESW), and good compatibility with electrodes. A polymer matrix in which the addition of plasticizers results in a swollen polymer matrix is termed as gel polymer electrolyte [2]. GPE possesses properties of both liquid and solid i.e. diffusive properties and cohesive properties. The plasticizer supports the diffusion of ions and the polymer matrix provides mechanical strength [3]. Many gel polymer electrolytes have been reported based on poly(acrylonitrile) (PAN), poly(methyl methacrylate) (PMMA), and poly(vinylidene fluoride) (PVDF), poly(vinylidene fluoride-hexafluoropropylene) (PVDF-HFP) [4]. The choice of polymer electrolyte plays a crucial role and mainly depends on two factors: (i) the existence of polar function group with electron donor group which can form coordination with cations (ii) low interruption to the rotation of bond [5]. The PVDF-HFP got attention from many researchers owing to the high dielectric constant ($\varepsilon = 8.4$) and the existence of

C–F group (electron-withdrawing functional groups) aid for the greater dissociation of salts subsequently increase the number of free charge carriers and induces net dipole moment [6]. Due to this high ionic conductivity close to liquid electrolyte can be achieved. The blending of semi-crystalline PVDF-HFP polymer with amorphous PMMA polymer has been considered in the present work to introduce the amorphous phase for transportation of free charge carriers and to provide mechanical integrity to GPE. It is also reported that the PMMA based PE enhances the interfacial stability when used in device. Moreover, the ester functional group in the PMMA containing carbon oxygen atom (C=O) as an electron donor make it for suitable for fabrication of gel polymer electrolyte system. Hence, the presence of the carbonyl group (C=O) makes the active coordination of it with cation due to which easier dissociation of alkali salt takes place ultimately aid for conductivity enhancement [7]. Ramesh et al. reported enhancement in ionic conductivity when Poly(vinyl chloride) (PVC) copolymerized with polymethyl methacrylate PMMA [8].

The proper choice of polymers and salt can provide better electrical properties because the interaction between the host polymer and salt plays a crucial role to achieve desirable ionic conductivity, chemical stability, and mechanical strength [9]. It is believed that the salt with low lattice energy and a polymer having high dielectric constant results in the dissociation of doping salt could provide high ionic conductivity as well as better stability. The polymer electrolyte with different lithium salt like $LiPF_6$ [10], $LiCF_3SO_3$ [11], LiTFSI [12], $LiClO_4$ [13] as a charge carriers have been reported by different research group [14]. Among all, $LiClO_4$ is a good choice as a dopant salt comprised of large size anions and small size cations [15]. The appreciable properties of $LiClO_4$ are low interfacial resistance with the lithium metal anode. In addition to these, this salt easily can make complexation due to high dissociation energy as it shows good solvability in most of the solvents [15]. Due to the interaction between the polar group of polymers and lithium ions, the lithium ion can be easily dissolved in the polymer matrix [16]. In this chapter, we aim to provide the electrical properties of the **PVDF-HFP:PMMA - PC:DEC - x wt.% $LiClO_4$ where x = 2, 4, 5, 7.5, 10 (Series (a))** has been carried out using electrochemical impedance spectroscopy (EIS).

Next, we aim to enhance the ionic conductivity and electrochemical properties of the GPE system. It can be enhanced by increasing the ion mobility by making the host polymer more flexible and free charge carriers. One of the approaches is to the addition of a proper amount of plasticizers into the host polymer which leads to enhancement of electrical

properties by enhancing the flexibility of the polymer chain. The plasticizers such as ethylene carbonate (EC), propylene carbonate (PC), diethyl carbonate (DEC), dimethyl carbonate (DMC), dimethylformamide (DMF), etc. have been used to improve overall properties [17]. Das et al. [18] reported the effect of different plasticizers on the conductivity and relaxation in blend polymer electrolytes. This low molecular weight plasticizer facilitates dissociation of the salt and upholds the liquid state within the polymer matrix [19]. Apart from this, it increases the amorphous nature of the polymer and softens the polymer backbone resulting in high segmental motion of polymer chains which assists the easy movement of ions through the polymer matrix. By keeping all in mind in the present study, a mixture of PC: DEC has been taken. PC has high dielectric constant ($\varepsilon \approx 64.4$, viscosity $\eta \approx$ 2.53 mPa S) aid for higher dissociation whereas DEC ($\varepsilon \approx 2.82$, viscosity $\eta \approx$ 0.748 mPa S) has lower viscosity assist for the easier movement of charge carriers through matrix [20]. Hence, the effect of plasticizers variation in **PVDF-HFP:PMMA - $LiClO_4$ - x wt.% PC:DEC where x = 20, 30, 40, 50, 60 (Series (b))** on electrical properties is investigated.

A large amount of plasticizers present in the gel polymer electrolyte creates attractive force with the polymer chain and reduces the cohesive force among the polymer chain, as a result, the ion moves easily through the polymer matrix and leads to enhancement in ionic conductivity. But, the mechanical strength becomes poor which is not suitable with the electrodes. Apart from losing mechanical strength, It is also reported that the addition of plasticizers into host polymer promotes the formation of the passive layer at the surface of metal lithium electrode and electrolyte surface while using as an electrolyte in battery applications [21]. The researchers have adopted a few methods to improve ionic conductivity such as blending, adding nanoparticles, and crosslinking, etc [22]. It is reported in the literature to improve the properties of GPE such as ionic conductivity, high mechanical and thermal stability, the addition of nanoparticles into the polymer matrix is an effective approach [23]. Nanofiller in the matrix, due to the high surface area of nanoparticles enhances surface area to volume ratio which aids in the better conduction pathway for the ion transport [24]. One of the pragmatic and simplest approaches is to the dispersion of nanofillers (inert insulating ceramic filler) such as SiO_2, TiO_2, ZrO_2, $BaTiO_3$ into the polymer matrix. Yamamoto et al [25] reported the enhancement in ionic conductivity and decrease in interfacial resistance between the lithium anode and polymer electrolyte by the addition of $BaTiO_3$. Nano-composite gel polymer blend electrolytes have

been of great interest to researchers due to their potential application in electrochemical devices such as batteries, supercapacitors, fuel cells, etc [24]. In the present chapter, the electrical properties of the **PVDF-HFP:PMMA - $LiClO_4$ - PC:DEC - x wt% Al_2O_3 where x = 0.5, 1, 2, 3, 4 (Series(c))** have been discussed. The effect of Al_2O_3 nanofiller in GPE on the electrical properties such as impedance, DC conductivity, AC conductivity, dielectric, modulus, ion transport behavior of PVDF-HFP:PMMA based gel polymer electrolyte has been reported.

In the present study, the electrochemical impedance spectroscopy (EIS) which is a versatile and powerful technique is adopted to carry out electrical properties and their interfaces with electrodes over a wide range of frequency and temperatures. It is used to carry out bulk properties, interfacial properties, and the ion conduction mechanism of all samples in the system. In the present chapter, the electrical properties, and ion conduction mechanism has been elaborated in terms of impedance (Z^*), temperature-dependent DC ionic conductivity (σ_{dc}), AC conductivity (σ'), dielectric permittivity (ε^*) and electric modulus (M^*). AC conductivity (frequency-dependent conductivity) has been a powerful tool to understand ion conduction mechanisms where the motion of the ions and dipoles are very sensitive to change in the frequency of the applied field. The frequency-dependent complex permittivity and loss tangent are influenced by the ion dynamics and the dipoles present in the polymer backbone [26]. The hopping mechanism and segmental relaxation of polymer chain result due to ion dynamics [18]. The dielectric relaxation behavior of dipoles in the polymer electrolyte and electrode polarization effect at low frequency can be understood by using frequency-dependent complex permittivity. The electric modulus (M^*) highlights the high-frequency region explains the phenomena of conductivity relaxation. To investigate bulk effect and conductivity relaxation in the polymer electrolyte with varying particular constituent of composition and at different temperatures, modulus formalism is used. The scaling has also been carried out to attain better understanding on ion dynamics. It is time-temperature superposition principle/ thermorheological simplicity is used to observe whether the conduction mechanism involving ion dynamics is temperature-dependent or not. The scaling of conductivity spectra at different temperatures results in a single master curve (time-temperature superposition) if the conduction mechanism is temperature independent. For scaling, Ghosh, and Summerfield scaling is approached [27].

5.2 Complex Impedance Analysis

Kramers-Kronig relationship

Electrochemical impedance spectroscopy is an important technique used to measure the electrochemical impedance of the system with the application of the AC field. The parameter electrochemical impedance plays an important role while using materials in the application. Hence, the validity of data obtained from electrochemical impedance measurements of polymer electrolyte should be evaluated before any interpretation of the experimentally measured data [28]. The EIS measurement is generally represented as a Nyquist plot which can be analyzed by using an equivalent circuit [29]. Kramers-Kronig (KK) relationship is a tool that is applied to check the validation of impedance data [30]. Before equivalent circuit fitting, the validity of the EIS data must be carried out using Kramers - Kronig relations. The Kramers - Kronig relationship relates the real and imaginary part of the frequency obtained from EIS data and is used to check internal consistency between the real and imaginary part of complex variables. The residual between calculated and measured impedance is used to determine consistency with the K-K relationship. In the present study, the residual values obtained from the Kramers-Kronig relationship for GPE containing 4 wt.% and 7.5 wt.% $LiClO_4$ are plotted in Figure 5.1. It is evident from the figure; the real and imaginary parts do not show deviation from the zero-error axis. It is a clear indication of data comply with linear K-K behavior.

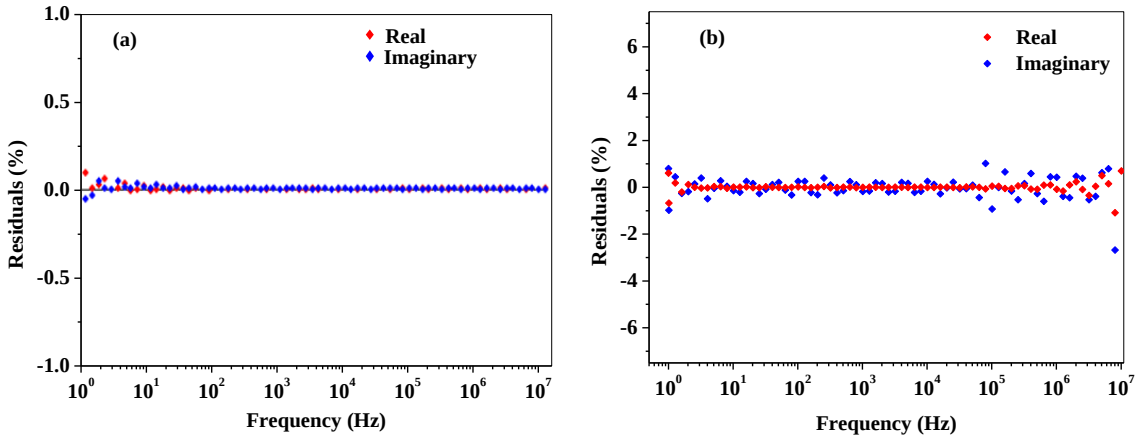

Figure 5.1 Residuals plots obtained from Kramers- Kronig relationship for GPE containing (a) 4 wt.% $LiClO_4$ (b) 7.5 wt.% $LiClO_4$ - Series (a).

From series b, the attained residuals data from the K-K test are plotted as a function of frequency for GPE holding 40 wt.% and 60 wt.% PC: DEC in Figure 5.2. Less deviation between real and imaginary data from the zero-axis except very low and high frequency indicates it comply with linear K-K behavior. Whereas, data are sensitive to non-K-K behavior and show distinct deviation from the zero-error axis for GPE having 60 wt.% PC: DEC. The reason for this is the presence of only low-frequency data and may be due to inhomogeneity between the electrode-electrolyte surface.

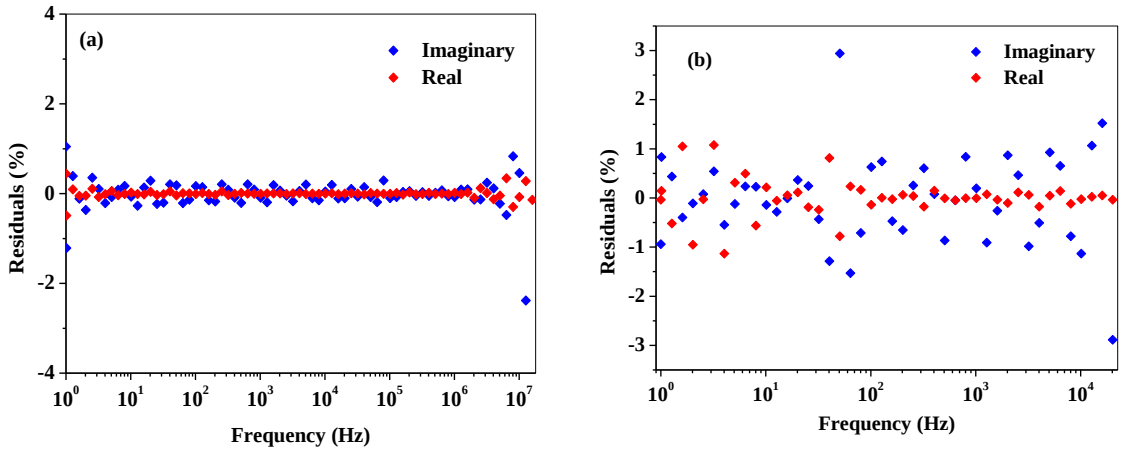

Figure 5.2 Residuals plot obtained from Kramers-Kronig relationship for GPE containing (a) 40 wt.% PC:DEC (b) 60 wt.% PC:DEC –Series (b).

From series C, the residual plots obtained from the K-K relationship are plotted for the NGPE containing 3 wt.% and 4 wt.% Al_2O_3 in Figure 5.3. The obtained data shows the stability except high-frequency region is an indication of satisfying Kramer-Kronig relationships.

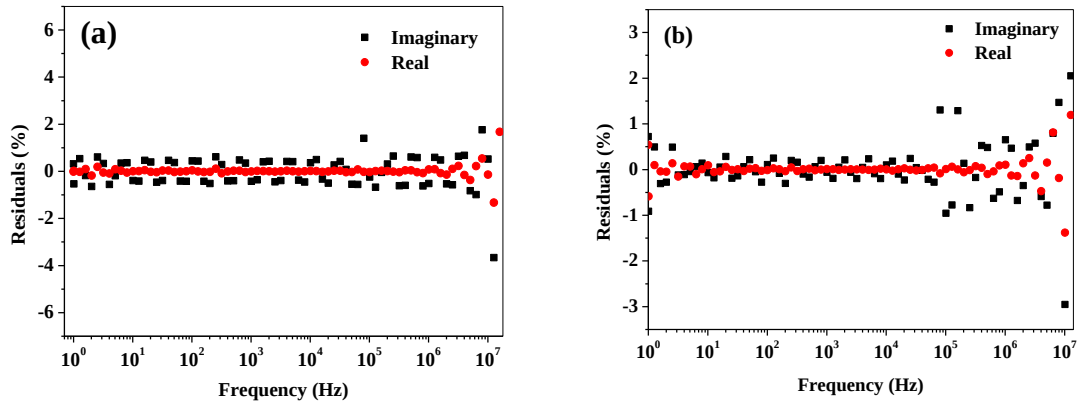

Figure 5.3 Residual plot obtained from Kramer-Kronig relationship for NCGPE containing (a) 3 wt.% Al_2O_3 (b) 4 wt.% Al_2O_3 - Series (c).

Complex Impedance Plots

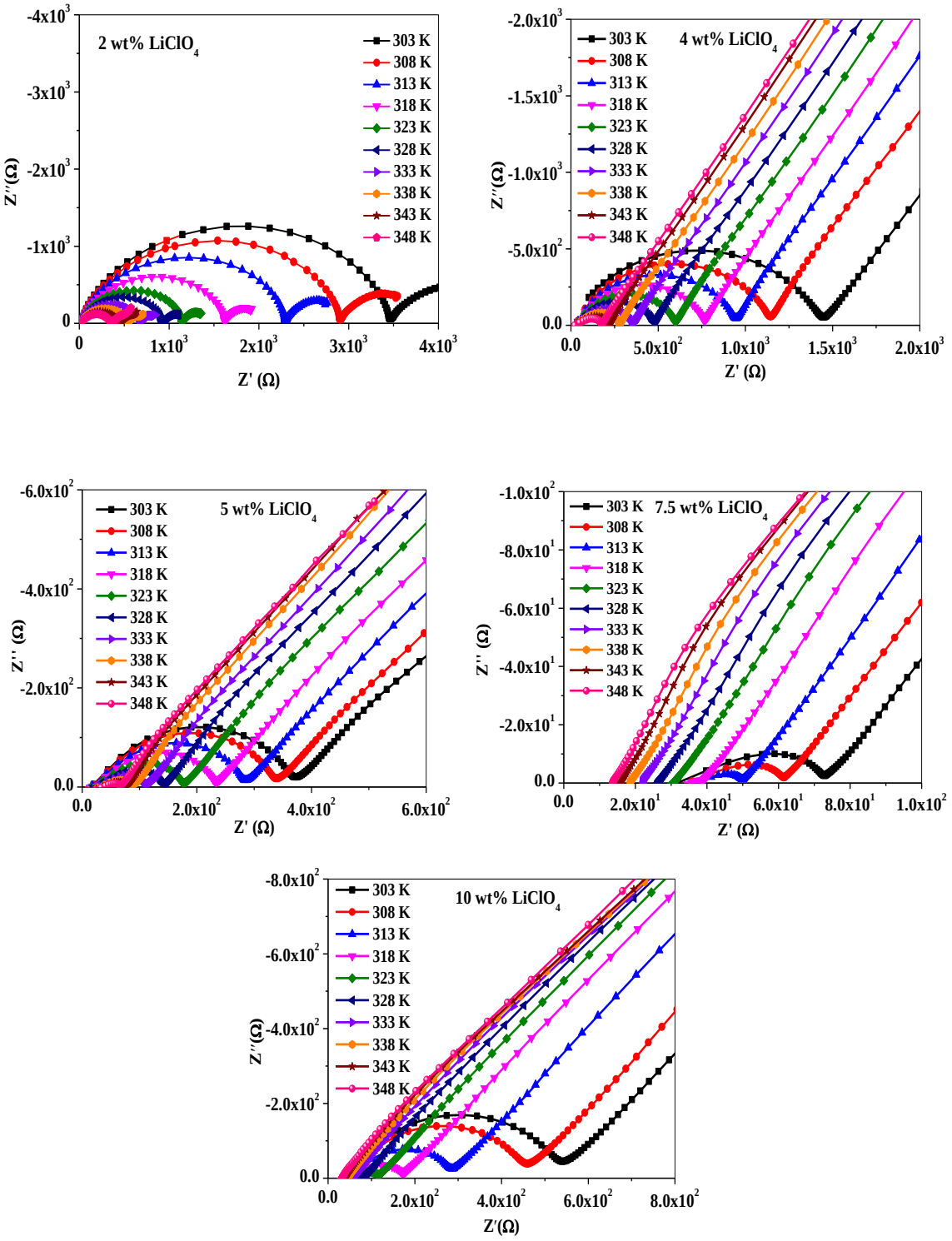

Figure 5.4 The complex impedance plot for different concentrations of $LiClO_4$ in the GPE system at different temperatures – Series (a).

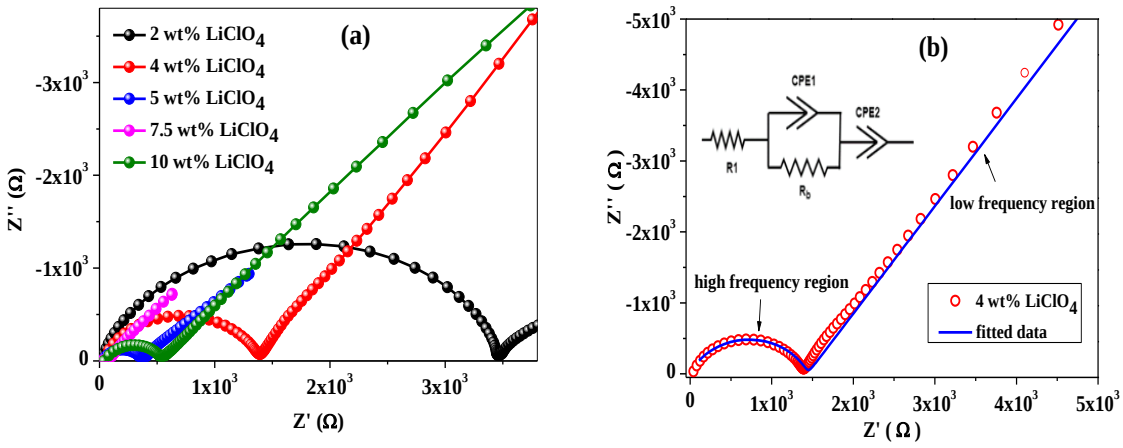

Figure 5.5 (a) The complex impedance plot for different concentrations of $LiClO_4$ in the GPE system at 303 K (b) Equivalent circuit fitting of impedance plot of GPE with 4 wt.% $LiClO_4$ at 303 K - Series(a).

Series (a): The electrical properties of the gel polymer electrolyte films with different amounts of $LiClO_4$ have been examined using the AC technique of complex impedance spectroscopy (CIS) analysis. Figure 5.4 shows the complex impedance plot for different concentrations of $LiClO_4$ in the GPE system in the temperature range 303 K to 348 K. The plot shows high-frequency depressed semicircle and low-frequency non-vertical spike. The high-frequency semicircle corresponds to a parallel combination of bulk resistor R_b and a constant phase element (CPE) and low-frequency spikes are attributed to double-layer formation at the electrode (blocking electrode)-electrolyte interface due to accumulation of charges [31]. A typical complex impedance plot of GPE containing 4 wt.% of $LiClO_4$ at 303 K along with their equivalent electrical circuit model (inset) fitted with experimental values by using EIS spectrum analyzer software is shown in Figure 5.5(b). The intercept on the real axis (z') of the plot at the low frequency of semicircle end and high-frequency end of spikes gives the value of bulk resistance (R_b). From the temperature-dependent complex impedance plot, the intercept of the real axis shift towards the origin i.e. bulk resistance decreases as temperature increases from 303K to 348 K. The decreases in resistance might be due to an increase in the segmental motion of the polymer chain with increasing temperature.

Figure 5.5(a) represents the complex impedance plot of GPE containing different concentrations of $LiClO_4$ at 303 K. The intercept of the semicircle on the real axis is found to decrease as the amount of salt is increased from 2 wt.% to 7.5 wt.% means bulk resistance decreases and the reverse trend has been observed for the sample having 10 wt.% $LiClO_4$.

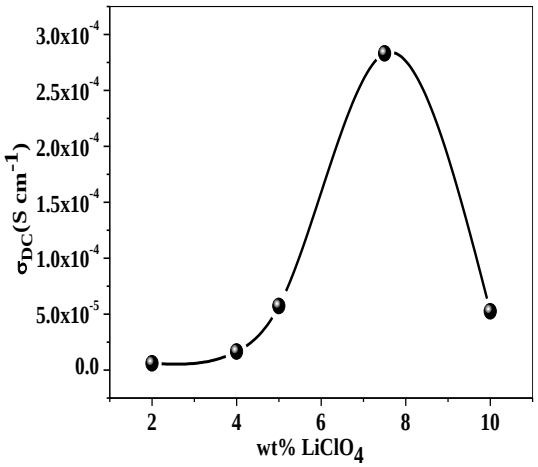

Figure 5.6 Variation of ionic conductivity as a function of $LiClO_4$ salt concentration at 303 K- Series (a).

From the measured value of bulk resistance (R_b), the conductivity (σ) has been calculated using the following relation,

$$\sigma = \frac{t}{R_b A} \tag{5.1}$$

The variation in conductivity as a function of wt.% of $LiClO_4$ at 303 K is plotted in Figure 5.6 and tabulated in Table 5.1. The increase in conductivity with increasing the amount of $LiClO_4$ can be attributed to an increase in charge carriers. From the theoretical aspect, conductivity is dependent to charge carriers, mobility, and charge on ion which can be formulated as [32]

$$\sigma_{dc} = \sum n_i \mu_i q_i \tag{5.2}$$

where n_i denotes the charge carrier density, μ_i is the ion mobility and q_i is the charge of the i ion. From Eq. 5.2, DC conductivity depends on three factors i.e. concentration of free charge carriers and mobility of the charge carrier. The increase in the amount of salt leads to an increase in the number of mobile lithium ions which results in enhancement of ionic conductivity reported by Ngai et al.[33]. The increased charge carriers disrupt the crystalline nature of the polymer and lead to an increase in the amorphousity which is also in good agreement with the XRD results [34]. The mobility of the ion is, therefore, increased due to this amorphous nature. Maximum ionic conductivity of the order of 2.83×10^{-4} S cm^{-1} is achieved for the sample having 7.5 wt.% $LiClO_4$. However, the ionic conductivity is found to decrease at 10 wt.% $LiClO_4$ concentration. This is due to the aggregation of charge carrier formation, which, consequently reduces the available path for the movement of ions. Apart

from this, the tendency of ions pair formation on the addition of more amount of salt also the reason of this reduced the ionic conductivity.

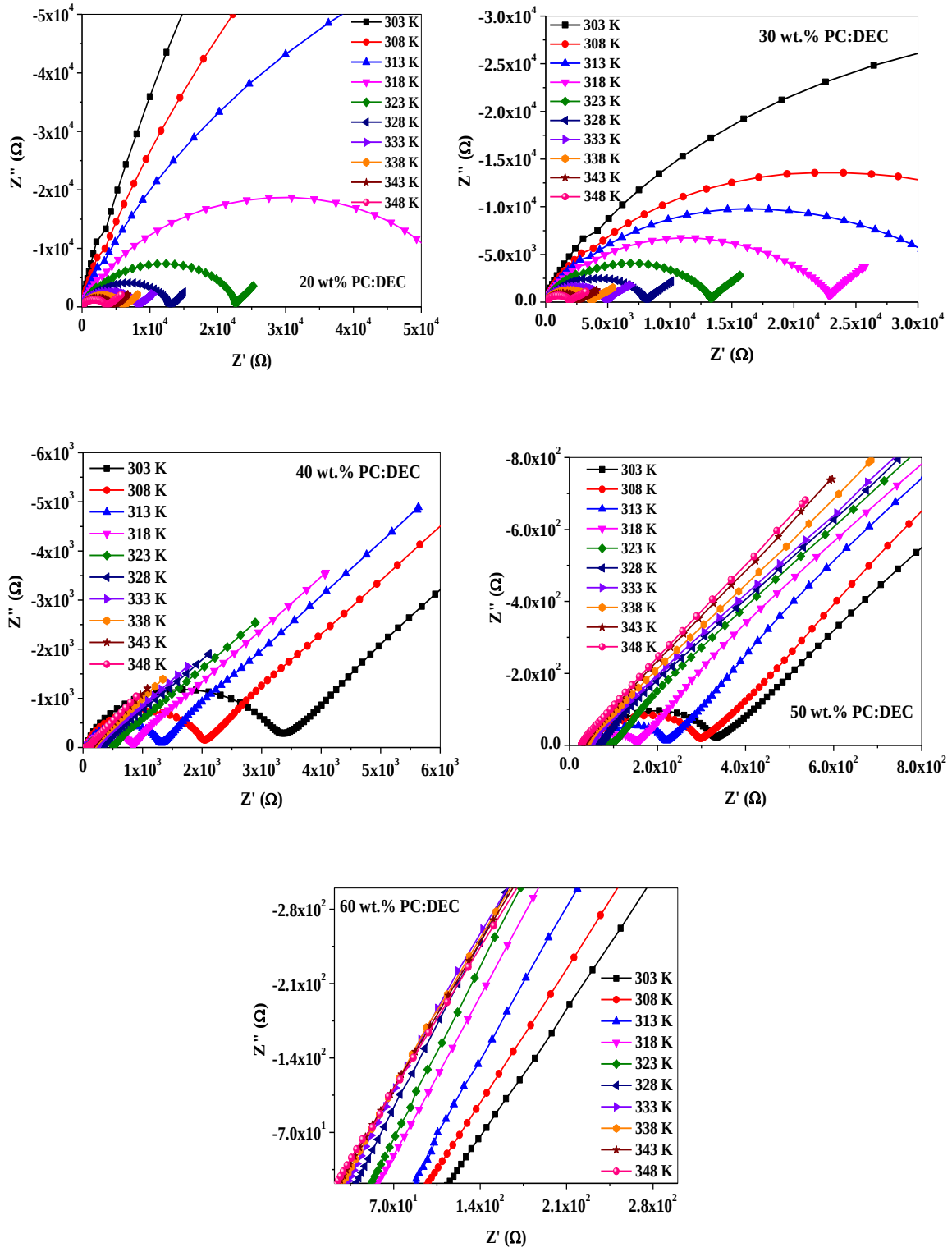

Figure 5.7 The complex impedance plot for different concentrations of PC:DEC in the GPE system at different temperatures - Series(b).

Series (b): In order to elucidate the influence of varying amount of PC:DEC plasticizer on electrical properties, the complex impedance plots for the GPE with different concentrations of PC:DEC plasticizers at different temperatures from 303 K to 348 K are depicted in Figure 5.7. The plots show the same features as discussed for the previous series but if we look at the complex impedance plot of GPE containing 60 wt.% PC:DEC, the semicircle diminishes and only a long tail is obtained implies this GPE system is the mainly ionic conductor. A similar type of behavior has also been reported for PEO based polymer electrolytes system by Kruppasamy et al. [35]. It is also observed from the figures that the intercept of high-frequency semicircle shifts towards origin indicates the decrease in the bulk resistance (R_b) of GPE as temperature increases.

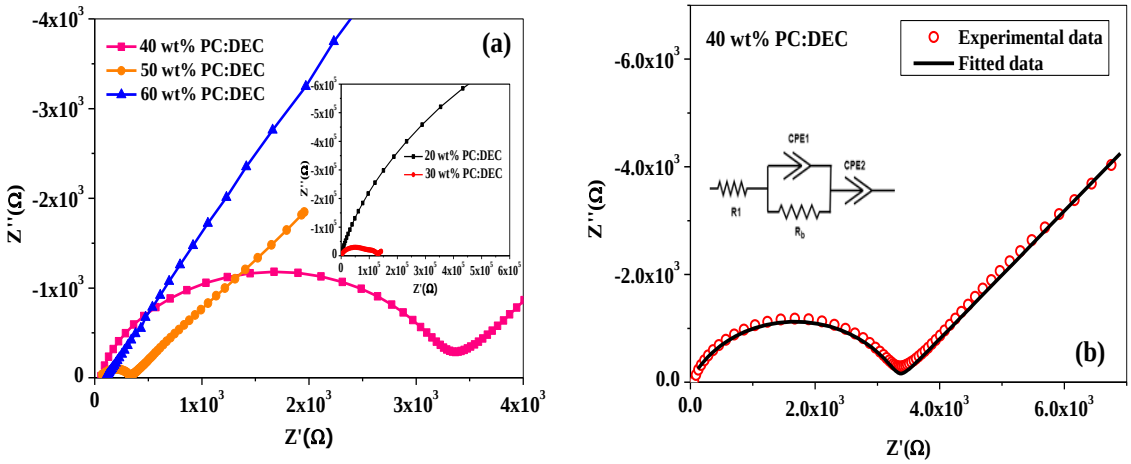

Figure 5.8 (a)The complex impedance plot for different concentrations of PC: DEC plasticizers in the GPE system at 303 K (b) Equivalent circuit fitting of the impedance plot of GPE with 40 wt.% PC:DEC at 303 K - Series (b).

The complex impedance plot for the GPE with variable concentrations of PC:DEC at 303 K is shown in Figure 5.8 (a). More clarity about the features can be examined using an equivalent circuit. Hence, the present GPE data is fitted with an equivalent circuit model and is depicted in Figure 5.8 (b) for the GPE system with 40 wt.% PC:DEC at 303 K. In the equivalent circuit, a high-frequency semicircle is represented by the parallel combination of a bulk resistor and a constant phase element (CPE1), and low frequency inclined and long-tail spikes are represented by constant phase element (CPE2) in series, where CPE is a leaky capacitor (i.e. hybrid between a capacitor and a resistor) [36]. CPE element in the circuit accounts for a non-ideal electrolyte system. The present system shows the depressed semicircle which has a wider distribution of relaxation time [37]. Such depressed semicircle

due to the presence of a distribution of relaxation time within the bulk electrolyte system has been reported by Patro et al. in their study [38]. With increasing the amount of PC: DEC, the reduction in the diameter of semicircle is observed, and complete disappearance semicircle at 60 wt.% of PC: DEC has been seen. The disappearance of the semicircle is an indication of the GPE system is a highly ionic conductor [39]. From the obtained bulk resistance, the ionic conductivity is calculated using Eq. 5.1. The variation in ionic conductivity with different concentrations of PC: DEC plasticizers at 303 K for PVDF−HFP:PMMA−$LiClO_4$-PC:DEC GPE system is shown in Figure 5.9. The values of ionic conductivity are also listed in Table 5.1. The continuous increase in the value of ionic conductivity from 1.24×10^{-8} S cm^{-1} to 3.97×10^{-4} S cm^{-1} as the concentration of plasticizers increases from 20 wt.% to 60 wt.%. The observed behavior might be due to the addition of a mixture of plasticizers with combined features such as high dielectric constant and lower viscosity which leads to an increase in the number of charge carriers as a result of salt dissociation in the polymer matrix. Sharma et al. reported that the plasticizers reduce the inter-ion coulomb interaction and a large number of ions take part in the conduction process [40]. And free charge carriers (Li^+ ions) migrate through a less viscous medium where mobility of ions enhances. A similar effect is discussed by Johan et al. [41] in PEO−$LiCF_3SO_3$–EC complexations with different concentrations of EC plasticizer. It is reported that when plasticizer is added to the system, it can interrupt polymer−polymer interaction due to polymer plasticizer interaction and ion plasticizer coordination. This process will create more free volume and a new path for the conduction of ions.

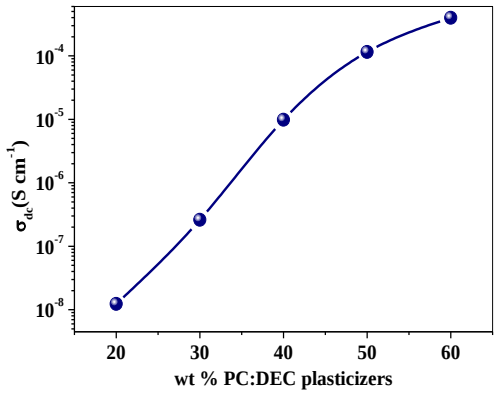

Figure 5.9 Variation of ionic conductivity as a function of PC:DEC plasticizers concentration at 303 K - Series(b).

It is a well-known fact that when the plasticizers are added to the system, it helps the conduction of ions through the polymer matrix because plasticizers are low molecular

weight and help in dissociating charge carriers resulting in a higher ionic conductivity [42]. Apart from this, the crystallinity of the polymer reduces which provides more space for the movement of ions. So, in general, the advantages of the addition of plasticizers are: (i) to increase the amorphous nature of polymer electrolyte (ii) dissociation of the salt as to increase the number of charge carriers for the participation in conduction process (iii) lower the glass transition temperature (T_g) of the polymer matrix [43].

Series (c): The complex impedance plots of nanocomposite gel polymer electrolyte systems at different temperatures are shown in Figure 5.10. The diameter of the semicircle decreases as the temperature increases. The intercept of semicircles on the real axis showing the bulk resistance (R_b) of the system shifts towards origin with an increase in temperature. At higher temperatures (almost > 333 K), the high-frequency semicircle disappears indicating that the present system is mainly ionic conductors [7]. For more clarification about the observed pattern of complex impedance plot, the obtained experimental data have been fitted with an equivalent circuit plotted in Figure 5.11 (b). In the diagram, open circles are experimental data and the solid line is fitted one. The equivalent circuit is represented in the inset of Figure 5.11(b). It is comprised of a parallel combination of constant phase element (CPE1) and bulk resistance (R_b) followed by constant phase element (CPE2) in series. A depressed semicircle in impedance plot, whose center lies below the real axis indicates the presence of a constant phase element. The CPE 2 corresponds to non-vertical inclined spikes. To investigate the effect of variation of Al_2O_3 nanofiller in GPE, the complex impedance plot of nanocomposite GPE with the variation of Al_2O_3 at 303 K has been plotted in Figure 5.11(a). It can be seen clearly that on the addition of nanofiller Al_2O_3, the bulk resistance (R_b) decreases with increasing the amount of nanoparticle from 0.5 to 2 wt.%, and a reverse trend has been observed beyond the 2 wt.% Al_2O_3.

The obtained ionic conductivity (σ_{dc}) (Eq. 5.1) values are plotted as a function of Al_2O_3 variation in Figure 5.12. The figure shows the increasing trend in ionic conductivity with increasing the amount of Al_2O_3 nano-particles in GPE up to an amount of 2 wt.%, however, beyond 2 wt.% the ionic conductivity drops. The increment and decrement in ionic conductivity can be explained by space charge enhancement and blocking effect. The change in DC conductivity with the variation of Al_2O_3 nanofiller can also be explained by the relation using Eq. 5.2. From that relation, one can say that DC conductivity depends on concentrations of charge carriers and mobility of charge carriers as q_i is a constant term.

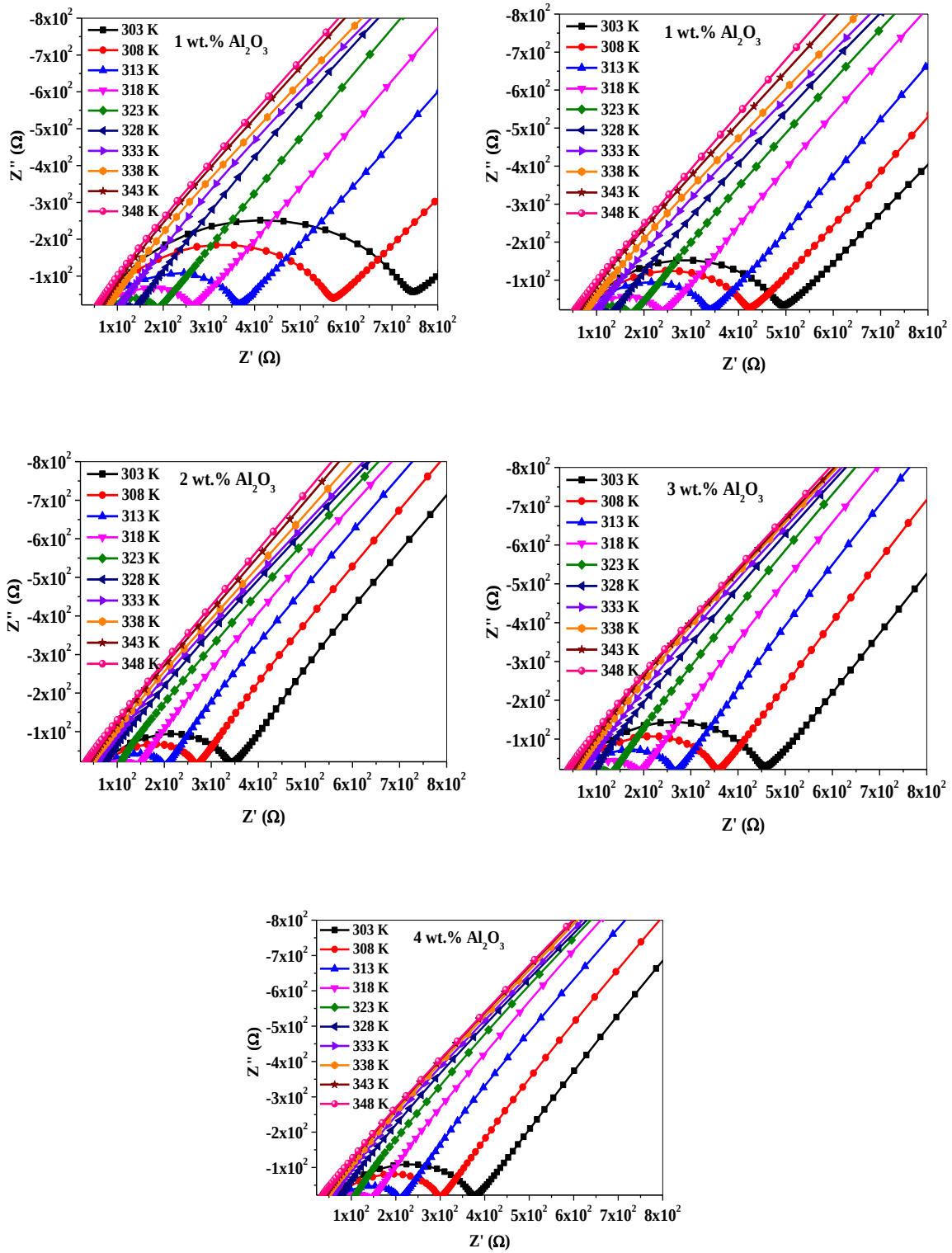

Figure 5.10 The complex impedance plot for different concentrations of Al_2O_3 in the GPE system at different temperatures – Series (c).

The addition of nanofiller enhances the amorphous nature as well as the conduction path for the transportation of Li^+ ions. Prasanth et al.[44] reported the enhancement in ionic conductivity by incorporating nano clay in poly (vinylidene fluoride) based nanocomposite

porous polymer membranes. He discussed in his study that the incorporation of nano clay in host polymer increase dissociation of lithium salt as well as provide conduction pathway for the transportation of Li^+ ion through the polymer matrix. However, on the other hand, as seen in the XRD study, the crystalline phase decreases with increasing the amount up to 2 wt.% due to dispersion of Al_2O_3 in the polymer matrix. The increasing amorphous phase with more free space favors the increase in ionic conductivity. The highest conductivity of the order of 1.62×10^{-4} S cm^{-1} is achieved for GPE having 2 wt.% Al_2O_3. On further addition of nanoparticles, cause a reduction in ionic conductivity might be due to agglomeration of nanoparticles into large particles inhibit the migration of the ion from one coordinating site to another. A similar phenomenon has also been observed by Arya et al.[45]. However, the ionic conductivity of all GPE systems containing nanoparticles is found to be of the order of 10^{-4} S cm^{-1}.

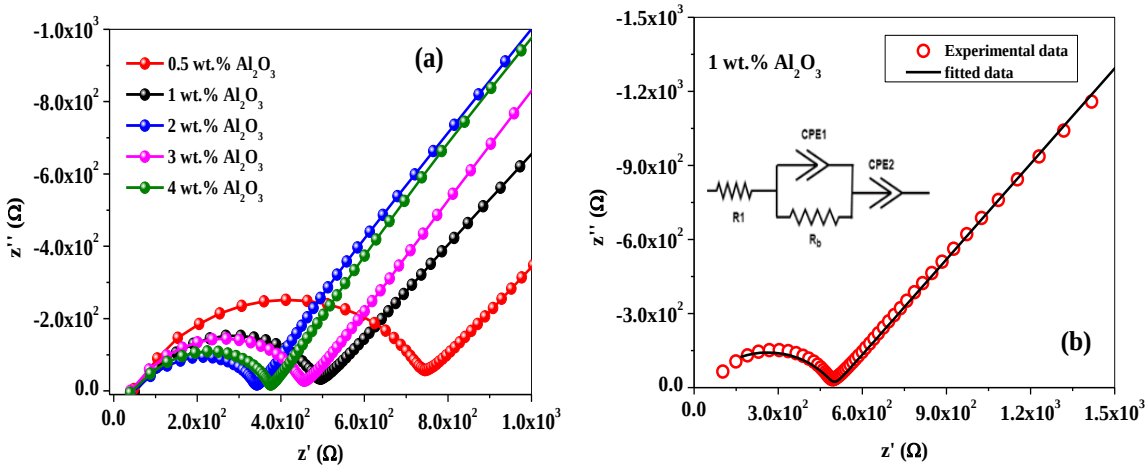

Figure 5.11 (a) The complex impedance plot for different concentrations of Al_2O_3 nano-particles in the GPE system at 303 K (b) Equivalent circuit fitting of the impedance plot of GPE containing 1 wt.% Al_2O_3 at 303 K - Series (c).

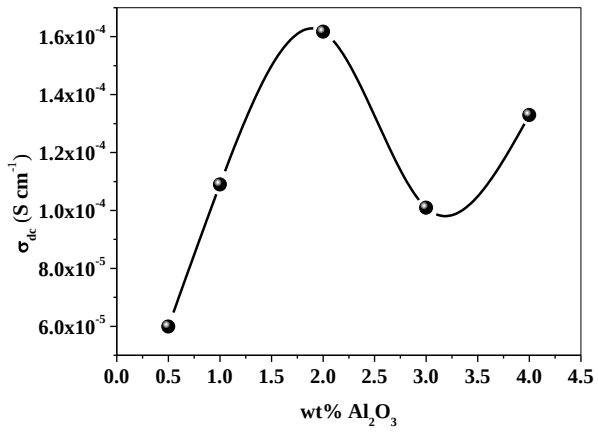

Figure 5.12 Variation of ionic conductivity as a function of Al_2O_3 concentration at 303 K - Series(c).

5.3 Temperature-Dependent DC Ionic Conductivity

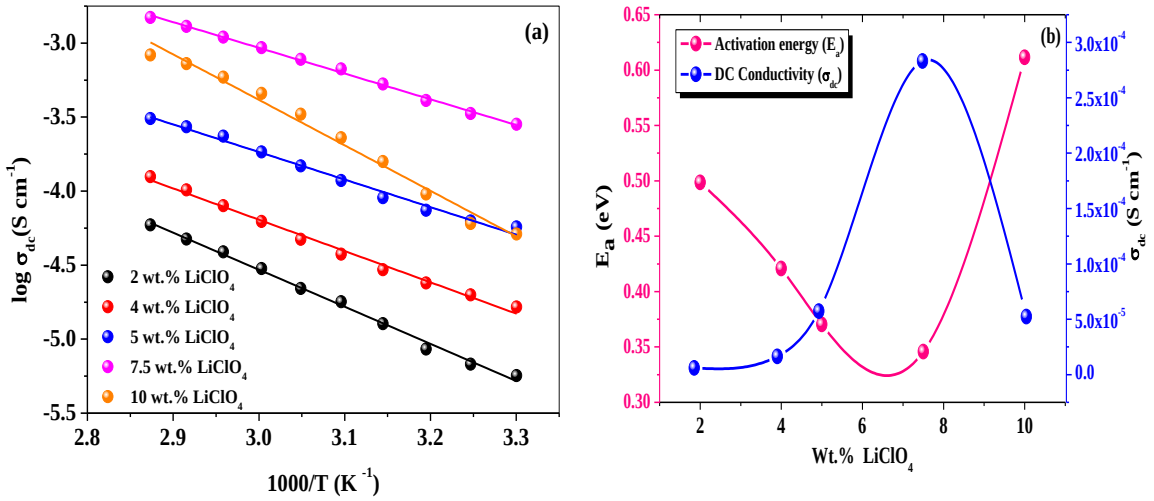

Figure 5.13 (a)Temperature dependence of ionic conductivity (log σ_{dc} versus 1000/T) of GPE with different concentrations of $LiClO_4$. (b) Variation of ionic conductivity and activation energy as a function of $LiClO_4$ salt concentration – Series (a).

The ionic conductivity of polymer electrolyte depends on temperature, types of ions, amount of salt, types of other additives, etc. The ionic conduction behavior or the conduction mechanism in the polymer electrolyte can be evaluated from the temperature-dependent ionic conductivity. Ratner et al.[46] reported that the temperature-dependent ionic conductivity generally obeys two types of ion transport models i.e. Arrhenius behavior and/or Vogel Tammann Fulcher (VTF) behavior. The linear relationship between the log σ_{dc} versus 1000/T signifies the Arrhenius behavior. This linear behavior indicates that the conduction mechanism is via the temperature assisted hopping mechanism and decoupled from the segmental motion of the polymer chain. Whereas, in VTF behavior, the non-linear relationship of log σ_{dc} versus 1000/T also suggests temperature dependent conduction mechanism involves ion hopping coupled with the polymer segmental motion.

Series (a): The variation of DC conductivity (log σ_{dc}) versus reciprocal temperature (1000/T) of the GPE system with different concentrations of $LiClO_4$ salt is depicted in Figure 5.13(a). The conductivity follows the linear behavior with increasing the temperature from 303 K to 348 K for all $LiClO_4$ salt concentrations. Arrhenius behavior conveys that the ion conduction mechanism is thermally activated and ions acquire more energy for the faster ionic motion. As a result, ions jump from one site to another empty site. This suggests that lower activation energy is coupled with a high ionic conductivity [46]. Mathew et al.,[46] reported in PVAc/PVDF/$LiClO_4$/x, where x = DMC, DEC, PC, GBL system that the

polymer expands and produces free volume with the rise in temperature so that mobile carriers or polymer chain segments can move through the free volume. In order to give a better understanding of the ionic conduction mechanism of the GPE films, the linear behavior of ($\log\sigma_{dc}$) versus reciprocal temperature (1000/T) data have been fitted to the Arrhenius relation expressed as

$$\sigma = \sigma_0 \exp\left(\frac{E_a}{K_B T}\right) \tag{5.3}$$

where σ_0 is the pre-exponential factor, E_a is the activation energy, K_B is the Boltzmann constant and T is the temperature in Kelvin. The linear plot of temperature-dependent conductivity is fitted with a linear fit with an R^2 value ~ 0.99 and a slope is extracted from it. From the values of the slope, activation energies for all GPE have been calculated. The activation energies as a function of $LiClO_4$ salt are plotted in Figure 5.13(b). It can be seen from Figure 5.13(b), the highest conducting sample exhibits minimum activation energy. The low activation energy (E_a) is required to energies the lithium-ion for physical transportation through polymer matrix which is caused by the completely amorphous nature [47]. According to Li et al. [48], ions or clusters of ions migrate in the pores of the polymer via amorphous domains swelled by electrolytes and along the molecular chain of the polymer. The migration of lithium-ion along the molecular chains of polymer is not appreciable. Hence, it can be stated that an increase in conductivity may be due to filled pores with electrolytes and swelled amorphous domain. Thereafter, ion clusters are formed, which mitigate the process of conduction in the polymer electrolyte.

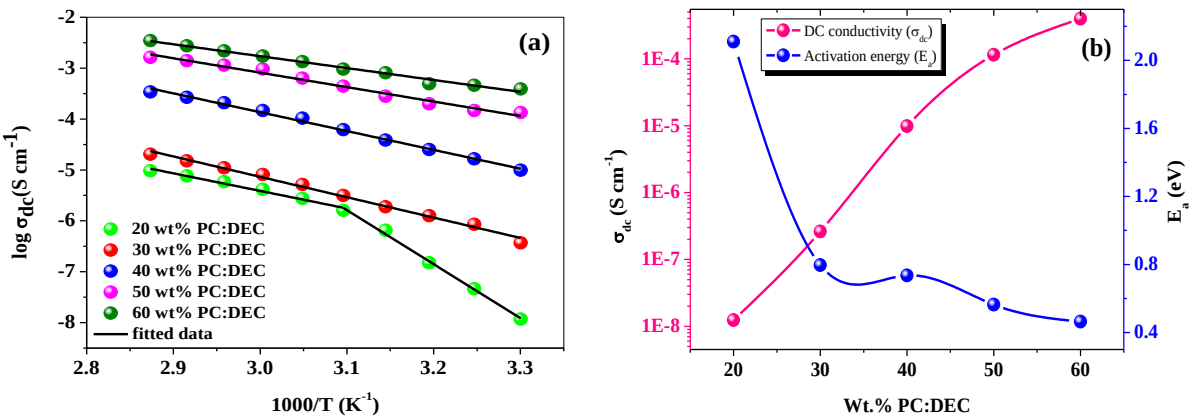

Figure 5.14 (a) Temperature dependence of ionic conductivity (log σ_{dc} versus 1000/T) of GPE with different concentrations of PC: DEC. (b) Variation of ionic conductivity and activation energy as a function of PC: DEC concentration - Series (b).

Series (b): The DC ionic conductivity as a function of reciprocal temperature for GPE with different amounts of PC:DEC is plotted in Figure 5.14(a). It is observed that the ionic conductivity increases with an increase in temperatures and linear behavior of σ_{dc} as a function of reciprocal temperature. This temperature-dependent ionic conductivity follows Arrhenius behavior. It suggests that it is a thermally activated process. According to Druger et al [49]., the increase in ionic conductivity with temperature is due to the segmental motion of the polymer chain. As a result of this, free volume in the polymer matrix increases with an increase in temperatures which permits the hopping of ions from one place to another. It causes an increase in the mobility of ions. It is also believed that with the progressive enhancement of the amorphous region due to an increase in temperature, the polymer chain acquires faster bond rotation, which produces polymer chain segmental motion. DC conductivity plot is fitted with the Arrhenius equation (Eq. 5.3) and activation energy E_a is calculated. The variation of ionic conductivity and activation energy versus concentration of PC: DEC is shown in Figure 5.14 (b). It can be seen from the figure that the ionic conductivity of the GPE system increases continuously with PC: DEC concentration and activation energy values decrease. The lowest activation energy of conduction of 0.46 eV is found for the highest conducting sample.

Series (c): The temperature-dependent DC ionic conductivity with a different weight percentage of Al_2O_3 over a temperature range from 303 K to 348 K is plotted in Figure 5.15 (a). The ionic conductivity increases with increasing temperature, because, the polymer chains acquired faster internal modes of vibration and make polymer chain segmental motion easier, which, in turn, enhances the hopping of ions through inter-chain and intra-chain movement. The linear behavior of the temperature-dependent conductivity plot suggests Arrhenius behavior and is fitted and activation energy is calculated. The calculated activation energy for all samples is plotted as a function of Al_2O_3 variation and shown in Figure 5.15(b). The lowest activation energy was found to be ≈ 0.51 eV for the sample having 2 wt.% Al_2O_3. The reason for decreased activation energy is attributed to the increased mobility of the ions due to the presence of Al_2O_3 in the polymer. DSC results are also agreeing with the fact that the melting temperature (T_m) of the composite gel polymer electrolyte decreases with the addition of nanofiller into GPE. This results in an enhancement of the polymer chain mobility and facilitates the migration of Li^+ ions through the polymer matrix. Pan et al. found a decrease in the activation energy with increasing the amount of TiO_2 nanofiller in PEO-$LiClO_4$ system due to reduced crystalline nature [50].

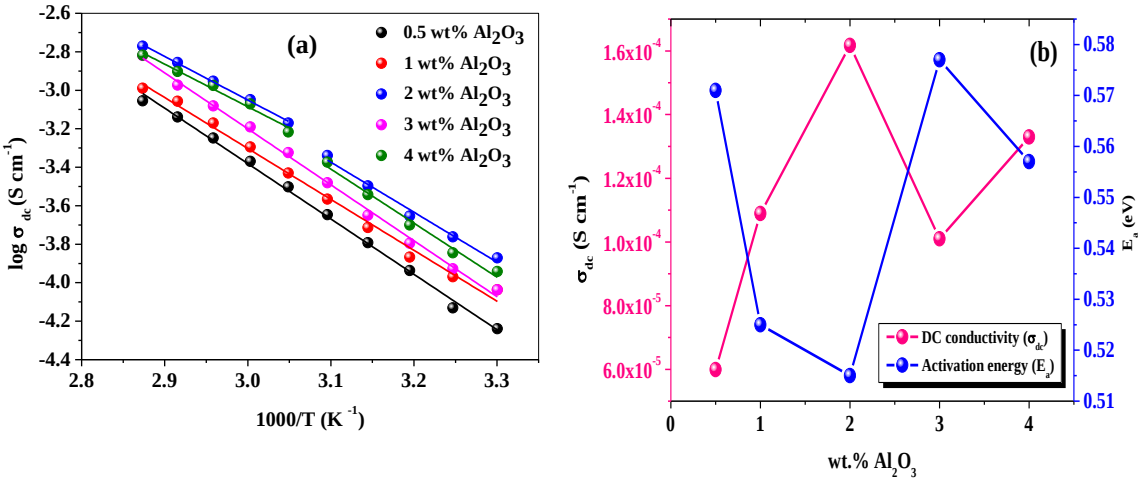

Figure 5.15 (a) Temperature dependence of ionic conductivity (log σ_{dc} versus 1000/T) of GPE with different concentrations of Al_2O_3. (b) Variation of ionic conductivity and activation energy as a function of Al_2O_3 concentration - Series(c).

Table 5.1 Values of DC conductivity (σ_{dc}) and activation energy (E_a) for all samples of Series (a), Series (b), and Series (c).

Samples	DC conductivity σ_{dc} (S cm^{-1}) (from R_b)	Activation energy (eV)
Series (a): PVDF-HFP:PMMA-$LiClO_4$-PC: DEC with different concentrations of $LiClO_4$		
2 wt.% $LiClO_4$	5.94×10^{-6}	0.49
4 wt.% $LiClO_4$	1.64×10^{-5}	0.42
5 wt.% $LiClO_4$	5.73×10^{-5}	0.37
7.5 wt.% $LiClO_4$	2.83×10^{-4}	0.34
10 wt.% $LiClO_4$	5.24×10^{-5}	0.61
Series(b): PVDF-HFP:PMMA-$LiClO_4$-PC:DEC with different concentrations of PC:DEC		
20 wt.% PC:DEC	1.24×10^{-8}	2.11
30 wt.% PC:DEC	2.61×10^{-7}	0.79
40 wt.% PC:DEC	9.82×10^{-6}	0.73
50 wt.% PC:DEC	1.15×10^{-4}	0.56
60 wt.% PC:DEC	3.97×10^{-4}	0.46
Series(c): PVDF-HFP:PMMA-$LiClO_4$-PC: DEC-Al_2O_3 with different concentrations of Al_2O_3		
0.5 wt.% Al_2O_3	5.99×10^{-5}	0.57
1 wt.% Al_2O_3	1.09×10^{-4}	0.52
2 wt.% Al_2O_3	1.62×10^{-4}	0.51
3 wt.% Al_2O_3	1.01×10^{-4}	0.57
4 wt.% Al_2O_3	1.33×10^{-4}	0.55

5.4 AC Conductivity

AC conductivity gives an understanding of electrical relaxation phenomena. This is commonly used to characterize the ion transport phenomenon occurring in ion-conducting material in the frequency domain [51]. To obtain this information, conductivity data has been analyzed in terms of complex conductivity $\sigma^*(\omega) = \sigma'(\omega) + i\sigma''(\omega)$, where σ' and σ'' is a real and imaginary part of AC conductivity. The formalism of AC conductivity is given in Chapter-2.

Series(a): The effect of $LiClO_4$ salt on the PVDF-HFP:PMMA-PC:DEC based gel polymer electrolyte in terms of frequency-dependent conductivity at different temperatures has been investigated.

Figure 5.16 shows the variation of conductivity as a function of the frequency of GPE at different temperatures 303 K to 348 K. It can be seen from the figure that the AC conductivity spectra show three different regions, (i) a low-frequency dispersive region, (ii) an intermediate frequency plateau region, and (iii) a high-frequency dispersion region [52]. However, all three features are not observed in all systems. The low-frequency region is not present in spectra of GPE with 2 wt.% $LiClO_4$ due to low conductivity whereas the disappearance of the high-frequency region in the spectra of GPE contains 7 wt.% $LiClO_4$ due to high conductivity. At the lower frequency region, the polarization starts at the electrode-electrolyte interface cause decrease in conductivity σ' [53]. This feature of polarization is due to the accumulation of charges at electrode-electrolyte. In the mid-frequency range, the values of σ' remain almost independent (constant) of frequency up to a certain value of frequency. This plateau region at the mid-frequency range corresponds to DC ionic conductivity. At the intermediate frequency range, the ion jumps from one vacant site to another and travels much faster which contributes towards DC conductivity. The conductivity σ' continues increasing with the increase in frequency. This crossover from DC conductivity to the dispersive conductivity is also termed as ac conductivity σ' . The frequency at which a transition from DC conductivity (plateau region) to conductivity dispersion is called crossover frequency (Hopping frequency) ω_p [54]. It is further affirmed that the hopping frequency shifts towards a higher frequency region with increasing temperature. A similar behavior of AC conductivity as a function of frequency for GPE with different concentrations of $LiClO_4$ content at 303 K is observed as shown in Figure 5.17.

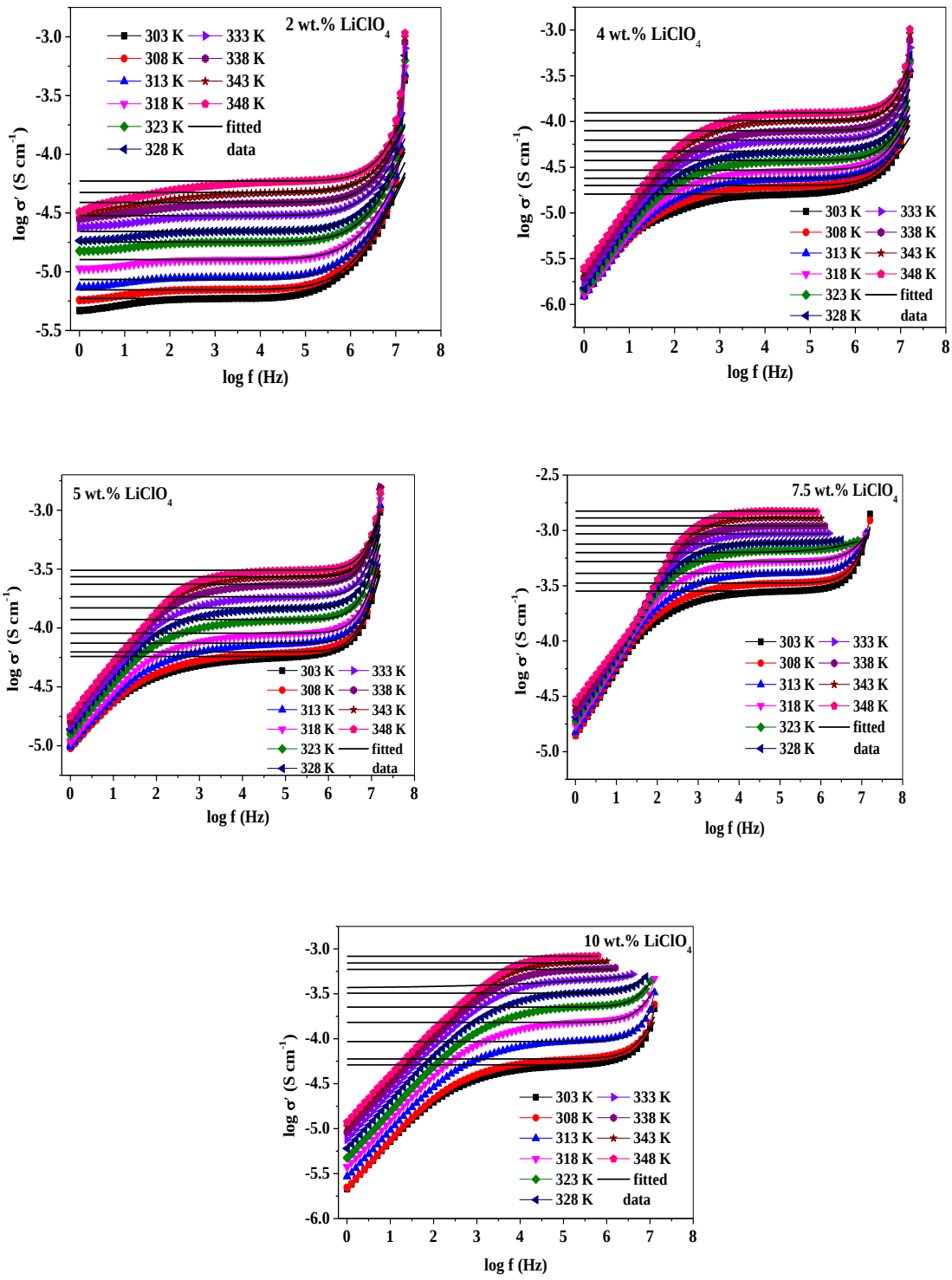

Figure 5.16 Variation of AC conductivity as a function of frequency (log σ′ versus log f) for different concentrations of $LiClO_4$ in the GPE system at different temperatures – Series (a).

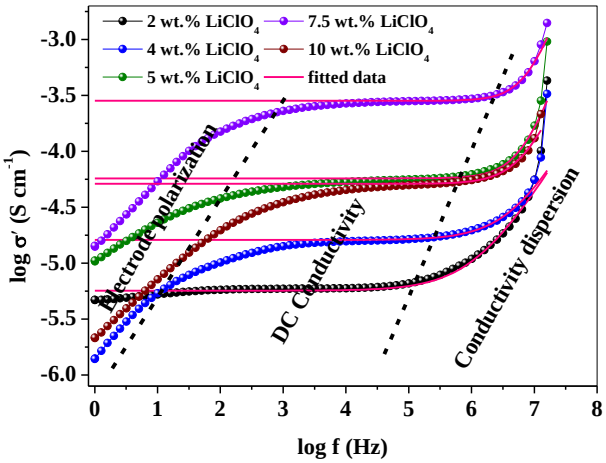

Figure 5.17 Variation of AC conductivity as a function of frequency (log σ′ versus log f) of GPE systems with different concentrations of $LiClO_4$ at 303 K - Series (a).

The behavior of AC ionic conductivity with frequency in the higher frequency region follows Jonscher's power law given by [55],

$$\sigma_{ac} = \sigma_{dc} + A\omega^{n} \tag{5.4}$$

where σ_{ac} is ionic conductivity at a particular frequency, σ_{dc} is frequency independent conductivity. A is the pre-exponential constant, ω is the angular frequency, and *n* is the power-law exponent. Since this behavior of power-law has been observed in a wide range of materials, it is also known as "Universal Power Paw" or "Universal behavior" [56]. Frequency exponent (*n*) measures the degree of interaction between mobile ions and the host polymer matrix. The values of *n* usually lie in the range, $0 < n < 1$. Frequency exponent (*n*) may also exceed unity reported elsewhere [57] In the present study, we have observed the values of $n > 1$ also [58]. The ionic conductivity is also ascribed by the factors like the concentration and the hopping frequency of mobile charge carriers [53] which can be estimated by the following Eq.5.5. Almond and west [59-61] have suggested a simple way to estimate hopping frequency from Eq. 5.4 by knowing the values of σ_{dc}, *A*, and *n*. Rewriting Jonscher's empirical equation

$$\sigma'(\omega) \propto \omega\left[\left(\frac{\omega}{\omega_p}\right)^{n_1-1} + \left(\frac{\omega}{\omega_p}\right)^{n_2-1}\right] \tag{5.5}$$

where n_1 and n_2 are empirical constant and ω_p is the hopping frequency. for frequency-independent conductivity $n_1 = 0$ and $n_2 = n$. Assuming a proportionality constant *K*, we have

$$\sigma'(\omega) = K\omega\left[\left(\frac{\omega}{\omega_p}\right)^{-1} + \left(\frac{\omega}{\omega_p}\right)^{n-1}\right] \tag{5.6}$$

$$\sigma'(\omega) = K\omega_p + K\omega_p^{1-n}\omega^n \tag{5.7}$$

On comparing Eq. 5.7 with Eq.5.4, one gets

$$\sigma_{dc} = K\omega_p \tag{5.8}$$

$$A = K\omega_p^{1-n} \tag{5.9}$$

On Comparing Eq. 5.8 and Eq. 5.9,

$$\sigma_{dc} = A\omega_p^{\,n} \quad \text{or} \quad A = \frac{\sigma_{dc}}{\omega_p^{\,n}} \tag{5.10}$$

Substituting Eq. 5.10 in Eq. 5.4,

$$\sigma_{ac} = \sigma_{dc}\left[1 + \left(\frac{\omega}{\omega_p}\right)^n\right] \tag{5.11}$$

It is assumed that at a particular frequency i.e. the hopping frequency (ω_p), ac conductivity becomes double of DC conductivity $\sigma_{ac} = 2\sigma_{dc}$ when $\omega = \omega_p$ (using Eq. 5.11). Substituting $\sigma_{ac} = 2\sigma_{dc}$ in Eq. 5.4., the expression for the hopping frequency ω_p becomes

$$\omega_p = \left(\frac{\sigma_{dc}}{A}\right)^{\frac{1}{n}} \tag{5 .12}$$

and

$$K = \frac{\sigma_{dc}T}{\omega_p} \tag{5.13}$$

The hopping frequency has been calculated for all gel polymer electrolytes using Eq. 5.12 at different temperatures. On a close inspection of the AC conductivity spectra, the frequency at which transition occurs from the plateau region to the dispersive region shifts towards a higher frequency side with an increase in temperature. Because an increase in temperature results in the expansion of polymer which facilitates the local empty spaces and expands the free volume. The hopping movement of ions is favored and the ions can hop with a higher frequency with shorter relaxation time.

To understand whether hopping frequency is a thermally activated process or not, the calculated hopping frequency (ω_p) versus inverse temperature(1000/T) has been plotted and shown in Figure 5.18(a). In the thermally activated hopping process, the hopping of ions

from one vacant site to another site takes place with increasing temperature. Linear behavior of this plot fitted using Arrhenius relation represented by

$$\omega_p = \omega_0 \exp\left(\frac{E_\omega}{K_B T}\right) \tag{5.14}$$

where ω_0 is the effective attempt frequency and E_ω is the energy required for hopping. The activation energies have been extracted using slope values of linear fit and tabulated in Table 5.2. Hopping frequency could not be obtained for the GPE having 7.5 wt.% $LiClO_4$ at all temperatures due to the absence of a high-frequency dispersion region. It may be noted that the activation energies for hopping are lower than the activation energies for conduction which suggest that the ions which are participating in conduction process have to overcome different potential barrier due to localized electrons in the amorphous polymer matrix. Similar results are also reported by Manish in his study for PbI_2 conducting glasses [62].

The mobile carrier concentration factor *K* is calculated using Eq. 5.13. Figure 5.19 shows the variation of mobile ion concentration *K* as a function of temperature. Carrier concentration increases slightly with an increase in temperature. The inset of Figure 5.19 illustrates that the carrier concentration term *K* is following the same trend as conductivity data with increasing salt concentration at 303 K.

The ion conduction mechanism can be determined based on the behavior of the frequency exponent (*n*) as a function of temperature. Mechanisms such as correlated barrier hopping (CBH) in which frequency exponent (*n*) decreases with temperature, in quantum mechanical tunneling (QMT), *n* is independent of temperature, the small polaron tunneling (SPT) shown an increases of *n* with temperature and the overlapping large polaron (OLP) in which frequency exponent(*n*) decreases with temperature and again increases [63]. In the CBH model, the conduction mechanism is associated with the charge carrier hopping process. QMT model is applicable to the system in which frequency dependent conductivity arises from the tunneling of charge carriers between the sites separated by a potential barrier. In the SPT model, small polarons are formed when a charge carrier deforms the surrounding lattice and a tunneling process is responsible. In this model, the charge carriers and lattice are strongly coupled. The variation of frequency exponent as a function of temperature for all GPE systems with different concentrations of $LiClO_4$ is shown in Figure 5.20. At higher temperatures, the frequency exponent(*n*) could not be obtained for GPE with 7.5 wt.% and 10 wt.% $LiClO_4$ due to the absence of a high-frequency dispersion region. The frequency

exponent n increases with temperature except for the GPE system with 7.5 wt.% $LiClO_4$. The SPT model can be applied in which small polarons are formed due to deformation of the surrounding structure by a charge carrier and conductivity rise might be due to the tunneling process. In our system, *n* decreases with temperature for the GPE system with 7.5 wt.% $LiClO_4$, hence, the applicability CBH model has been observed. For the GPE system with 7.5 wt.% $LiClO_4$, the conduction mechanism is associated with the hopping process of Li^+ charge carriers. This is due to the high amorphous nature of GPE, where hopping of charge carriers easily takes place.

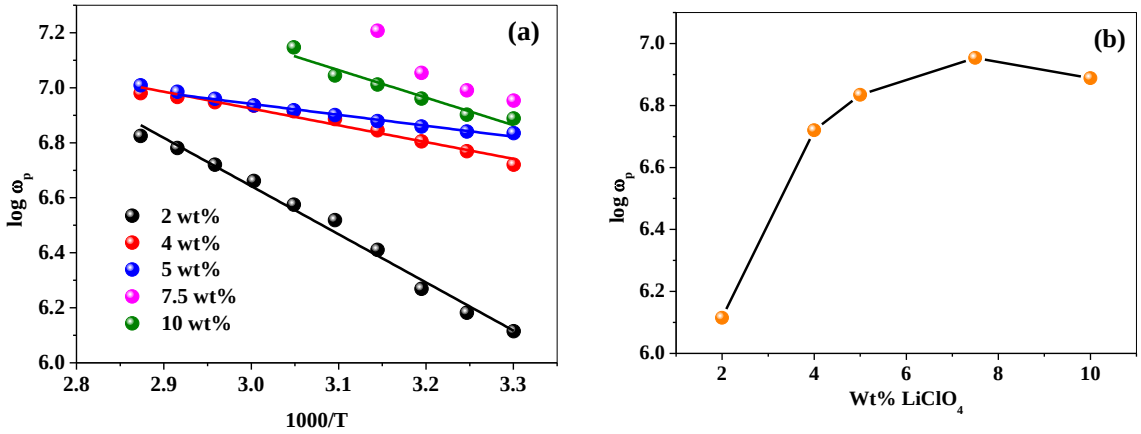

Figure 5.18 (a) log ω_p versus 1000/T for different concentrations of $LiClO_4$ in the GPE system. (b) Variation of hopping frequency as a function of $LiClO_4$ concentration at 303 K – Series (a).

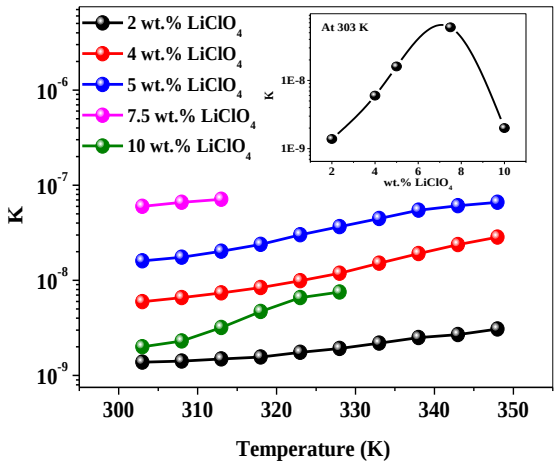

Figure 5.19 Variation of mobile ion factor *K* as a function of the temperature of GPE with different $LiClO_4$ content (inset: Variation of *K* with $LiClO_4$ content at 303 K) – Series (a).

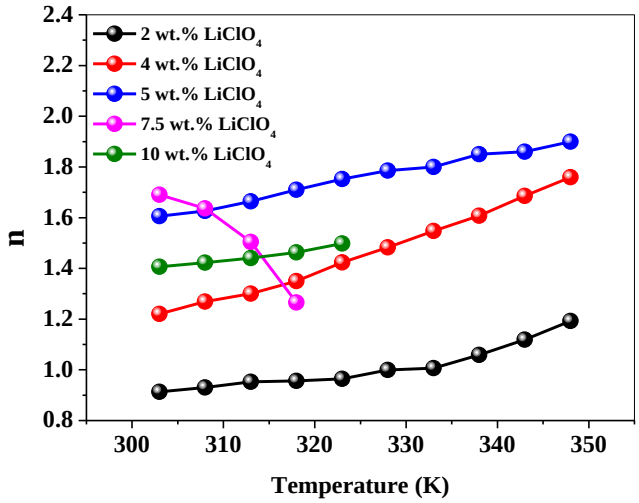

Figure 5.20 Frequency exponent as a function of temperature for all GPE system with different $LiClO_4$ concentration – Series (a)

Series(b): The effect of PC: DEC plasticizer concentrations in PVDF-HFP: PMMA based gel polymer electrolyte in terms of AC conductivity at different temperatures ranging from 303 K to 348 K is studied. Figure 5.21 shows the variation of ionic conductivity as a function of frequency at different temperatures with different concentrations of PC: DEC plasticizers. Similar features are observed for AC conductivity data as discussed in series (a). At lower frequency, the dispersive region is due to space charge polarization i.e. buildup of charges at the interface of electrode-electrolyte due to blocking electrode [52]. A plateau region in the mid-frequency range is ascribed to DC conductivity as a result of the hopping of charges/ions due to long-range diffusion from one site to another vacant site [53]. A dispersion region in the high-frequency range, where ionic conductivity continues to increase with increasing frequency and represents bulk phenomena [64]. According to Arya et al., in the high frequency region, short-range motion of ions or a correlated forward-backward motion of the ion occurs which is because of the fast periodic reversal effect of the applied field, and diffusion of ions in a longer path is not feasible [65]. Variation of AC conductivity with frequency obeys Jonscher's power law (Eq. 5.4). For the GPE system with 60 wt.% PC: DEC, the high-frequency dispersive regions are not seen at any temperatures because of the high conducting nature of the GPE where the bulk region is absent. The high-frequency dispersive region is not visible in the experimental frequency range due to the fast ion transport dynamic of the electrolytes system as reported by Bandara et al. in his study [66].

Hopping frequency is found to shift towards high frequency side with increasing temperatures. Shifting towards the higher frequency side is attributed to an increase in the polymer chain's flexibility at high temperatures and hopping process gets faster with temperature.

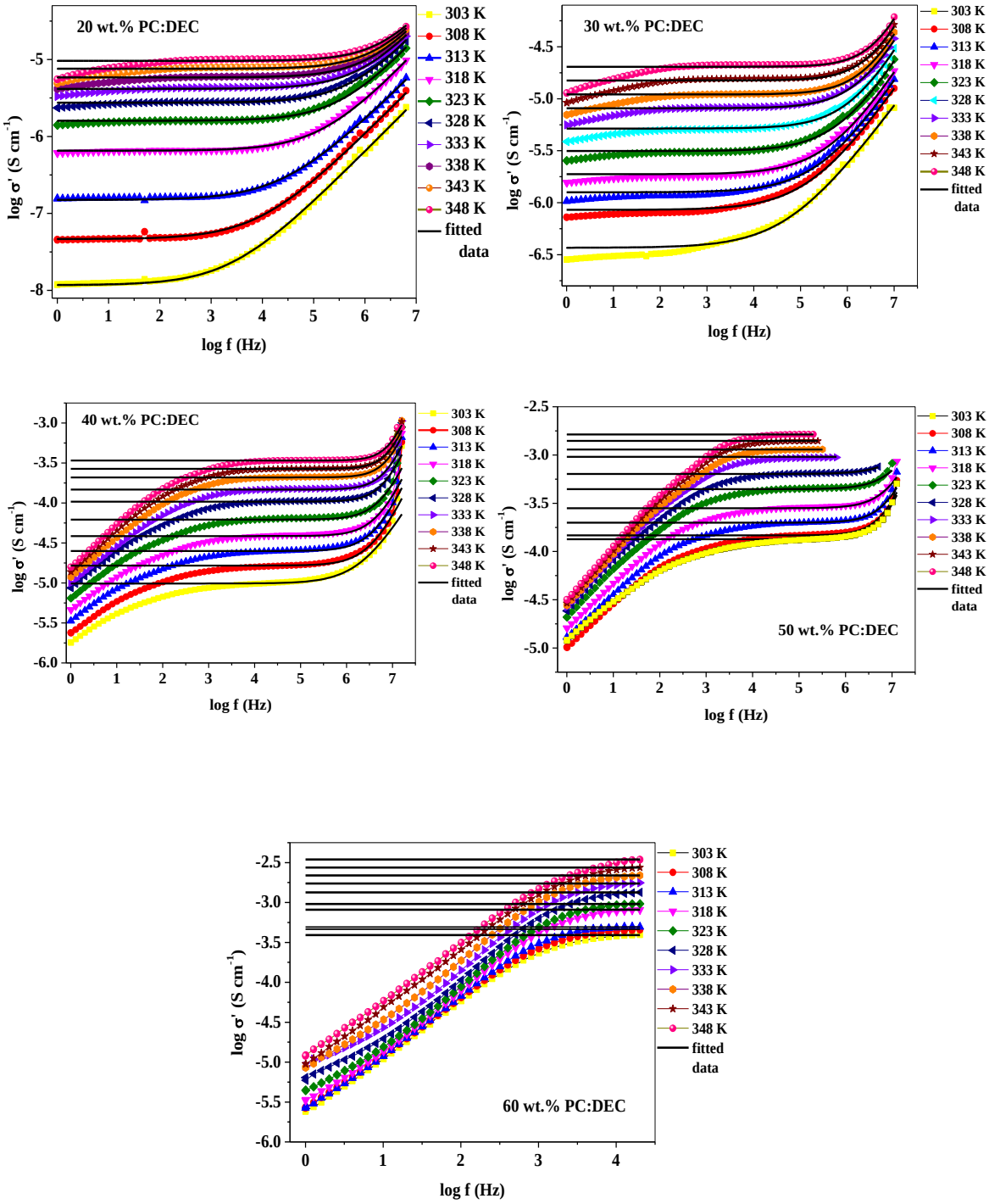

Figure 5.21 Variation of AC conductivity as a function of frequency (log σ′ versus log f) for different concentrations of PC: DEC in the GPE system at different temperatures - Series (b)

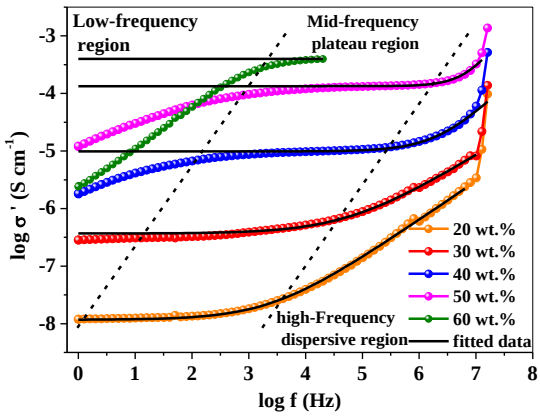

Figure 5.22 Variation in AC conductivity as a function of frequency (log σ′ versus log f) of GPE system with different concentrations of PC: DEC at 303 K - Series (b).

Figure 5.22 shows the AC conductivity as a function of frequency for the GPE having different wt.% of PC: DEC at 303 K. Two features are revealed from the AC conductivity spectra as the content of PC: DEC increases from 20 wt.% to 60 wt.% PC: DEC (i) the conductivity increases due to an increase in the free charge carriers as a result of salt dissociation (ii) the hopping frequency shift toward the higher frequency side may due to an increase in the amorphous nature of the GPE system. In addition to these, the experimental data of AC conductivity spectra are fitted (black solid lines) with Eq. 5.4. and fitted as well as calculated parameters are tabulated in Table 5.2.

The hopping frequency (ω_p) as a function of inverse temperature for the GPE with different concentrations of PC: DEC is plotted in Figure 5.23(a). An increase in the hopping frequency with the rise in temperature is an indication of the thermally activated process. It means the rate of hopping of ions from one site to another available vacant site increases with the temperature. The linear behavior of the plot is fitted with the Arrhenius relation (Eq. 5.14) and activation energy for the hopping of ion is calculated which is listed in Table 5.2.

The mobile carrier concentration factor K is calculated using Eq. 5.13. Figure 5.24 shows the variation of mobile ion concentration K as a function of temperature for the GPE with different wt.% PC: DEC plasticizers. Carrier concentration term K almost remains invariant with changing temperature for GPE system containing a low amount of PC: DEC plasticizers i.e. 20 and 30 wt.% PC: DEC. The inset of Figure 5.24 shows that the carrier concentration term K increases with increasing the amount of the plasticizer in the polymer matrix.

The variation of frequency exponent as a function of temperature for all GPE systems with different concentrations of PC: DEC is shown in Figure 5.25. The GPE system with 20, 30, and 40 wt.% PC: DEC shows an increase in frequency exponent (*n*) indicates the small polaron tunneling (SPT) model is applicable. The decreasing trend of *n* indicates the CBH model is appropriate to probe the ion conduction mechanism in the GPE system with 50 wt.% PC: DEC. For a high conducting sample (GPE containing 60 wt.% PC: DEC), *n* could not be evaluated due to the absence of high-frequency regions in AC conductivity spectra.

Table 5.2 Fitting parameters σ_{dc}, *A*, *n* from the Jonscher's power law and calculated ω_p and τ for all GPE systems of Series (a), Series (b), and Series (c).

Samples	**σ_{dc} (S cm^{-1})**	***A***	***n***	**Hopping frequency ω_p (Hz)**	**Relaxation time τ (s)**	**E_ω (eV)**
Series (a): PVDF-HFP:PMMA-$LiClO_4$-PC: DEC with different concentrations of $LiClO_4$						
2 wt.% $LiClO_4$	5.94×10^{-6}	1.55×10^{-11}	0.91	1.30×10^{6}	7.68×10^{-7}	0.33
4 wt.% $LiClO_4$	1.65×10^{-5}	1.04×10^{-13}	1.22	5.25×10^{6}	1.91×10^{-7}	0.11
5 wt.% $LiClO_4$	5.73×10^{-5}	6.06×10^{-16}	1.61	6.83×10^{6}	1.46×10^{-7}	0.08
7.5 wt.% $LiClO_4$	2.83×10^{-4}	4.98×10^{-16}	1.69	8.98×10^{6}	1.11×10^{-7}	-
10 wt.% $LiClO_4$	5.12×10^{-5}	1.05×10^{-14}	1.40	7.73×10^{6}	1.29×10^{-7}	0.18
Series (b): PVDF-HFP:PMMA-$LiClO_4$-PC:DEC with different concentrations of PC:DEC						
20 wt.% PC:DEC	1.53×10^{-8}	3.45×10^{-11}	0.70	5.39×10^{3}	1.85×10^{-4}	1.74
30 wt.% PC:DEC	3.96×10^{-7}	2.52×10^{-10}	0.64	8.59×10^{4}	1.16×10^{-5}	0.80
40 wt.% PC:DEC	1.01×10^{-5}	1.86×10^{-13}	1.23	1.95×10^{6}	5.13×10^{-7}	0.31
50 wt.% PC:DEC	1.34×10^{-4}	6.24×10^{-15}	1.49	8.40×10^{6}	1.19×10^{-7}	0.26
60 wt.% PC:DEC	3.91×10^{-4}	-	-	-	-	-
Series (c): PVDF-HFP:PMMA-$LiClO_4$-PC: DEC-Al_2O_3 with different concentrations of Al_2O_3						
0.5 wt.% Al_2O_3	5.72×10^{-5}	2.92×10^{-14}	1.35	7.74×10^{6}	1.29×10^{-7}	0.18
1 wt.% Al_2O_3	9.73×10^{-5}	5.64×10^{-15}	1.46	9.08×10^{6}	1.10×10^{-7}	0.12
2 wt.% Al_2O_3	1.34×10^{-4}	6.85×10^{-15}	1.47	1.01×10^{7}	9.90×10^{-8}	0.10
3 wt.% Al_2O_3	9.46×10^{-5}	2.48×10^{-13}	1.23	8.71×10^{6}	1.15×10^{-7}	0.14
4 wt.% Al_2O_3	1.13×10^{-4}	8.00×10^{-15}	1.45	9.86×10^{6}	1.01×10^{-7}	0.11

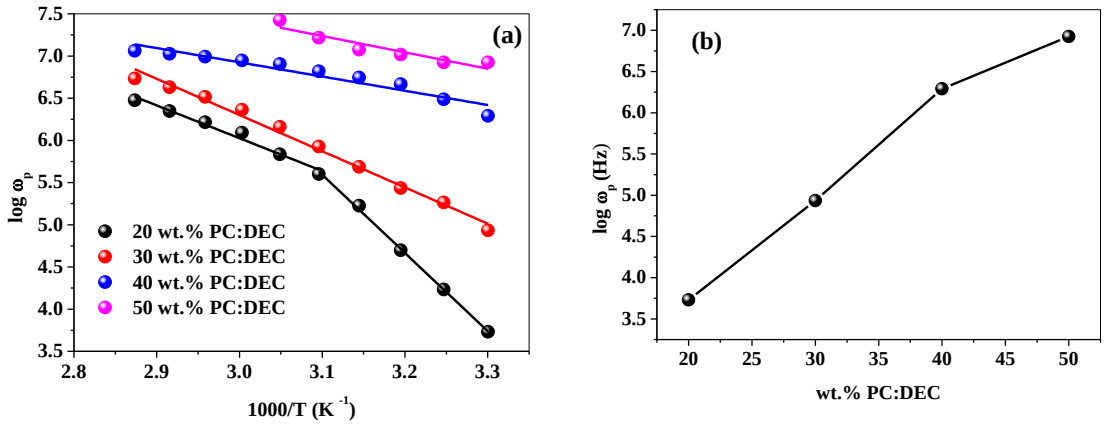

Figure 5.23 (a) log ω_p versus 1000/T for different concentrations of PC: DEC in the GPE system (b) Variation of hopping frequency as a function of PC: DEC concentration at 303 K - Series(b).

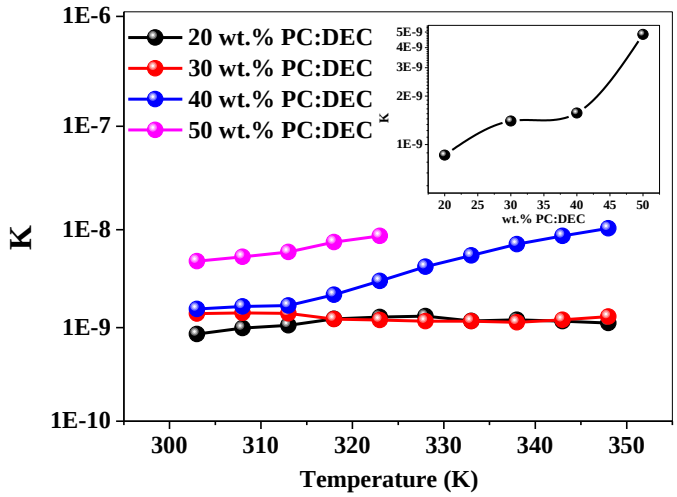

Figure 5.24 Variation of mobile ion factor **K** as a function of the temperature of GPE with different PC: DEC content. (inset: Variation of K with PC: DEC content at 303K) – Series (b)

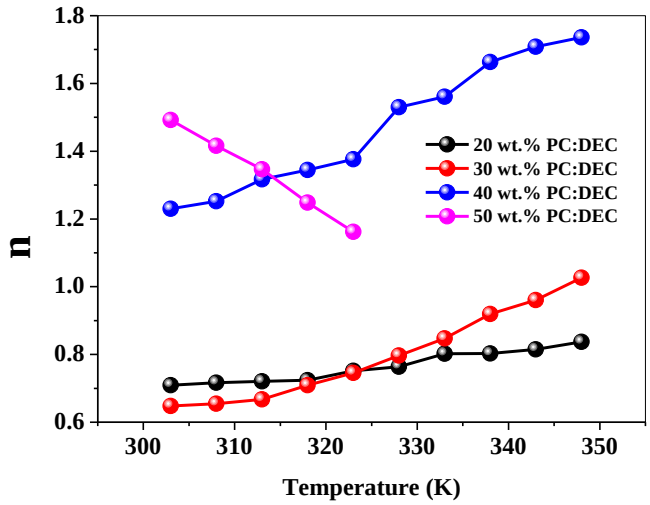

Figure 5.25 Frequency exponent as a function of temperature for all GPE system with different PC: DEC concentrations – Series (b)

Series(c): Figure 5.26 represents the ac conductivity plot for the NCGPE system with Al_2O_3 nanofiller at different temperatures from 303 K to 308 K which shows similar behavior as discussed earlier. The AC conductivity increases due to the rapid ion migration with the increasing frequency of applied AC voltage. Also, with an increase in temperature, it increases. However, the high-frequency dispersion region corresponds to bulk phenomena has not been observed at higher temperatures for all NCGPE systems. This might be due to an increase in conductivity for which the frequency falls outside the measured frequency range. Another interesting feature is visible that the crossover frequency (a region where plateau to frequency dispersion region occurs) is shifting towards the higher frequency side with an increase in temperatures. Figure 5.27 shows the AC conductivity for NCGPE with different concentrations of Al_2O_3 nano-filler. The σ' shows all three distinct regions at room temperature as discussed earlier. AC conductivity increases with the incorporation of Al_2O_3 amount up to 2 wt.% thereafter it decreases and again at 4 wt.% increases. The data were fitted to Jonscher's power law shown by solid lines in Figure 5.27. The fitted and calculated parameters are given in Table 5.2.

The variation of the logarithmic value of hopping frequency versus 1000/T plot is shown in Figure 5.28(a). The increase in the hopping frequency with temperature shows the thermally activated process. The linear behavior of the plot is fitted with the Arrhenius relation (Eq. 5.14) and activation energy for the hopping of ion is calculated which are tabulated in Table 5.2. It has been observed from Figure 5.28(b), the rise in the hopping frequency(ω_p) with the incorporation of Al_2O_3 nano-filler amount from 0.5 wt.% to 2 wt.% may be due to increased amorphous nature which is in good agreement with our XRD result of the series (c). At 3 wt.% Al_2O_3, the fall in ω_p is detected might be due to cluster formation of Al_2O_3 nanofiller or aggregation of free ions.

The variation of mobile carrier concentration factor K as a function of temperature for all NCGPE systems and as a function of Al_2O_3 variation at 303 K (inset) is represented in Figure 5.29. A slight increment in carrier concentration with changing temperature is seen whereas the inset shows that the ion concentration factor K is in accordance with conductivity data with Al_2O_3 at 303 K. The variation of power-law exponent (n) as a function of temperature for the NCGPE system is plotted in Figure 5.30. The values are observed between 1.23 to 1.86. The increasing value of n with temperatures suggests that the small polaron tunneling model is applicable for the present system.

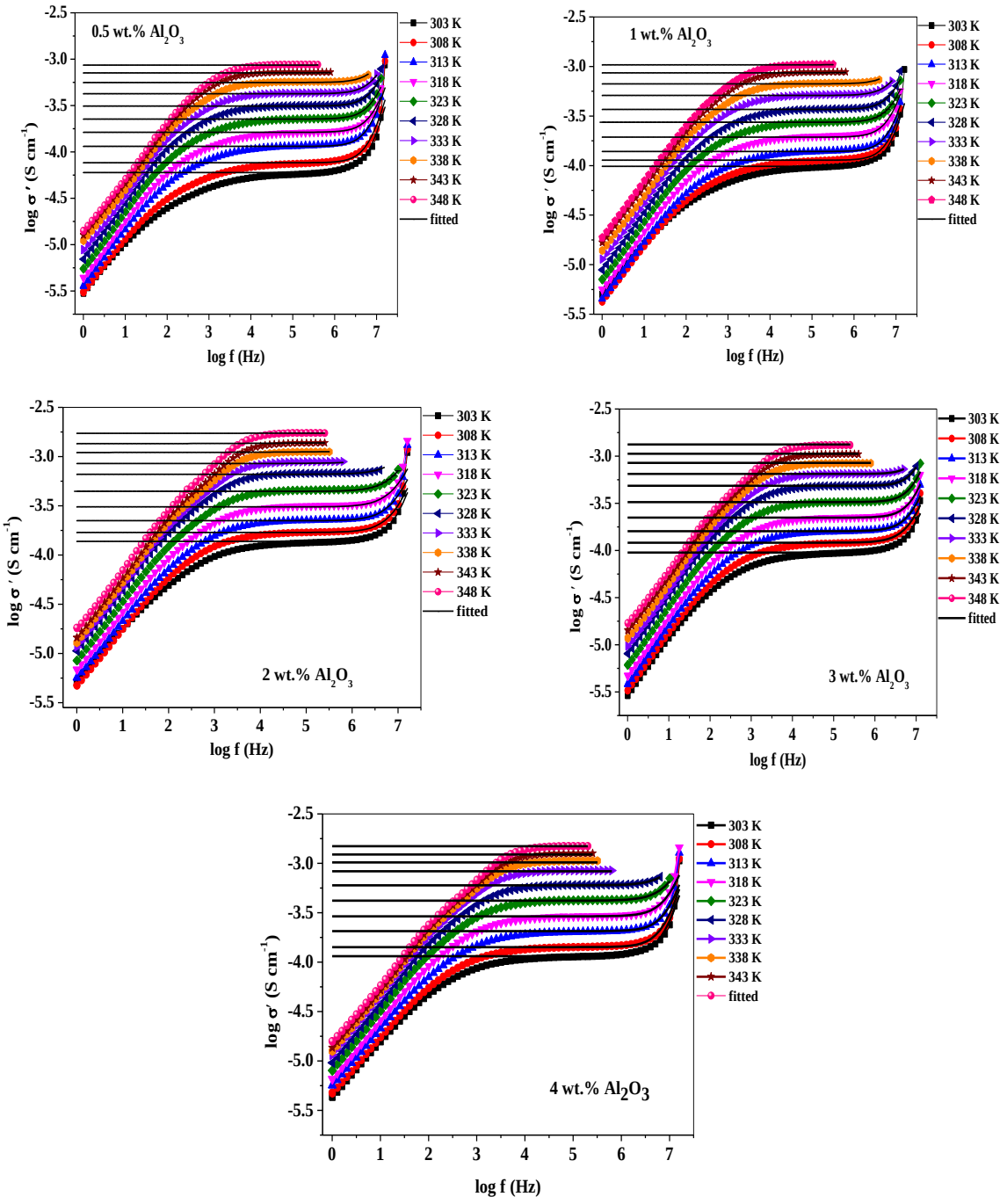

Figure 5.26 Variation of AC conductivity as a function of frequency (log σ′ versus log f) for different concentrations of Al_2O_3 in the GPE system at different temperatures – Series (c).

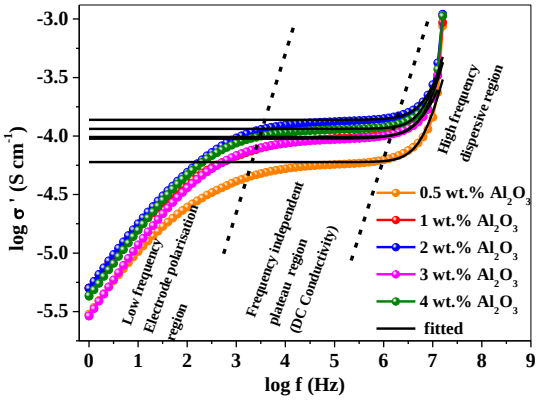

Figure 5.27 Variation of AC conductivity as a function of frequency (log σ′ versus log f) of GPE system with different concentrations of Al_2O_3 at 303 K – Series (c).

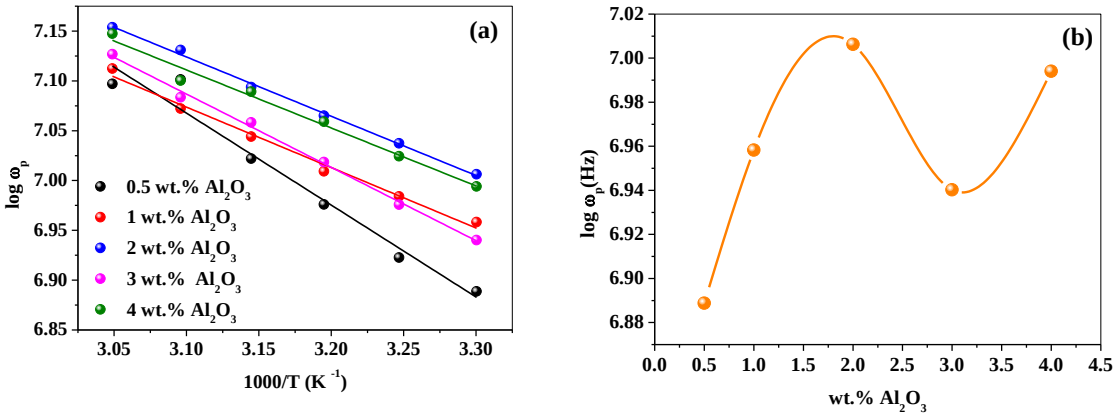

Figure 5.28 (a) log ω_p versus 1000/T for different concentrations of Al_2O_3 nanofiller in the GPE system. (b) Variation of hopping frequency as a function of Al_2O_3 nanofiller at 303 K – Series (c).

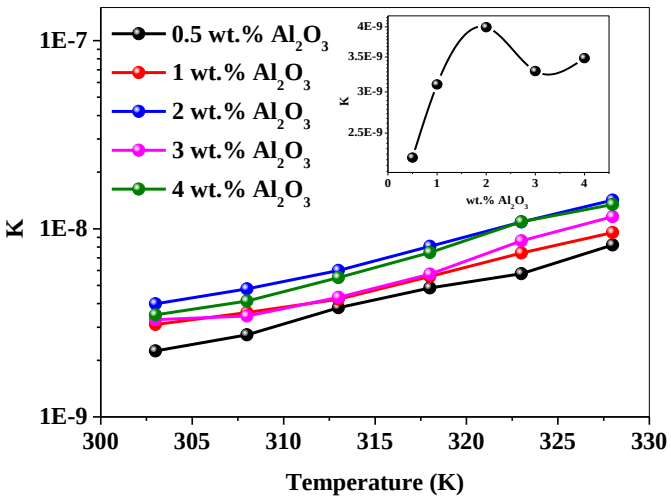

Figure 5.29 Variation of mobile ion factor *K* as a function of the temperature of NCGPE with different Al_2O_3 content (inset: Variation of *K* with Al_2O_3 content at 303 K – Series (c).

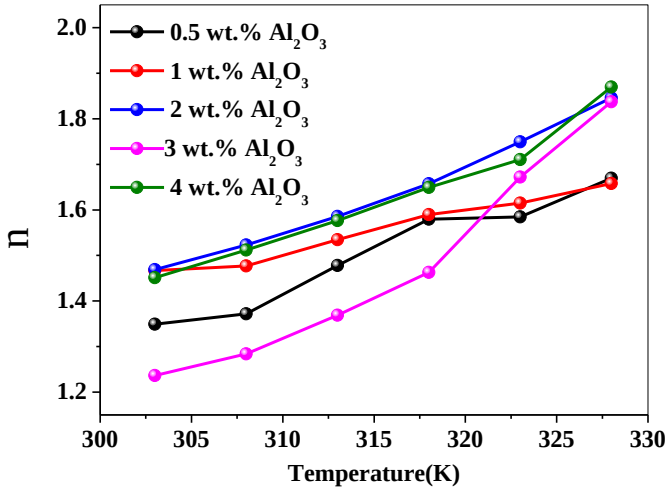

Figure 5.30 Frequency exponent as a function of temperature for all NCGPE system with different Al_2O_3 concentration – Series (c).

Scaling of AC Conductivity

To gain an insight into the temperature and composition dependence of the ion dynamics, the scaling behavior of the conductivity spectra has been studied. The scaling (time-temperature superposition principle/thermorheological simplicity) is a tool that helps us to examine whether the conduction mechanism involving ion dynamics is temperature-dependent or not. Various scaling laws have been proposed for scaling the AC conductivity data by Summerfield [67], Roling [68], Sidebottom [69], and Ghosh [70].

We have used Ghosh scaling, according to that the scaling of AC conductivity follows the following relation [70]

$$\frac{\sigma'}{\sigma_{dc}} = F\left(\frac{f}{f_p}\right) \tag{5.15}$$

where F is the scaling function which is independent of temperature.

Series(a): Figure 5.31 shows the scaled ac conductivity spectra by using Ghosh scaling relation at different temperatures for the GPE containing 2 wt.%, 4 wt.%, and 5 wt.% $LiClO_4$.

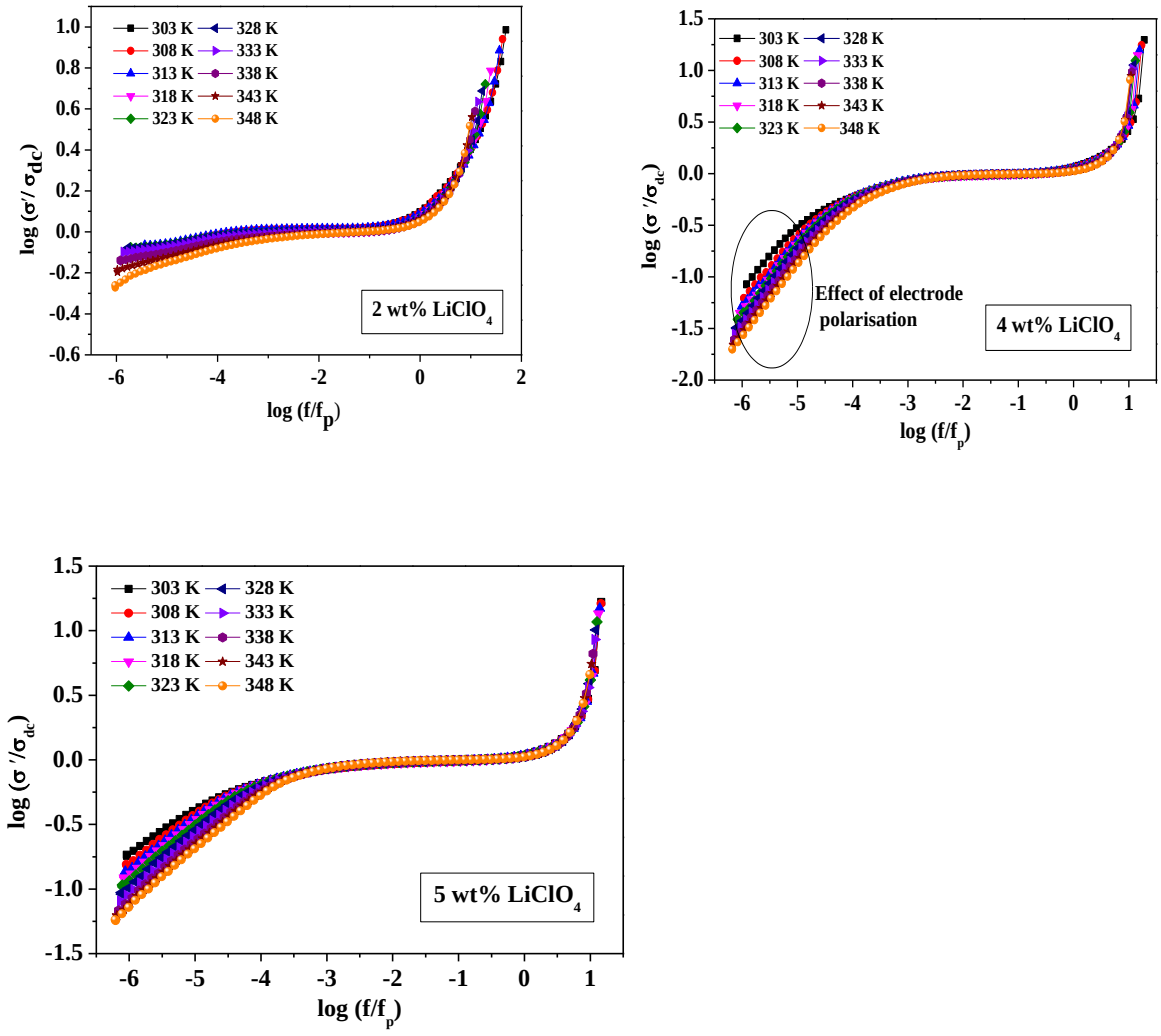

Figure 5.31 Scaled conductivity spectra for different concentrations of $LiClO_4$ in the GPE system at different temperatures (using Eq. 5.15) – Series (a).

It is observed that the scaled spectra merges on a common master curve. The nearly perfect overlapped scaled data suggests that the present GPE system follows the time-temperature superposition principle. Pal et al. observed this behavior for the lithium salt-based plasticized polymer electrolyte system [71]. However, the scaling for the GPE system with 7.5 wt.% and 10 wt.% $LiClO_4$ could not be achieved due to the unavailability of hopping frequency at higher temperatures as the high-frequency dispersion region is not observed in these samples. In such a situation, another scaling known as Summerfield scaling is adopted [70]. Summerfield scaling method for ac conductivity scaling which can be given as

$$\frac{\sigma'}{\sigma_{dc}} = F\left(\frac{f}{\sigma_{dc}T}\cdot x\right) \tag{5.16}$$

where σ' is ac conductivity, σ_{dc} is dc conductivity at a particular temperature, T is absolute temperature, f is the frequency and, x is concentration factor. Assuming the constant value of charge carrier concentration with temperature for the sake of simplicity, rewriting the above equation as [68]

$$\frac{\sigma'}{\sigma_{dc}} = F\left(\frac{f}{\sigma_{dc}T}\right) \tag{5.17}$$

The main advantage of the above-mentioned scaling law is direct utilization of available quantities which is present in Eq. 5.17. Scaling of the GPE sample containing different wt.% $LiClO_4$ at different temperatures is shown in Figure 5.32, from which we note that the scaled spectra at different temperatures for all gel polymer electrolytes almost merge on a common master curve except at higher frequencies dispersion region where it deviates slightly at all temperatures. Interestingly, the GPE with 7.5 wt.% shows the perfect overlapping in the entire frequency range which indicates that Li^+ ion experiences same environment to relax following same ion dynamics in the entire temperature range indicating the existence of the time-temperature superposition (TTS) principle. Thus, we can conclude that the relaxation dynamics of charge carriers in the electrolyte follow a common mechanism throughout the entire temperature range which indicates the temperature-independent nature of the ion conduction mechanism.

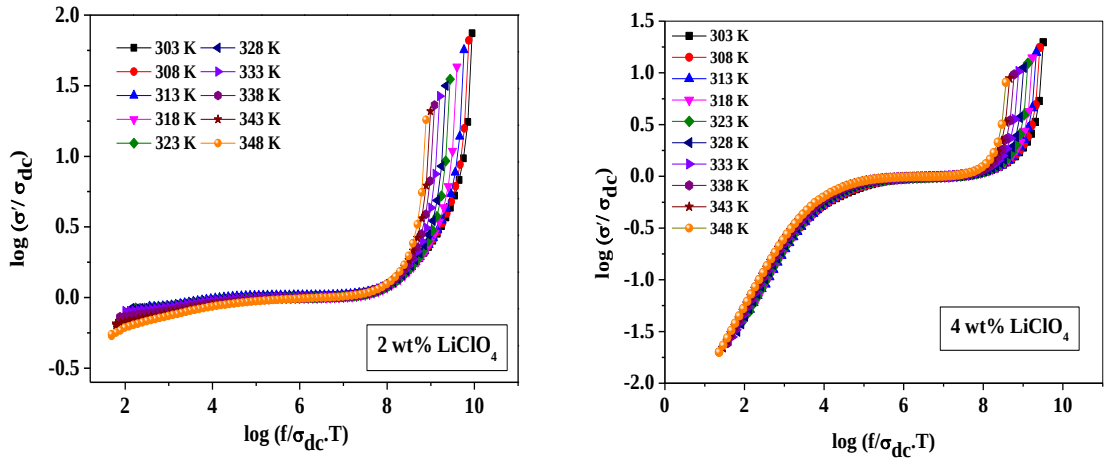

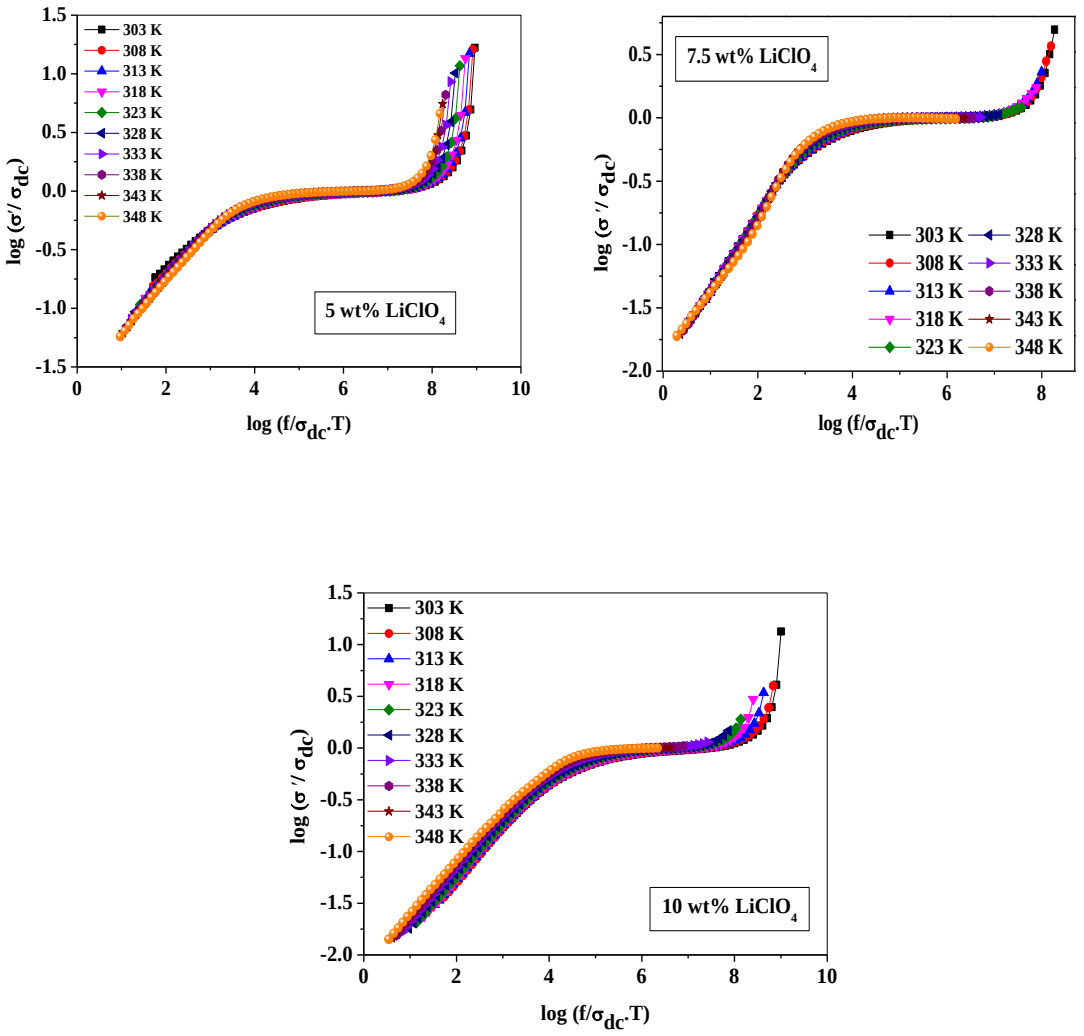

Figure 5.32 Scaled conductivity spectra for different concentrations of $LiClO_4$ in the GPE system at different temperatures (Using Eq. 5.17) – Series (a).

Scaling of σ′ of GPE with different concentrations of $LiClO_4$ at 303 K is shown in Figure 5.33**.** This scaling aims to show whether there is any effect of variation in $LiClO_4$ salt concentration on charge carrier as well as structural change. The spectra clearly show that the scaling does not result in any single master curve. As the scaling does not follow the 'Time-concentration superposition principle', one can conclude that structure of the GPE system considerably changes with variation of $LiClO_4$ salt concentration, stating the relaxation mechanism of the present GPE system composition dependent. Das et al. [72] also reported a similar behavior in PEO-PVDF-HFP-$LiClO_4$ blend polymer electrolytes where relaxation dynamics of charge carriers do not follow the common mechanism at different salt concentrations.

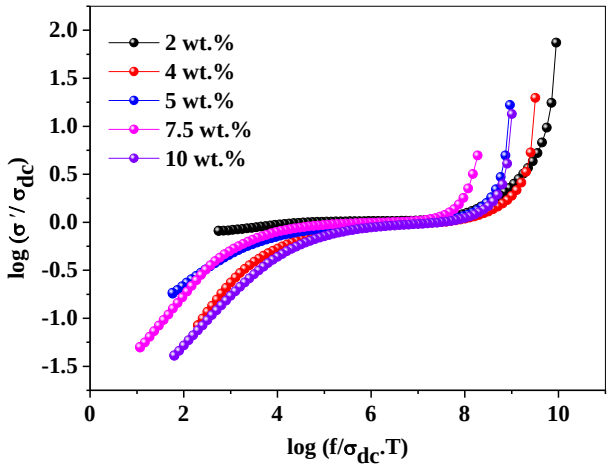

Figure 5.33 AC conductivity scaling spectrum of GPE containing different concentrations of $LiClO_4$ at 303 K (Using Eq. 5.17) – Series (a).

Series (b): The scaled spectra of GPE with 20, 30, and 40 wt.% PC:DEC at different temperatures are shown in Figure 5.34. All conductivity data at different temperatures merge into a single master curve. However, such scaling could not be achieved for the GPE system containing 50 and 60 wt.% PC:DEC because of the values of f_p are not known. This indicates the system obeys the time-temperature superposition principle. This type of scaling has also been attempted by Ghosh et al. in lithium-ion conducting glass systems [70].

According to Patro et al., crossover frequency corresponding to each temperature is activated by the thermal energy of $\sigma_{dc}T$, hence $f_p = \sigma_{dc}T$ can be chosen as a scaling parameter and one major advantage of it to utilize direct available quantities rather than calculating hopping frequency [38]. Hence, another approach for scaling known as Summerfield scaling is adopted for which directly available data can be utilized to scale the data. The scaled spectra with different concentrations of PC: DEC plasticizer at different temperatures are shown in Figure 5.35. It can be seen that AC conductivity spectra at different temperatures have successfully collapsed to a common master curve indicating the time-temperature superposition principle. This means the ion dynamics of the system do not change with an increase in temperature. The scaling has been achieved for all the systems except 60 wt.% PC:DEC in the low-frequency region where accumulation of charges at the electrode-electrolyte surface or the presence of inhomogeneity is observed. Now the scaled spectra for GPE having a different amount of PC: DEC at 303 K is shown in Figure 5.36.

All data also show perfect merging except slight deviation in polarization region due to the different carrier concentration with the variation of PC: DEC amount.

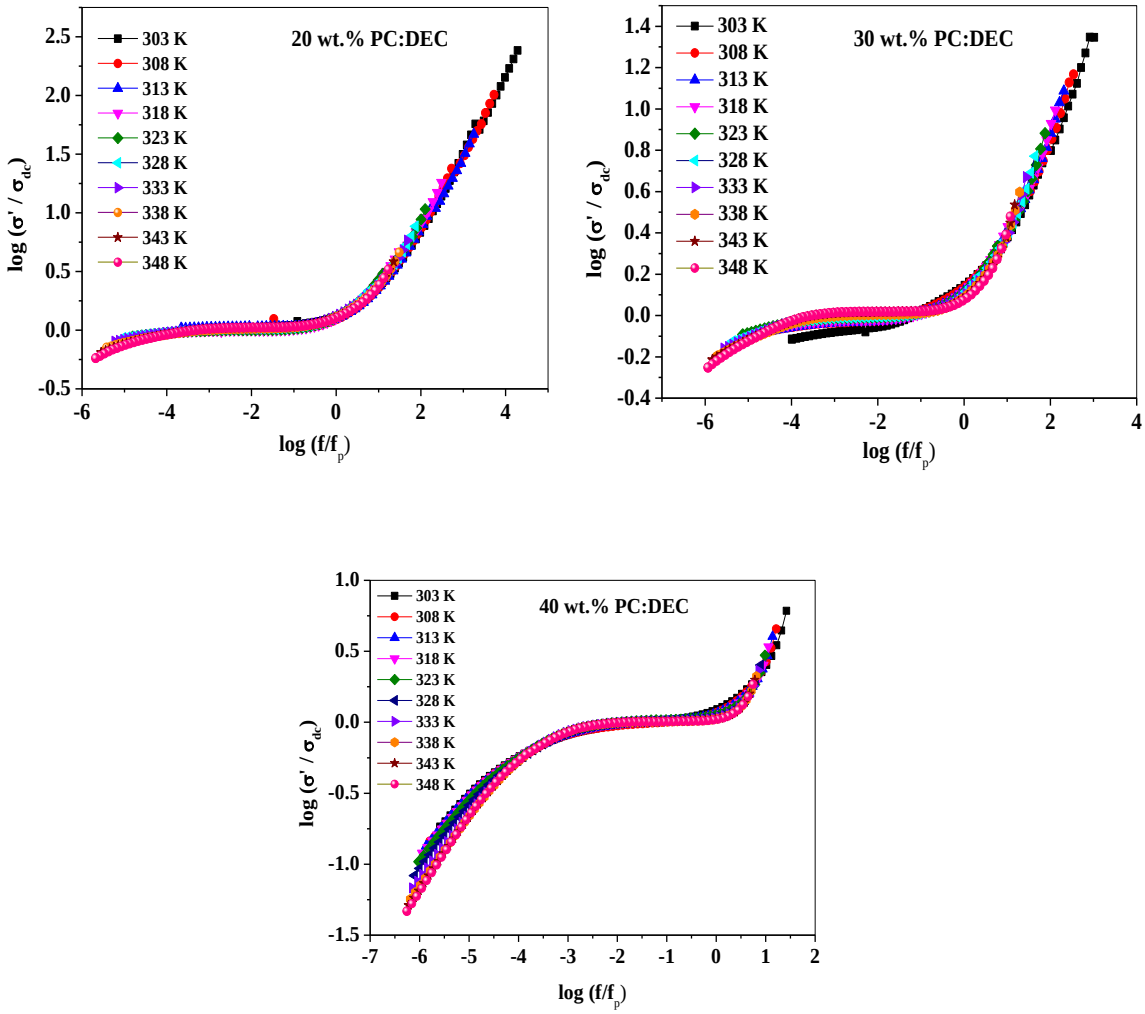

Figure 5.34 Scaled conductivity spectra for different concentrations of PC: DEC in the GPE system at different temperatures (using Eq . (5.15) – Series (b).

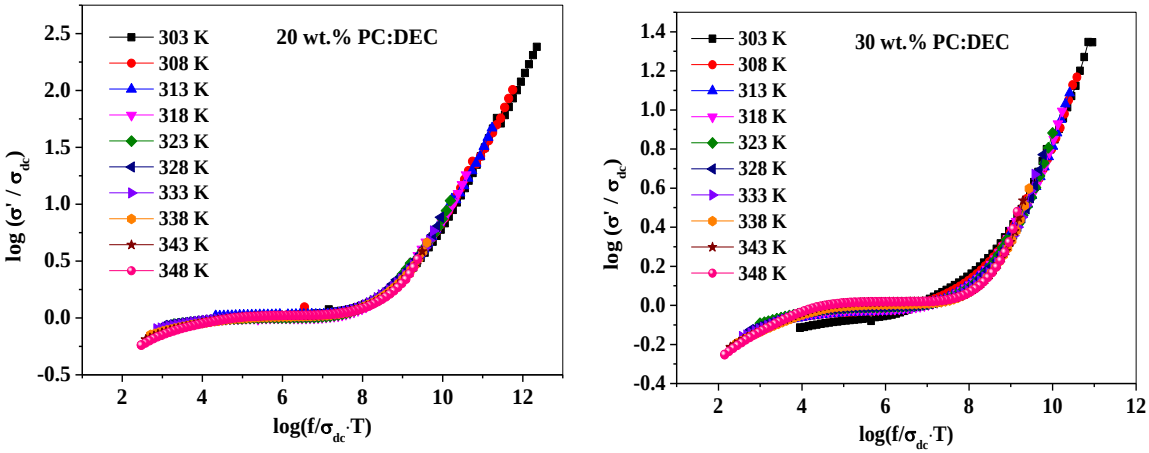

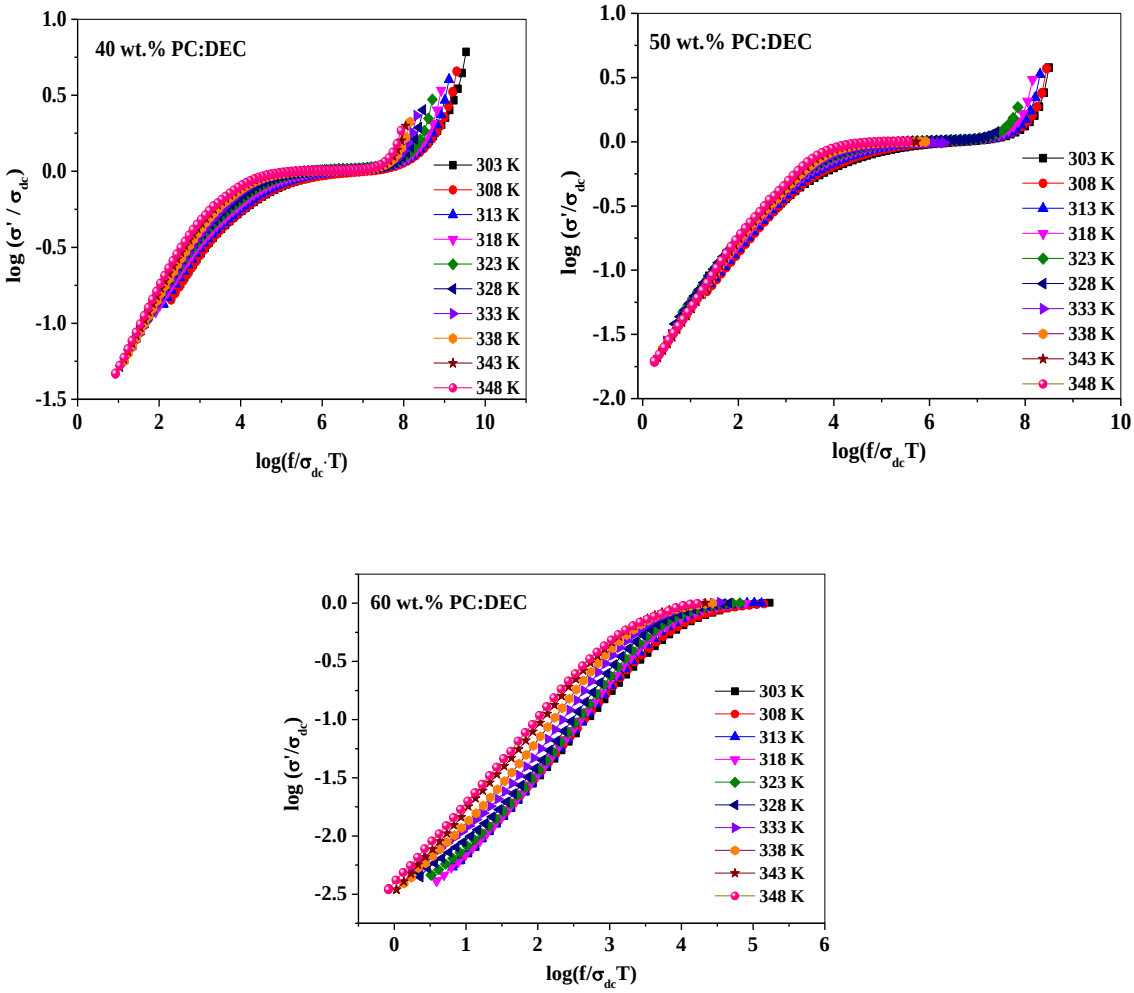

Figure 5.35 Scaled conductivity spectra for different concentrations of PC: DEC in the GPE system at different temperatures (Using Eq. 5.17) – Series (b).

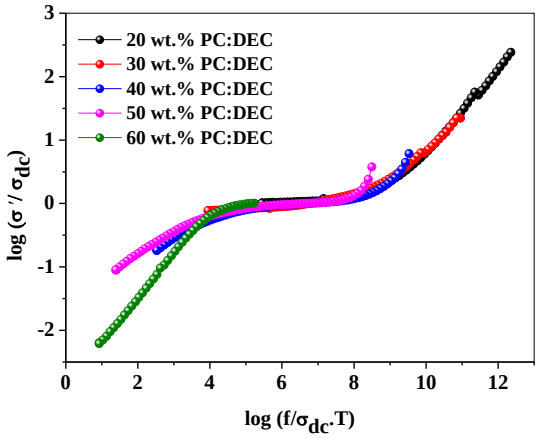

Figure 5.36 AC conductivity scaling spectrum of GPE containing different concentration PC: DEC at 303 K (Using Eq. 5.17) – Series (b).

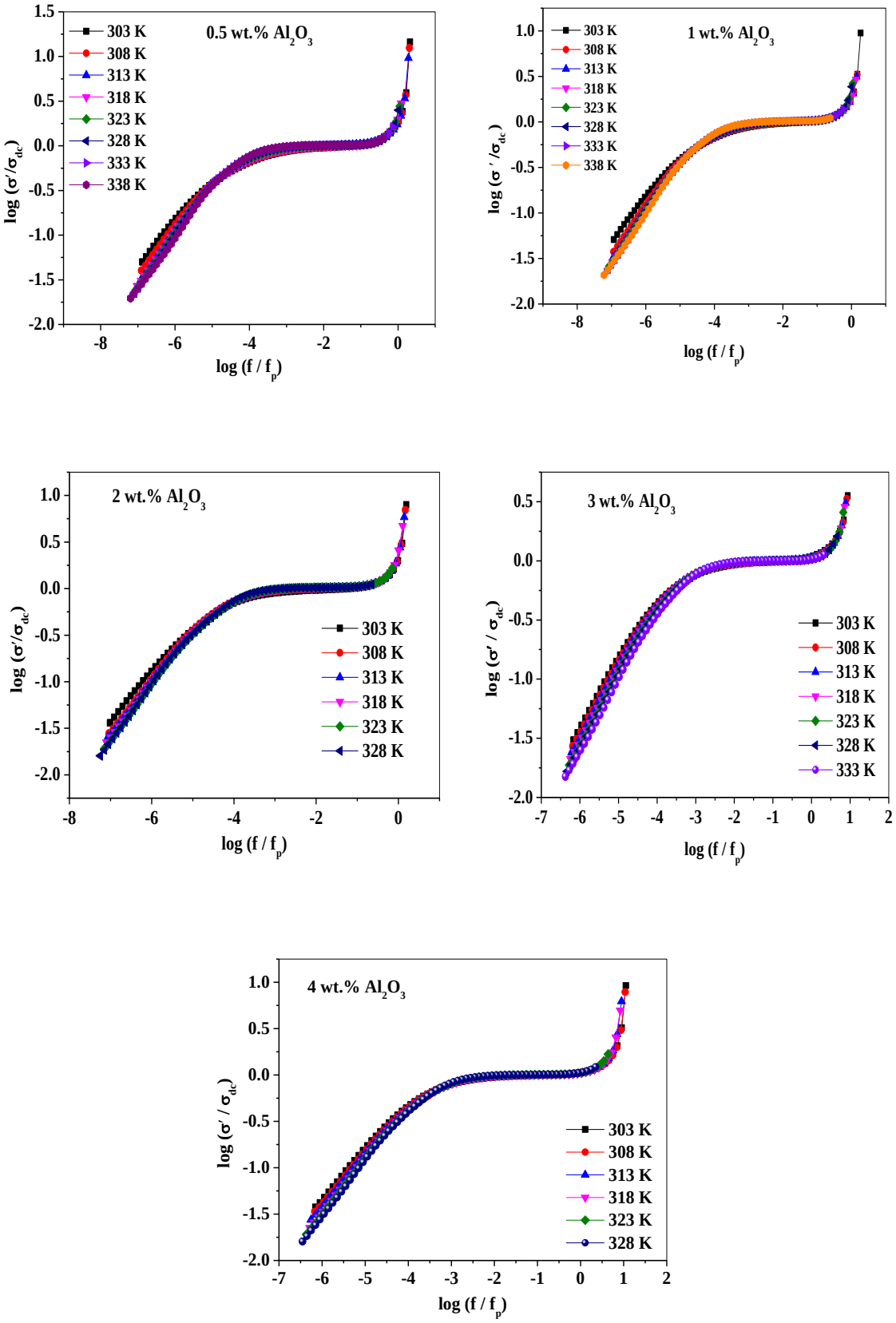

Figure 5.37 Scaled conductivity spectra for different concentrations of Al_2O_3 in the GPE system at different temperatures (using Eq. 5.15) – Series (c).

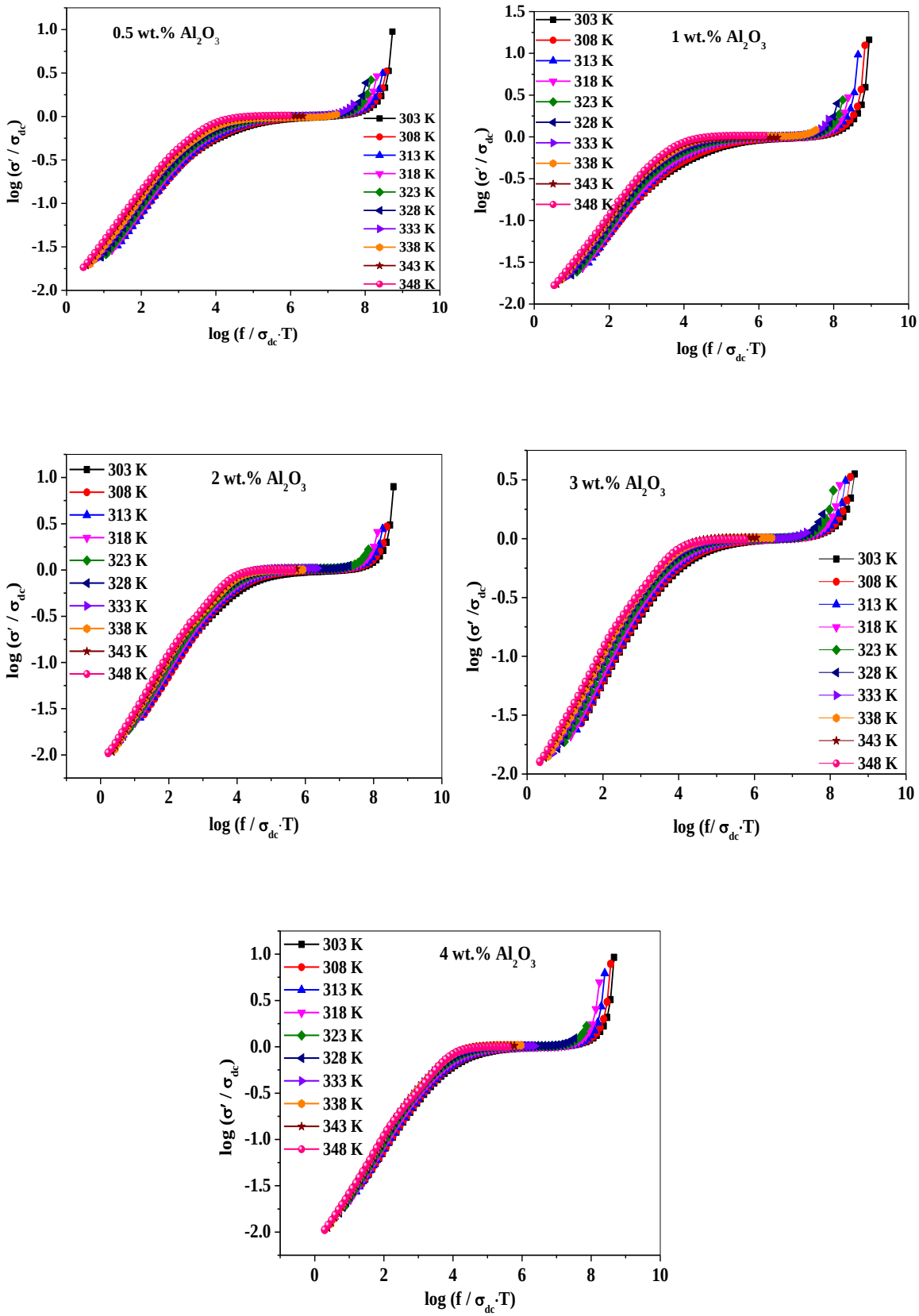

Figure 5.38 Scaled conductivity spectra for different concentrations of Al_2O_3 in the GPE system at different temperatures (Using Eq. 5.17) – Series (c).

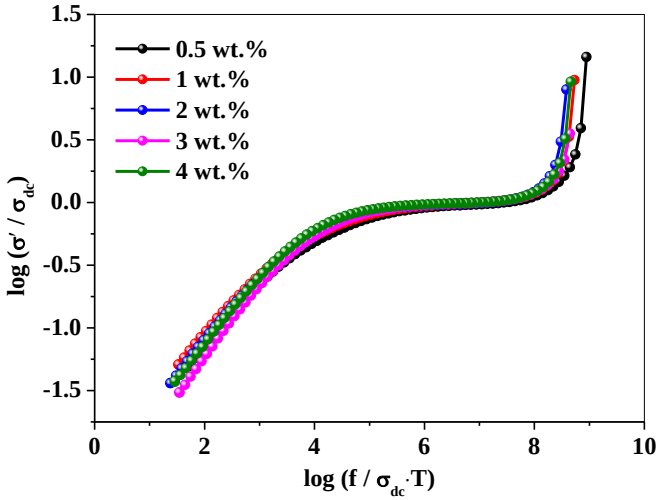

Figure 5.39 AC conductivity scaling spectrum of GPE containing different concentrations of Al_2O_3 at 303 K (Using Eq. 5.17) – Series (c).

Series (c): Figure 5.37 represents scaled ac conductivity spectra according to Ghosh scaling of all NCGPE samples in the temperature range 303- 348K. Spectra in Figure 5.37 shows overlapped or perfectly merged onto the master curve except at the low-frequency dispersion region for all compositions. The perfect merging of all data onto the master curve is an indication of obeying the time-temperature superposition principle. The present nanocomposites follow the common nature of the relaxation dynamics of charge carriers at all temperatures. Chaurasia et al. in their PEO-$LiPF_6$-$BMIMPF_6$ system also reported the similar nature [73]. However, due to the absence of a high-frequency region and hence unavailability of the Jonscher's fitting parameters for the as conductivity spectra at higher temperature > 338 K, scaling is not achieved for that data. To overcome this problem, the Summerfield relation (Eq. 5.17) is adopted for the scaling and shown in Figure 5.38. It shows less perfection in terms of overlapping as compared to the Ghosh Scaling method [74].

The scaled data for the NCGPE system at 303 K using Summerfield relation is shown in Figure 5.39. It nearly follows the perfect Time-concentration superposition principle which leads us to conclude that there might be no change in the carrier concentration and structure of the NCGPE system with a variation of Al_2O_3 nano-particles.

5.5 Dielectric Analysis

The dielectric response of polymer electrolyte is commenced from the application of the AC field due to which dipoles are able to orient themselves in the direction of the applied field. This builds up the polarization at the electrode-electrolyte interface due to the different dipoles present in the polymer backbone. The built-up polarization depends on the ability of dipole in the polymer chain as well as the temperature of the system. Temperature alters the arrangement of the polymer chain and hence polarization. To get insight into dielectric properties, it is well explained in terms of energy storage and energy dissipation in the gel polymer electrolyte. In the present study, the dielectric analysis is used to investigate dipolar relaxation in the dipolar materials. Arya et al. [26] have investigated the influence of $NaPF_6$ salt concentration on the dielectric properties of PEO-PVP-based solid polymer electrolyte and found an increase in the dielectric constant of the salt added polymer matrix and lowering the relaxation time compared to the salt-free system. In the present study dielectric analysis has been carried out to observe the effect of composition and temperature variation for the GPE systems.

The dielectric study has been analyzed in terms of dielectric constant (ε′) and dielectric loss (ε′′). The complex dielectric formalism can be written as

$$\varepsilon^* = \varepsilon' + j\varepsilon'' = \frac{Z''}{\omega C_0 (Z'^2 + Z''^2)} + j\frac{Z'}{\omega C_0 (Z'^2 + Z''^2)} \tag{5.18}$$

where ε' and ε'' are real part (dielectric constant) and imaginary part (dielectric loss) of the complex dielectric. Z' and Z'' are real and imaginary parts of the complex impedance plot, respectively. C_0 is the vacuum capacitance [1].

Series (a): The dielectric constant as a function of frequency at different temperatures from 303 K to 348 K are shown in Figure 5.40. All plots show a decrease in the dielectric constant with increasing frequency. At lower frequency region, the high value of dielectric constant (ε′) is ascribed to the dominance of space charge polarization (electrode polarization) which is caused by blocking of mobile ions at the interface of the electrode-electrolyte due to blocking metallic electrode where ions are not permitted to transfer into external circuit [75]. As a result, Li^+ ions get piled up near electrodes which leads to the building of space charge polarization. At lower frequencies, the ions generally show a slow periodic reversal, while

at a higher frequency region, diffusion, as well as dipole orientation in the direction of the applied field, is not feasible due to the high frequency of the applied field [76]. Hence, the dielectric constant decreases and show an almost constant value [26].

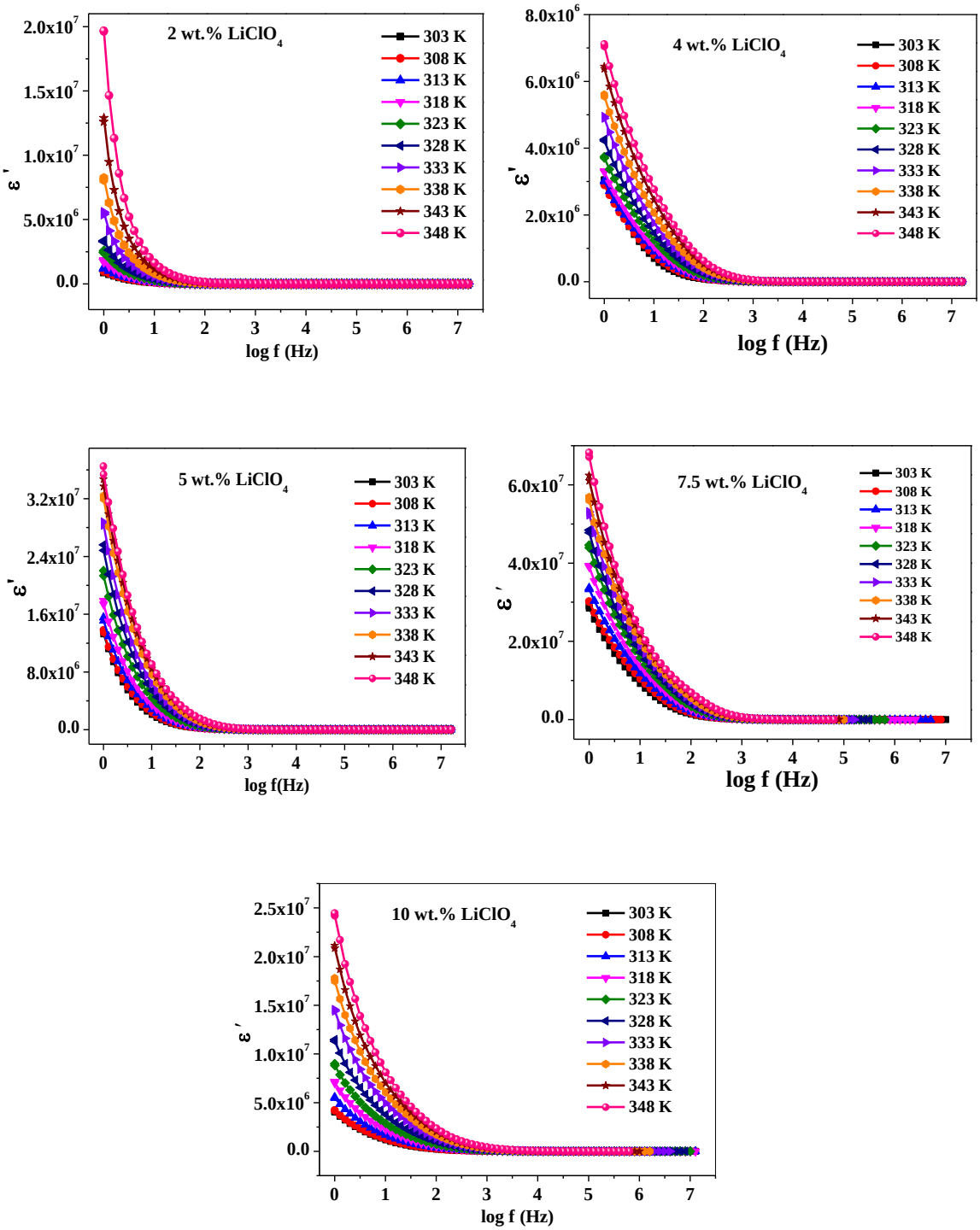

Figure 5.40 Dielectric constant (ε′) as a function of frequency for different concentrations of $LiClO_4$ in the GPE system at different temperatures – Series (a).

The temperature-dependent dielectric constant (ε′) at 10^1 Hz, 10^2 Hz, 10^3 Hz, and 10^4 Hz frequencies for the GPE with 4 wt.% and 7.5 wt.% is shown in Figure 5.41. From the figure, it can be seen that the dielectric constant ***ε′*** also increases with an increase in the temperature because of greater freedom of movement of the dipole molecular chain. As temperature increases, the free volume increases, and a decrease in viscosity of GPE. Bhargav et al.[77] reported that for non-polar, ε′ is independent of temperature whereas in the case of polar polymer ε′ increases with increasing temperature and for their study on PVA-NAI system, he found to increase in ε′ as an increment in temperature due to dipole facilitation.

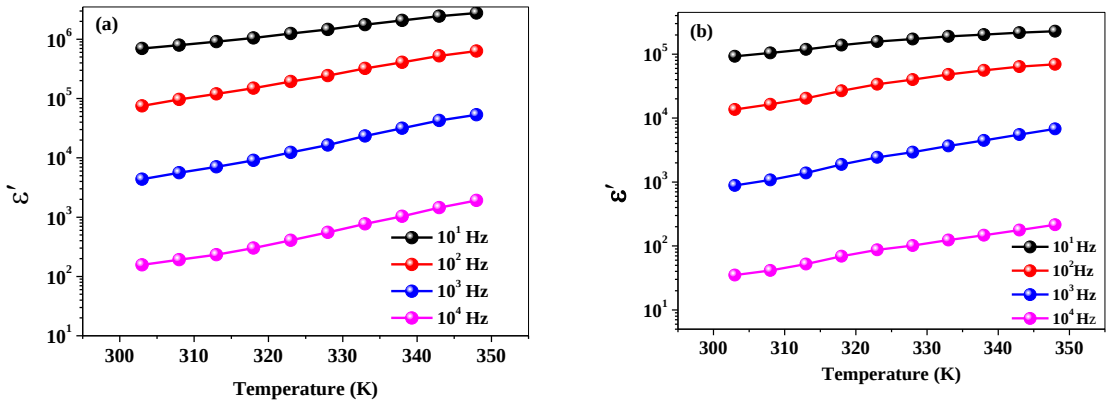

Figure 5.41 Temperature dependent dielectric constant (ε′) at different frequencies for GPE containing (a) 4 wt.% $LiClO_4$ (b) 7.5 wt.% $LiClO_4$ – Series (a).

Figure 5.42 (a) shows the dependence of dielectric constant with frequency for different concentrations of salt. The increase in dielectric constant with increasing the amount of salt up to 7.5 wt.% may be due to an increase in density of charge carriers as a result of salt dissociation in the polymer matrix [78]. At 10 wt.% $LiClO_4$ content, due to coulomb interaction between Li^+ cations and ClO_4^- anions form ion pairs. Hence, the dielectric constant decreases at 10 wt.% of $LiClO_4$. At a lower frequency i.e. 10 Hz, the dielectric constant is found to be maximum as shown in Figure 5.42(b). With the incorporation of $LiClO_4$ salt content, an increase in dielectric constant from 9.9×10^4 for 2 wt.% to 9.1×10^6 for 7.5 wt.% is observed which is due to increase in charge carrier density but its value drops beyond 7.5 wt.% $LiClO_4$ concentration.

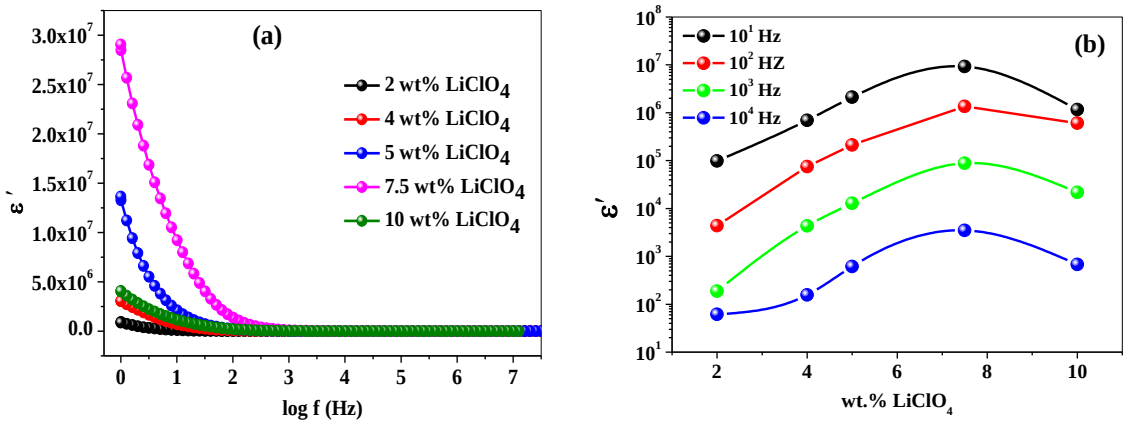

Figure 5.42 (a) Dielectric constant (ε′) versus log f for different concentrations of $LiClO_4$ salt in the GPE system at 303 K. (b) Variation of ε′ as a function of $LiClO_4$ concentrations at different frequencies at 303 K – Series (a).

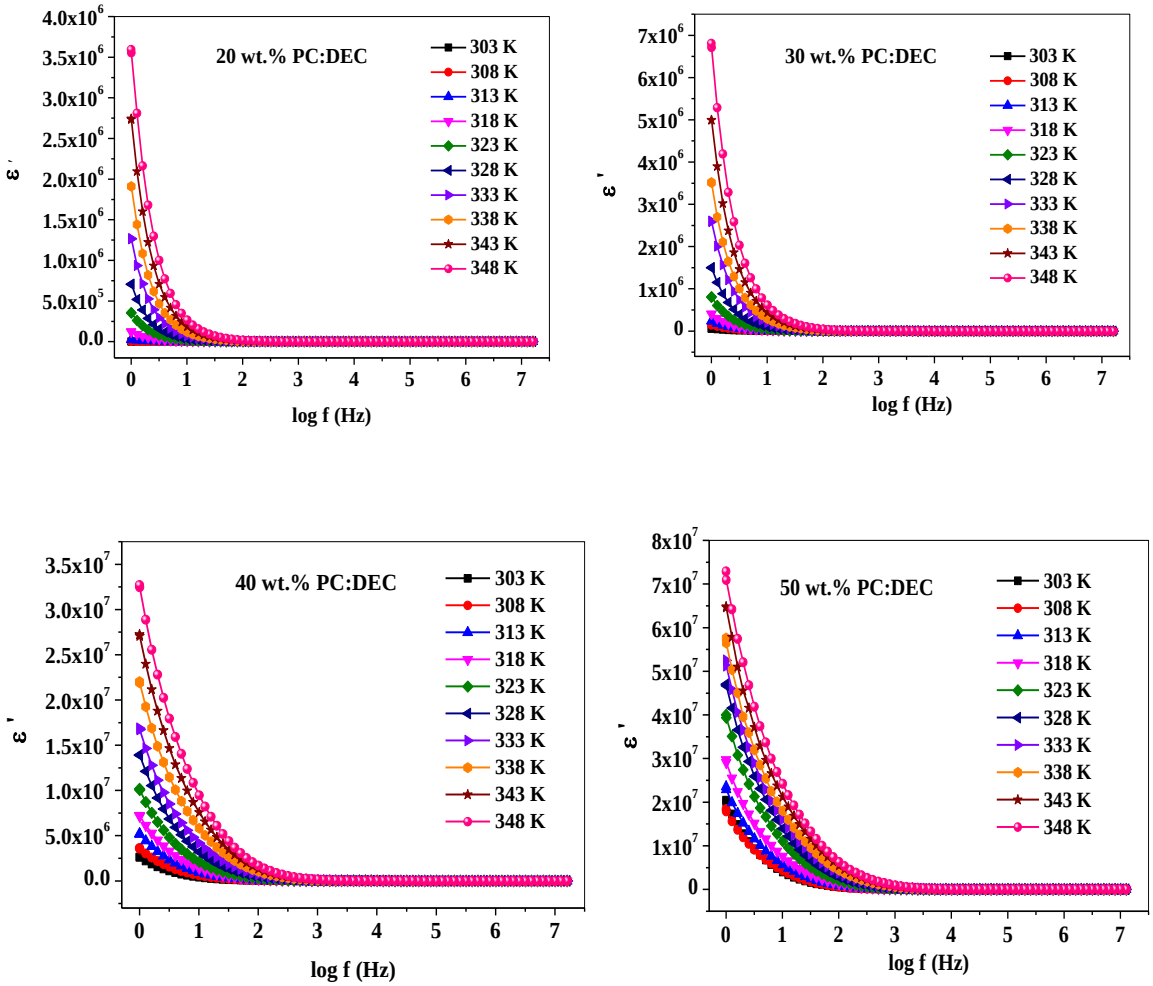

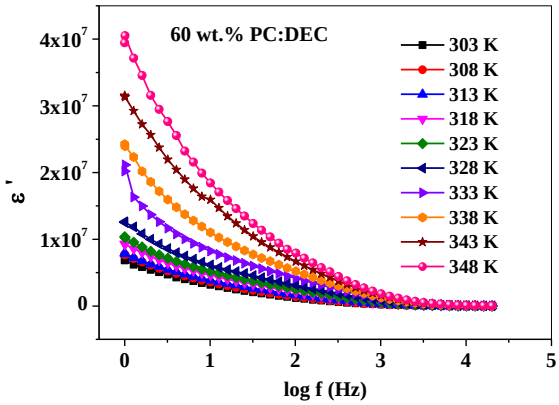

Figure 5.43 Dielectric constant (ε′) as a function of frequency for different concentrations of PC: DEC in the GPE system at different temperatures – Series (b).

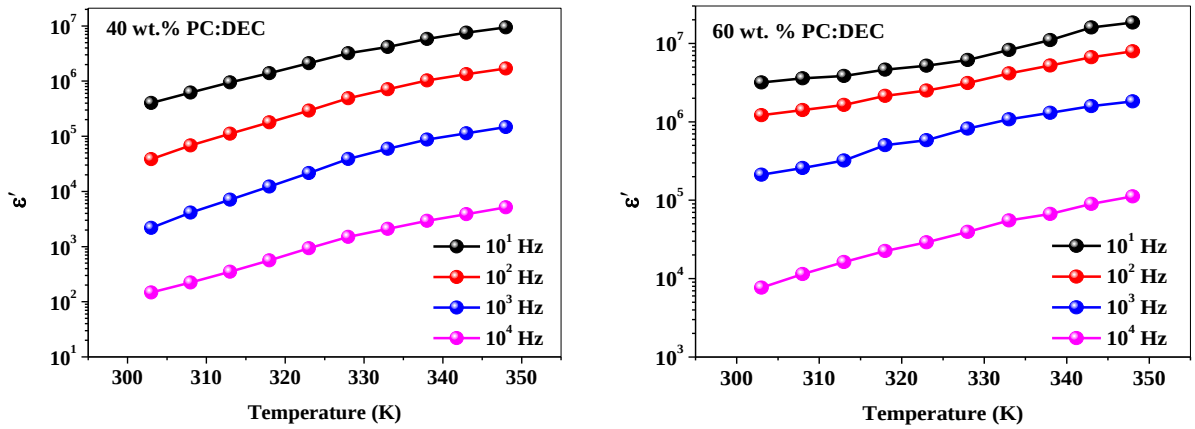

Figure 5.44 Temperature dependent dielectric constant (ε′) at different frequencies for GPE containing (a) 40 wt.% PC:DEC (b) 60 wt.% PC:DEC – Series (b).

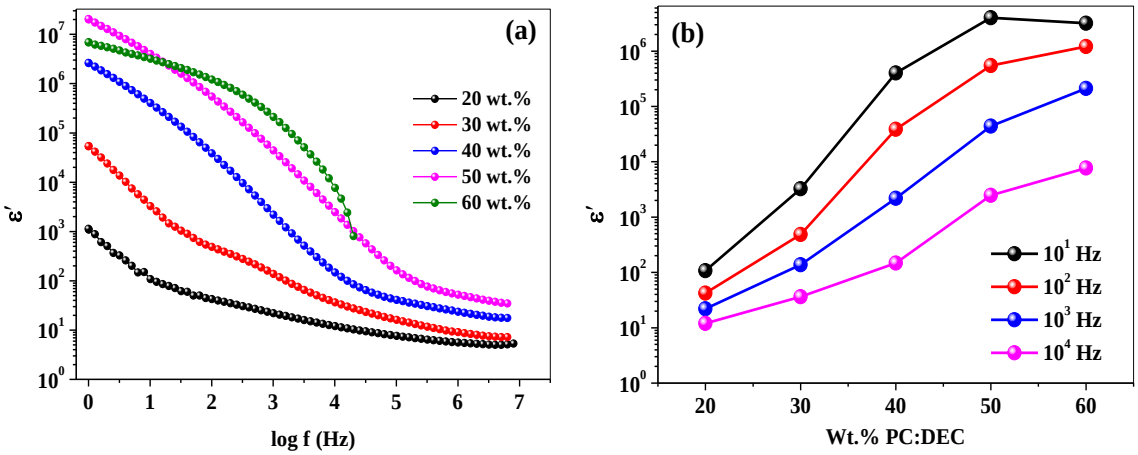

Figure 5.45 (a) Dielectric constant (ε′) versus log f for different concentrations of PC:DEC in the GPE system at 303 K. (b) Variation in ε′ as a function of PC: DEC concentration at different frequencies at 303 K – Series (b).

Series (b): The dielectric constant (ε′) versus log f for different amount of PC: DEC in polymer electrolyte at different temperatures is depicted in Figure 5.43. In the low-

frequency region, the value of the dielectric constant is high due to the ability of orientation of dipoles with the frequency of the applied field while the dielectric constant decreases with increasing frequency. The dielectric constant (ε′) also increases as temperature varies from 303 K to 348 K as shown in Figure 5.44. According to free volume theory, at higher temperature, an increase in amorphous nature with free volume causes dipoles to orient easily through this phase. Apart from this, the rise in temperature can cause a decrease in viscosity of GPE which in turn facilitates the movement or jiggling of dipoles through the polymer matrix. Thakur et al.[79] reported that the rise in temperature enhances the Brownian or molecular motion of the polymer chain resulting in increase of dielectric constant of PMMA based system.

The variation of the dielectric constant with different amount of PC:DEC plasticizers at 303K is shown in Figure 5.45(a). Fast periodic reversal effect of applied AC field at higher frequency does not allow dipoles to orient, hence ε′ decreases but at low frequency, space charge polarization leads to an increase in dielectric constant. It can be seen from Figure 5.45(b), the value of the dielectric constant increases with increasing the concentrations of PC:DEC plasticizers. When low molecular weight PC:DEC plasticizers are added to the polymer, free charge carrier density increases as a result of ion dissociation [80]. At 10 Hz, the value of dielectric constant is 42.39 for 20 wt.% whereas, 3.18×10^{6} for 60 wt.% PC:DEC is observed.

Series (C): To understand the effect of Al_2O_3 nano-filler on dielectric properties, the dielectric constant is analyzed. The dielectric constant (ε′) as a function of frequency is plotted in Figure 5.46 for all nanocomposite gel polymer electrolyte system at different temperatures from 303 K to 348 K. The value of ε′ is high at low frequency due to the contribution of polarization at the electrode-electrolyte surface. The dominance of electrode polarization is mainly due to the accumulation of charges at the blocking electrode. Localized dipoles are able to reorient themselves in the direction of the applied AC field at low frequency whereas it unbales to follow the direction of the field at a higher frequency. Hence dielectric constant decreases as frequency increases. However, the dielectric constant increases with increasing temperature shown in Figure 5.47. The increase in the free volume and flexibility of the polymer chains takes place with a rise in temperature. As a result of this, ε′ increases with increasing temperatures.

The dielectric constant as a function of Al_2O_3 variation at 303 K is plotted in Figure 5.48(a). Similar features are observed as discussed earlier in this section. The dielectric constant as a function of Al_2O_3 at different frequencies i.e. 10^1 Hz, 10^2 Hz, 10^3 Hz, and 10^4 Hz is shown in Figure 5.48(b). Two prominent features can be seen (i) high dielectric constant at low frequency (10^1 Hz) (ii) high value of dielectric constant at 2 wt.% Al_2O_3. As the amount of Al_2O_3 nanoparticles is increased from the 0.5 wt.% to 2 wt.%, the dielectric constant increases which might be due to increased amorphous nature which can be seen from the XRD pattern of this NGPE as discussed in Chapter 4 and it is also worthwhile to mention that the available oxygen atom at the surface of the Al_2O_3 nanoparticles which act as Lewis acid sites having a tendency to attractions which result in increased conductivity [81]. The effect of ZrO_2 nanoparticles on ionic conductivity in PEO-$NaClO_4$ polymer electrolyte system is principally due to Lewis acid-base interaction between polymer chain and nanofiller as reported by Arup Dey et al.[82]. Croce et al. also reported and demonstrated a model to show the effect of Al_2O_3 nanofiller [22]. According to him, the interactions between surface groups of nanoparticles and polymer chain segments results in a rise in ionic conductivity due to increase in the fraction of free ions and available new conduction pathway for the transportation of ion. Hema et al. reported that the incorporation of TiO_2 nano-filler in PVA: PVDF based polymer electrolyte increases the dielectric constant due to increase in the number of charge carriers[83].

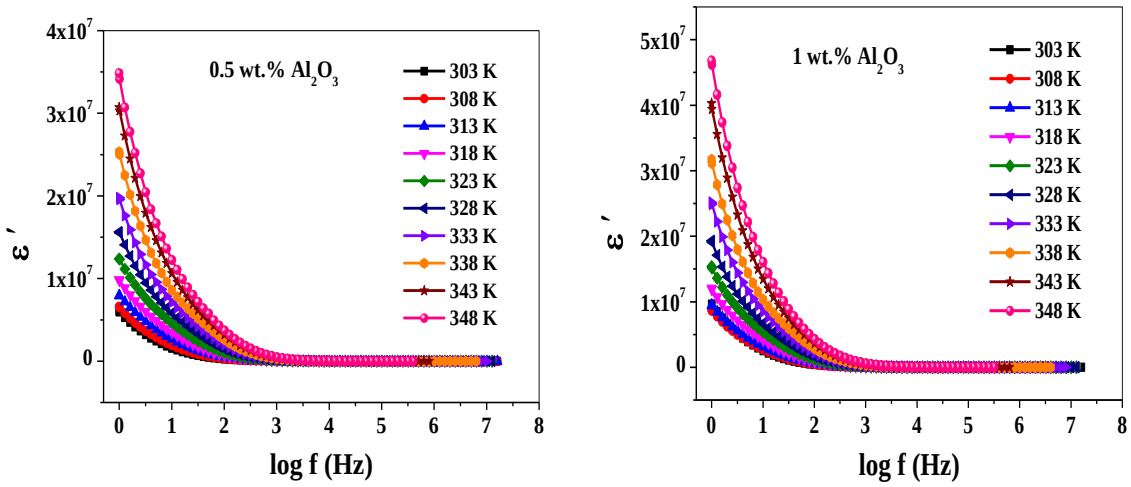

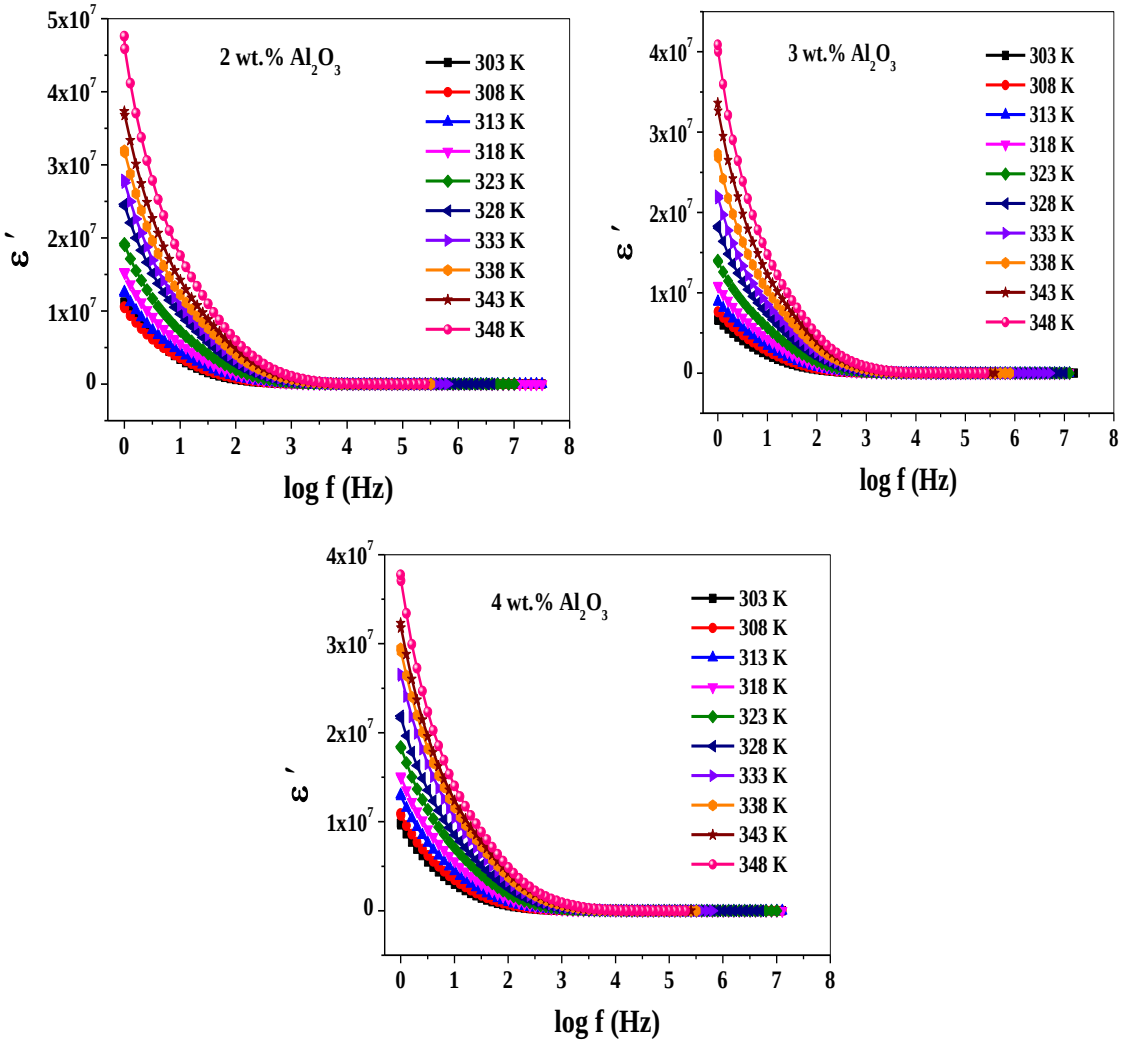

Figure 5.46 Dielectric constant (ε′) as a function of frequency for different concentrations of Al_2O_3 in the GPE system at different temperatures – Series (c).

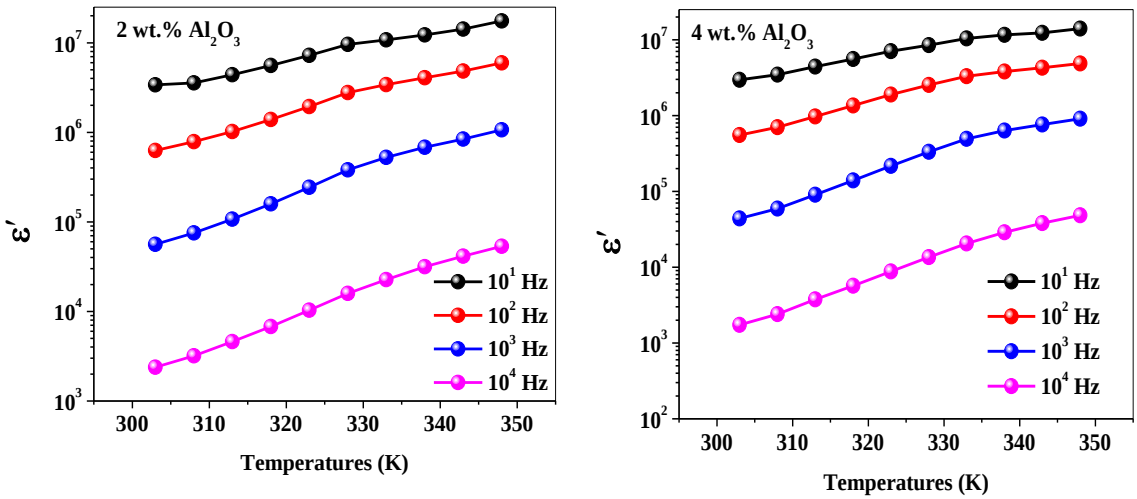

Figure 5.47 Temperature dependent dielectric constant (ε′) at different frequencies for NCGPE containing (a) 2 wt.% Al_2O_3 (b) 4 wt.% Al_2O_3 – Series (c).

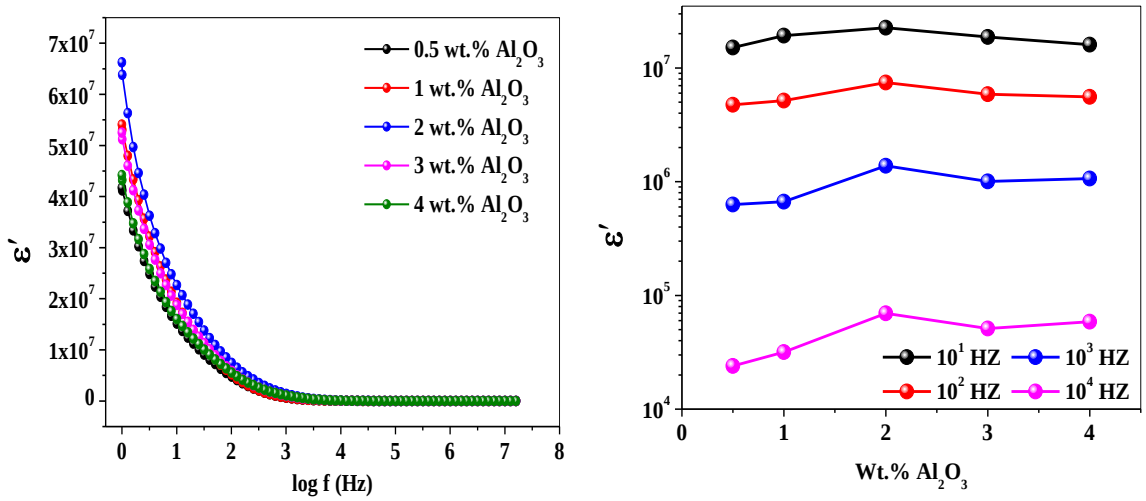

Figure 5.48 (a) Dielectric constant (ε′) versus log f for different concentrations of Al_2O_3 nano-filler in the GPE system at 303 K (b) Variations in ε′ as a function of Al_2O_3 concentration at different frequencies at 303 K – Series (c).

Tangent Loss (Tan δ)

The electrode polarization in dielectric loss is at a lower frequency is so prominent so that another relaxation process is masked. Hence further analysis of dielectric behavior has been done using tangent loss formalism (tan δ). Tangent loss is the ratio of energy dissipation to energy storage also called the dissipation factor. Mathematically, it can be expressed as

$$\tan\delta = \frac{\varepsilon''}{\varepsilon'} \tag{5.19}$$

where ε″ and ε′ is dielectric loss and dielectric constant respectively.

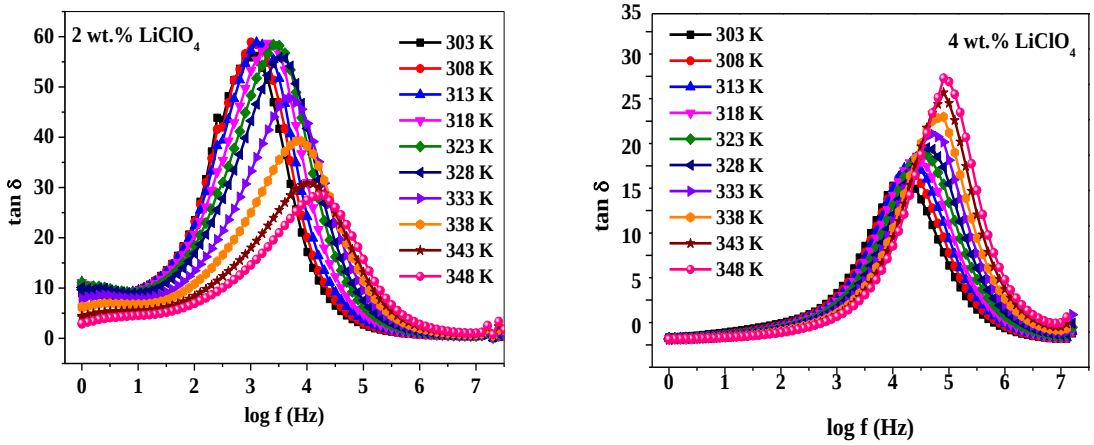

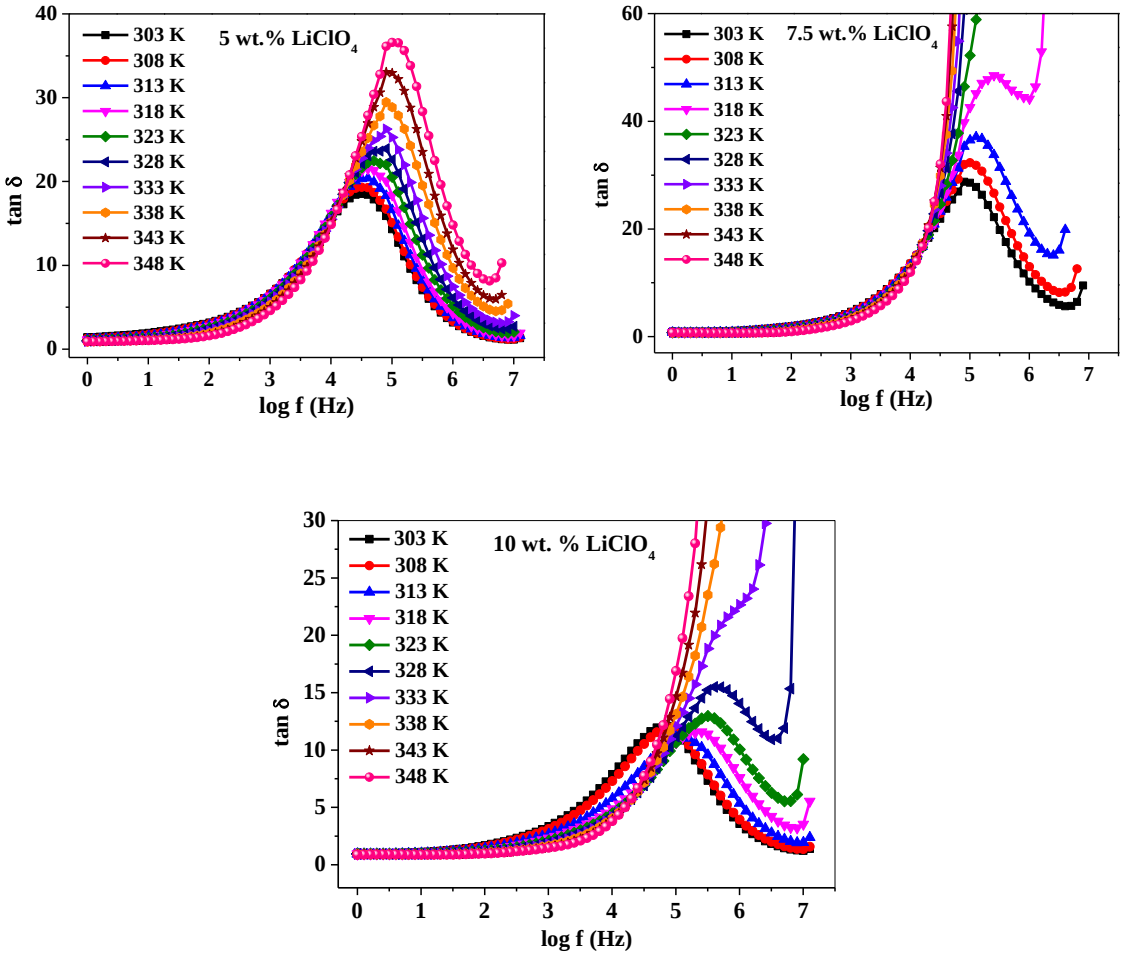

Figure 5.49 Variation of loss tangent (tanδ) versus log f for different concentrations of $LiClO_4$ salt in the GPE system at different temperatures – Series (a).

Series (a): Variation of loss tangent for the GPE system contains different wt.% $LiClO_4$ at different temperatures 303 K to 348 K is shown in Figure 5.49. From the plot of tangent loss, it is clear that tan δ value is lower at very low and very high frequency. This is due to polarization or accumulation of charges near the electrode-electrolyte surface at a lower frequency and the inability of the dipole in the direction of the applied field at a higher frequency. At mid-frequency region, tanδ attain maximum value in all the GPE systems with different $LiClO_4$ salt concentrations. The tangent loss shows the characteristic peak at a particular frequency is called relaxation frequency. It is also observed to a shift in frequency corresponds to maximum loss towards the higher frequency side with an increase in temperatures. The peak in tanδ and shifting with temperature suggest the occurrence of the dielectric relaxation process. Similar behavior is also reported by many researchers. This indicates the relaxation time decreases according to the relation between frequency and

relaxation time are given as $\omega\tau=1$, where $\omega=2\pi f$. The observed phenomena might be due to increasing the polymer chain segmental motion as well as an increase in the free volume of polymer matrix where ion of the dipole can easily orient and diffusion takes place.

The tangent loss of the GPE system at different concentrations of $LiClO_4$ salt at 303 K is depicted in Figure 5.50. At the mid-frequency range, the value of $tan\delta$ is maximum indicates dissipation of energy where diffusion of ions takes place. Apart from this, an increase in the amount of $LiClO_4$ to GPE from 2 wt.% to 4 wt.% causes to shift in peak towards the higher frequency side, whereas a reverse trend has been observed for the GPE system containing 10 wt.% of $LiClO_4$ salt. The reduction in the relaxation time with an increase in the amount of $LiClO_4$ salt may be due to increasing the amorphous nature. The polymer chains easily orient through the amorphous regions.

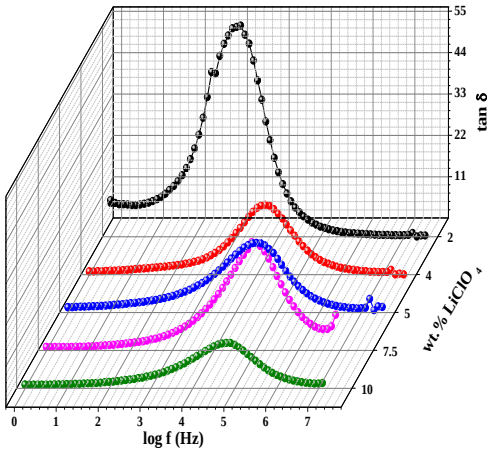

Figure 5.50 Variation of loss tangent (tanδ) versus log f for different concentrations of $LiClO_4$ salt in the GPE system at 303 K – Series (a).

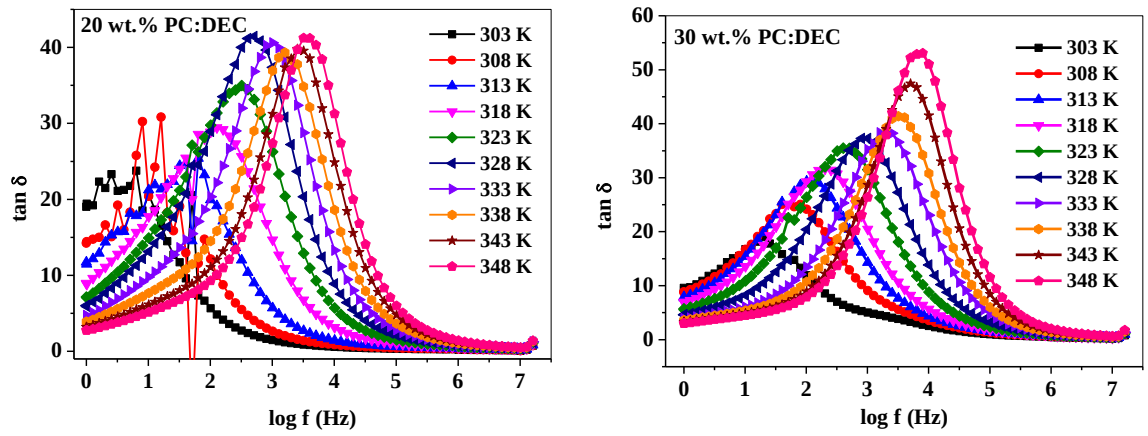

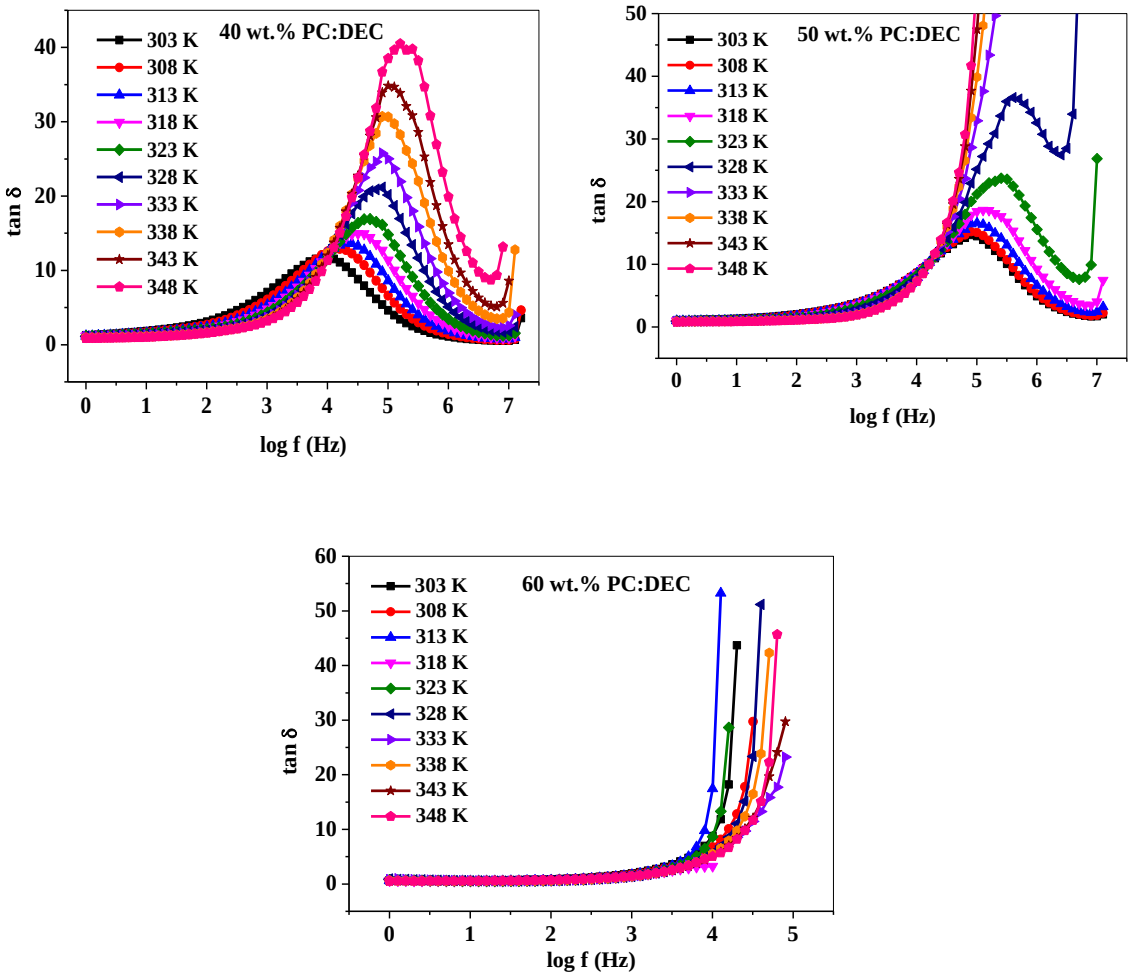

Figure 5.51 Variation of loss tangent (tanδ) versus log f for different concentrations of PC: DEC at different temperatures – Series (b).

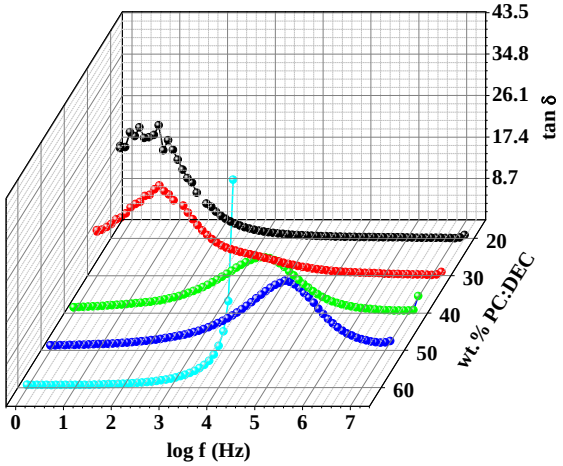

Figure 5.52 Variation of loss tangent (tanδ) versus log f for different concentrations of PC: DEC in the GPE system at 303 K – Series (b).

Series (b): Tangent loss for the GPE with a different weight percentage of PC: DEC plasticizers at different temperatures from 303 K to 348 K is shown in Figure 5.51. At very low and high frequency, the value of the tangent loss is low whereas at mid-frequency the value is high. The high values indicate the dominance of the ohmic component over the capacitive component. At low frequency, the capacitive behavior of polymer electrolytes grows whereas ohmic behavior is almost independent. The tanδ spectrum shows a well-defined characteristic peak at a particular frequency called relaxation peak. However, this peak is not observed for the sample with 50 wt.% PC: DEC at higher temperatures and 60 wt.% PC: DEC at all temperature range due to high ionic conductivity. Another feature of spectra shows of shifting of peaks towards higher frequency side with increasing temperatures which is an indication of the thermally activated relaxation process. The characteristics peak is also observed to shift towards higher frequency with the increment in the amount of PC: DEC from 20 wt.% to 60 wt.%, as shown in Figure 5.52. This behavior indicates the decrease in the relaxation time. As more amount of plasticizers are incorporated into the polymer matrix, it grows the higher number of amorphous regions and the packing of molecules becomes loose. The polymer chain becomes more flexible to orient through the amorphous region resulting in a decrease in relaxation time τ.

Series (c): The variation of tangent loss as a function of frequency for nanocomposite gel polymer electrolyte with different wt.% Al_2O_3 at different temperatures from 303 K to 348 K are shown in Figure 5.53. One can notice that the tangent loss is very low at low frequency, increases with an increase in frequency attaining maximum value (Peak), and subsequently decreases with increasing frequency. Other conclusions are: (i) the height of the peak increases (ii) the peaks shift towards the higher frequency side with a rise in temperature. The peak at a different temperature is the relaxation peak that corresponds to electrode polarization. With an increase in temperature, the peak shifts towards the higher frequency side and the relaxation time is found to be decreased as temperature increases. The relaxation process is thermally activated and similar behavior has been observed for all samples.

To investigate the ion dynamics of the present electrolyte with the incorporation of Al_2O_3 nanofiller, the tangent loss as a function of Al_2O_3 concentration at 303 K is plotted in Figure 5.54. The feature observed is as discussed above. The addition of Al_2O_3 from 0.5 wt.% to 2

wt.% the peak shift towards the higher frequency side. A shorter relaxation time has been found for the highest conducting sample.

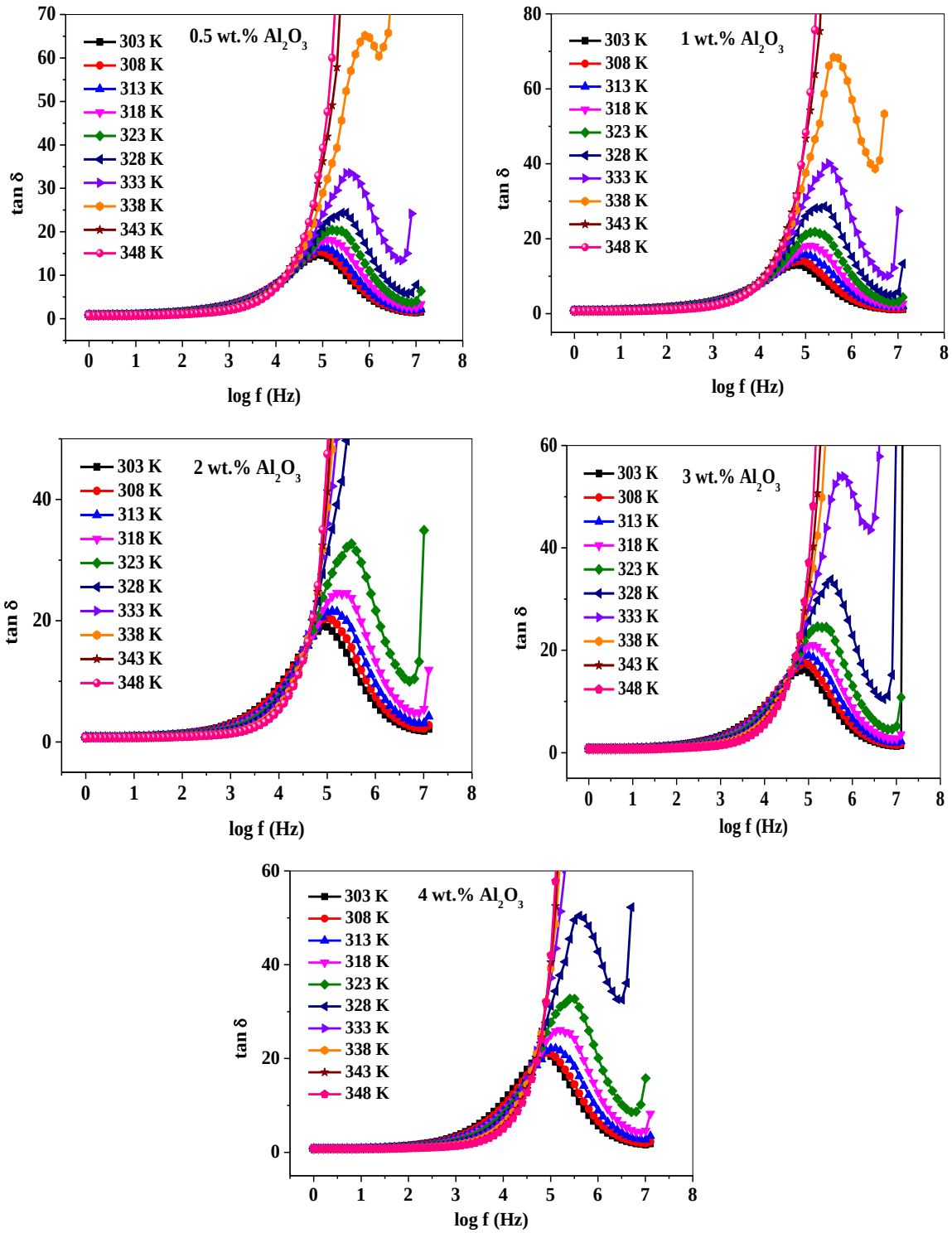

Figure 5.53 Variation of loss tangent (tan δ) versus log f for different concentrations of Al_2O_3 in the GPE system at different temperatures – Series (c).

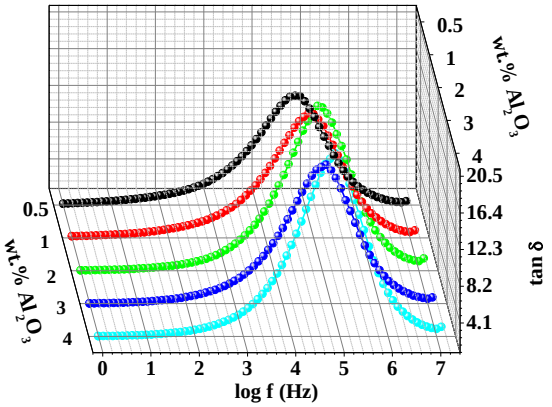

Figure 5.54 Variation of loss tangent (tanδ) versus log f for different concentrations of Al_2O_3 in the GPE system at 303 K – Series (c).

Scaling of tan δ

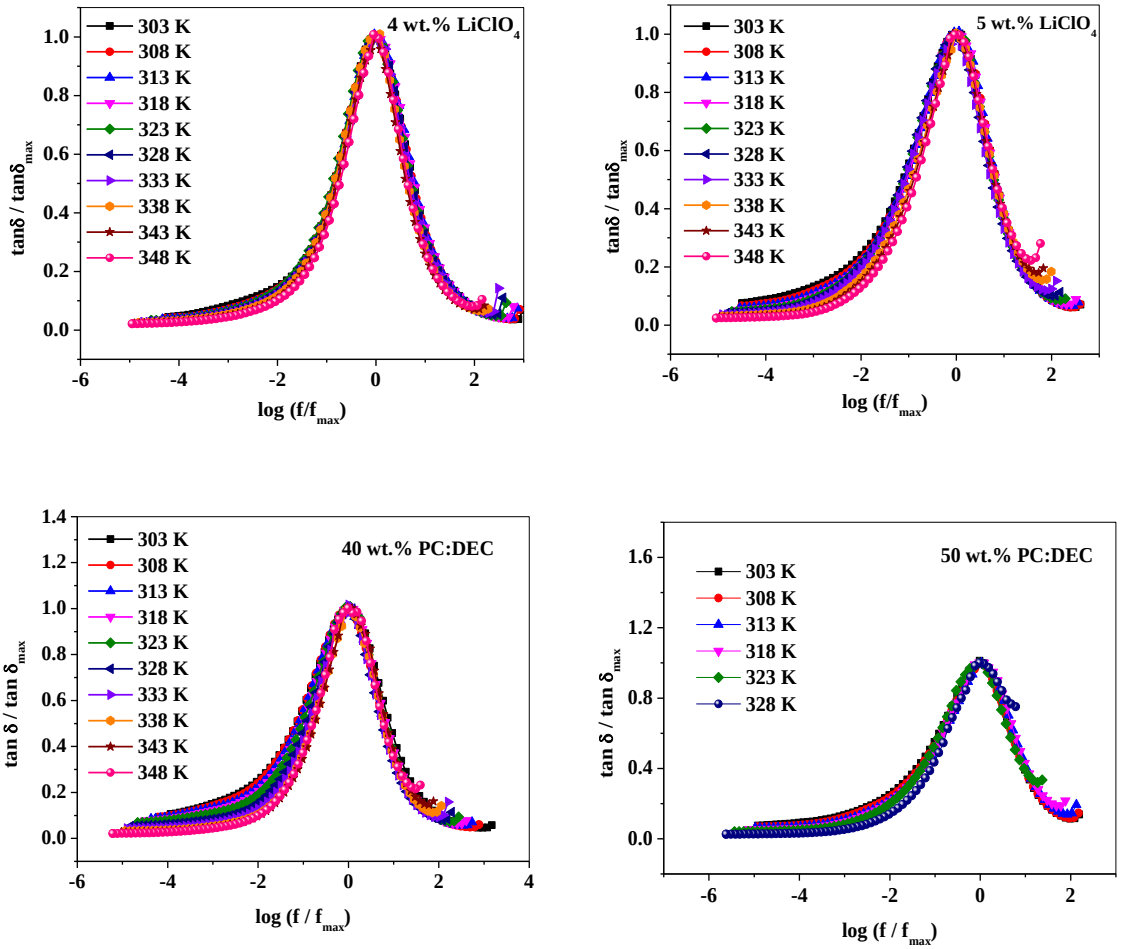

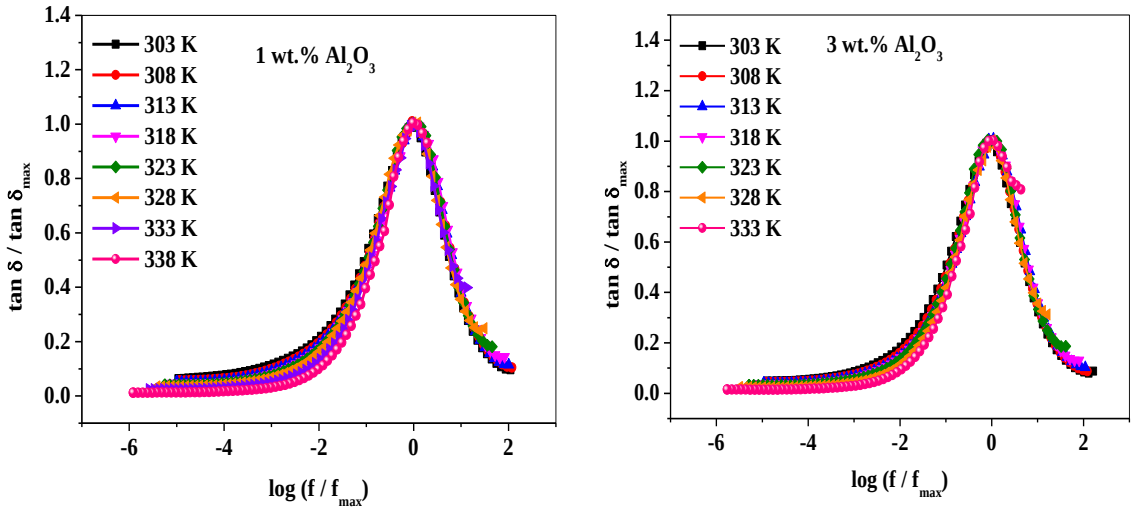

Figure 5.55 Scaled spectra of tangent loss for GPE with 4 wt.% and 5 wt.% $LiClO_4$ (Series a), 40 wt.%, and 50 wt.% PC: DEC (Series b), NCGPE with 1 wt.% and 3 wt.% Al_2O_3 (Series c)

The scaling of tan δ also provides ion dynamics behavior whether it is temperature-dependent or independent. If it is temperature independent, the scaled data tend to merge onto a master curve and one can say the ion dynamics follow the time-temperature superposition principle (TTSP). In the present study, tangent loss data is scaled where x characteristics frequency is used as a scaling parameter on the x-axis and tan δ_{max} as scaling parameter on the y-axis. The relation is given as

$$\frac{\tan\delta}{\tan\delta_{max}} = \frac{f}{f_{max}} \tag{5.20}$$

The scaled spectra for the particular GPE system from each series are shown in Figure 5.55. The spectra at a different temperature almost merge to a single master curve except for data at the low-frequency side. This suggests that the ion dynamics are temperature independent. The deviation at the lower frequency side may be due to the electrode-polarization effect.

5.6 Modulus Analysis

The ac response of the electrolyte can also be analyzed in terms of the electric modulus. In the low-frequency region, dielectric permittivity data are concealed by interfacial and electrode polarization and the relaxation process is hardly observed. To overcome these problems, a new formalism was developed by Macedo et al. [84] known as modulus formalism used to investigate relaxation behavior. In modulus representation, the

relaxation phenomenon becomes distinct as an electrode and interfacial polarizations are suppressed. Electrical modulus formalism has been used to study conductivity relaxation in a wide variety of materials [85-87]. The relaxation process is due to the distribution of relaxation time in non-homogeneous and mixed-phase material.

The electric modulus can be given as [88],

$$M^* = M' + j\,M'' = j\omega C_0 Z^* \tag{5.21}$$

where M′ is a real part of modulus and M′′ is the imaginary part of modulus. It is also defined as the inverse of the dielectric function given below

$$M^* = \frac{1}{\varepsilon^*} \tag{5.22}$$

Details of modulus formalism are also given in chapter 2.

Series (a): The M′′ (imaginary part of the modulus) as a function of frequency for GPE with different concentrations of $LiClO_4$ at different temperatures 303 K to 348 K is shown in Figure 5.56.

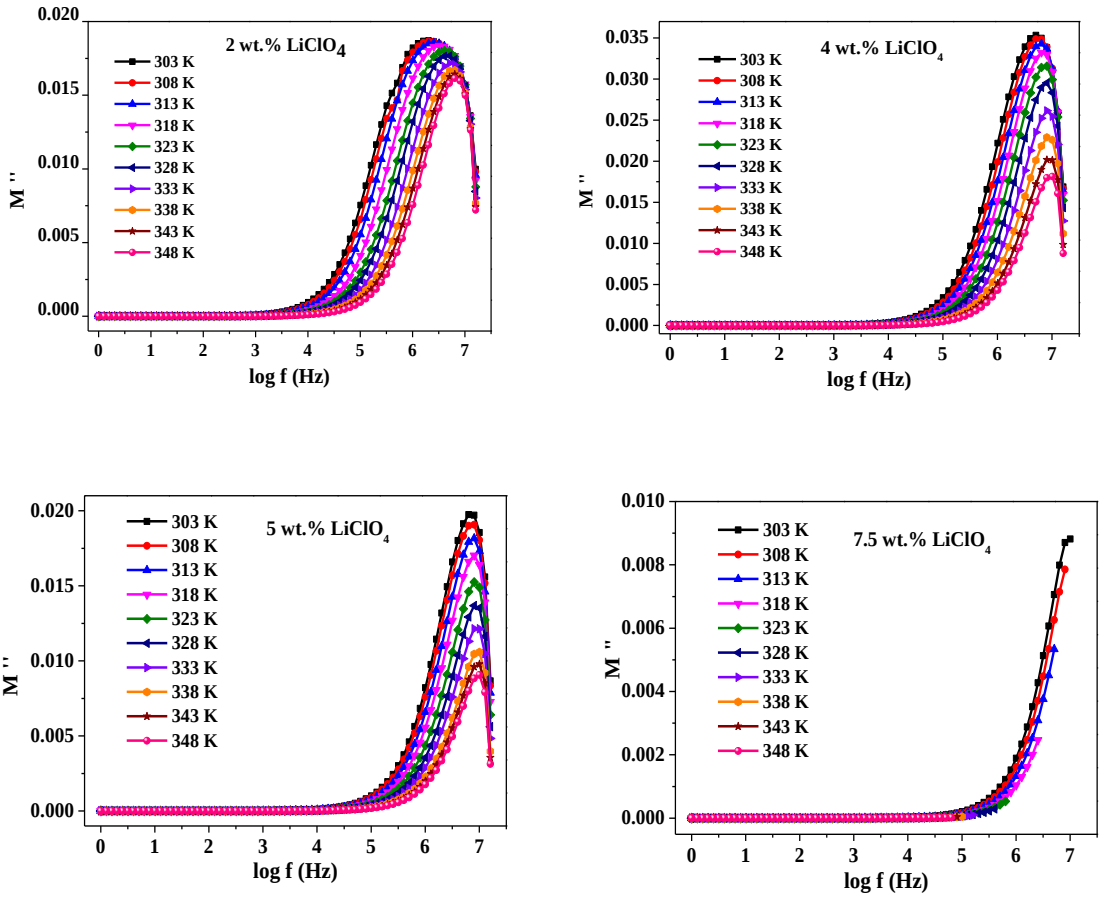

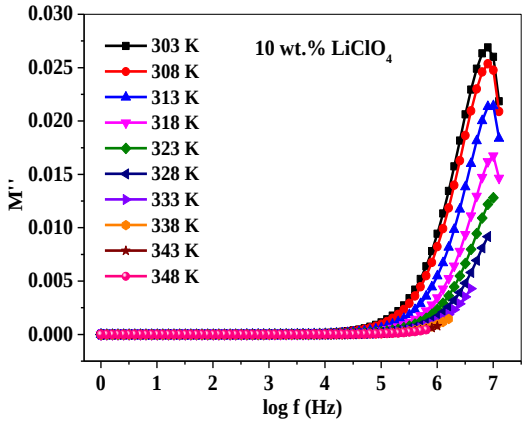

Figure 5.56 Variations in the imaginary part of modulus (M″) versus log f for different concentrations of $LiClO_4$ salt in the GPE system at different temperatures – Series (a).

The M″ tends to zero at low-frequency region whereas dispersion region at the high-frequency region. The low-frequency plateau region is due to the accumulation of charges at the electrode-electrolyte interface or polarization effect. M″ spectra show a characteristic peak at a particular frequency. With increasing the temperature, the peak is shifting towards the higher frequency side and the height of the peak is also changes. This peak indicates a relaxation phenomenon and confirms the ion-conducting nature of the system. Similar features have been reported by Manindra et al. [76] in their biopolymer containing NH_4I salt. The shifting of the peak towards the higher frequency side with increasing temperature indicating faster ionic motion leads to a decrease in the relaxation time and the charge carriers are thermally activated, reported by Das et al. [54]. The frequency corresponds to peak maxima M″ is conductivity relaxation frequency. From which conductivity relaxation time τ_m can be obtained using relation $\omega\tau = 1$. Another feature is observed here that the peak M″ is broader than the ideal Debye peak and asymmetric. It can be interpreted as being the consequence of the distribution of relaxation time [89].

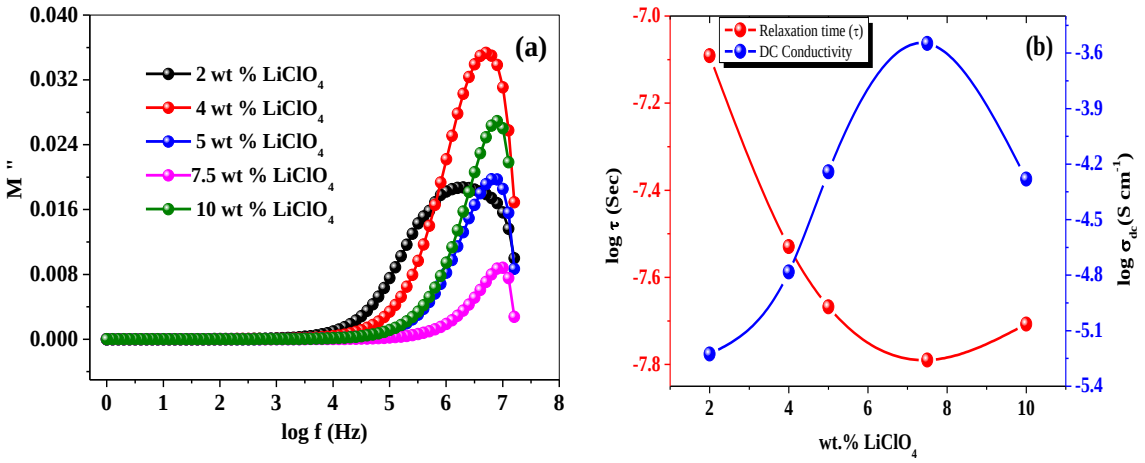

Figure 5.57 (a) M′′ versus log f for different concentrations of $LiClO_4$ in the GPE system at 303 K (b) Variation of conductivity relaxation time and DC conductivity as a function of $LiClO_4$ concentration at 303 K – Series (a).

The M′′ versus log f at 303 K for gel polymer electrolyte containing different amounts of $LiClO_4$ salt is shown in Figure 5.57(a). The spectrum shows a characteristic peak at a particular frequency called conductivity relaxation peak/frequency, below which the ions have long-range mobility, and above it, ions are confined in a narrow potential well [88]. Another feature is drawn from the spectra that the peak shift towards the higher frequency side with an increase in salt concentrations up to 7.5 wt.% $LiClO_4$. This behavior suggests that the charge carrier hopping is taking place which might be due to an increase in amorphous nature with increasing the amount of salt up to 7.5 wt.% $LiClO_4$. At 10 wt.% $LiClO_4$, the peak shift towards the lower frequency side indicates slow relaxation time. It might be due to a decrease in charge carriers due to aggregation of charge carriers which causes a decrease in the amorphous nature of the film. This is in good agreement with the XRD pattern of GPE having 10 wt.% $LiClO_4$. The obtained conductivity relaxation time τ_m is using relation $\omega\tau = 1$ and DC conductivity as a function of wt.% of $LiClO_4$ is plotted in Figure 5.57(b). The lowest relaxation time is found for the highest conducting sample.

In addition to these, the asymmetric nature of peak in M′′ spectra can be interpreted as being the consequence of the distribution of relaxation time and non-exponential behavior of the conductivity relaxation. The complex electric modulus in the form of a Fourier transform is given by the following relation

$$M^* = M_\infty \left[1 - \int_0^\infty \exp(-i\omega t) \frac{d\phi(t)}{dt} \right] \tag{5.23}$$

$M_\infty = \frac{1}{\varepsilon_\infty}$, where ε_∞ is the limiting high-frequency real part of permittivity and the function $\phi(t)$ is the relaxation function or Kohlrauch–Williams–Watts (KWW) function.

Due to ion-ion and ion-lattice correlation in the ion-conducting materials, it gives rise to non-Debye behavior which can be explained using stretched exponential functions of the Kohlrausch-Williams-Watts (KWW) [90]

$$\phi(t) = e^{-(t/\tau)^{\beta}} \tag{5.24}$$

where β is the nonexponential parameter, $0 < \beta < 1$ is an exponent indicating departure from the Debye relaxation (β=1), and τ is the relaxation time. The parameter β for all the samples can be evaluated by knowing the full width at half maximum (FWHM) from M″ spectra which are calculated using the following formula

$$\beta = \frac{1.14}{FWHM} \tag{5.25}$$

and are listed in Table 5.3. From Table 5.3, the deviated values of β (β ≠1) suggest a greater departure from the ideal Debye response.

Table 5.3 β exponent values of KWW function for different concentrations of $LiClO_4$ salt in the GPE system at different temperatures – Series (a).

Temperature (K)	**2 wt.% $LiClO_4$**	**4 wt.% $LiClO_4$**	**5 wt.% $LiClO_4$**	**7.5 wt.% $LiClO_4$**	**10 wt.% $LiClO_4$**
303	0.28	0.57	0.79	0.89	0.75
308	0.32	0.62	0.80	0.91	0.77
313	0.34	0.66	0.83	0.90	0.85
318	0.39	0.70	0.88	-	0.91
323	0.45	0.77	0.94	-	0.93
328	0.48	0.81	0.99	-	0.99
333	0.55	0.87	1.04	-	1.06
338	0.60	0.94	1.10	-	1.08
343	0.65	0.96	1.13	-	-
348	0.70	0.99	1.17	-	-

Series (b): The imaginary part of modulus (M′′) as a function of the log of frequency for the GPE system with different wt.% PC: DEC at different temperatures is plotted in Figure 5.58. The spectra attain a lower value of M″ at lower frequencies which confirms the ion conduction process in the polymer matrix whereas the maximum value (peak) at a particular frequency(f_{max}) corresponds to the bulk effect. According to Druger et al., an increase in M″ at a higher frequency is related to jumping of ion from one site to another site over a long distance [49]. The frequency region where $f < f_{max}$ corresponds to long-range mobility and higher frequency ($f > f_{max}$) part is attributed to ions spatially confined in a narrow potential well and the frequency range where the peak occurs indicates the transition between long- and short-range mobility as reported by Sharma et al. [88]. It is also observed that the position of the peak at f_{max} shifts towards the higher frequency side with the rise in temperature indicates the occurrence of the relaxation phenomenon which is thermally activated.

Figure 5.59(a) shows the M″ versus log f for the GPE with different wt.% of PC:DEC at 303 K. The conclusion is drawn from the spectra that the position of the peak maximum is shifted to higher frequencies side indicates the occurrence of a relaxation phenomenon with an increasing amount of PC:DEC. The frequency corresponds to peak falls outside the measured frequency range for the GPE system contain 60 wt.% PC:DEC, hence, a peak is not observed. The height of the peak at high-frequency changes with plasticizer PC:DEC concentration. This behavior suggests that the charge carrier hopping has taken place due to the addition of plasticizer might be due to the increase in the amorphous nature of GPE. The relaxation time is observed to be decreasing with increasing the amount of PC:DEC plasticizers as shown in Figure 5.59(b).

Moreover, the asymmetric and broad nature of conductivity relaxation can be explained by Kohlrausch–Williams–Watts function (Eq. 5.24). β is calculated using Eq. 5.25 and tabulated in Table 5.4. The observed values, if found other than β=1 indicates the non-Debye nature of the system.

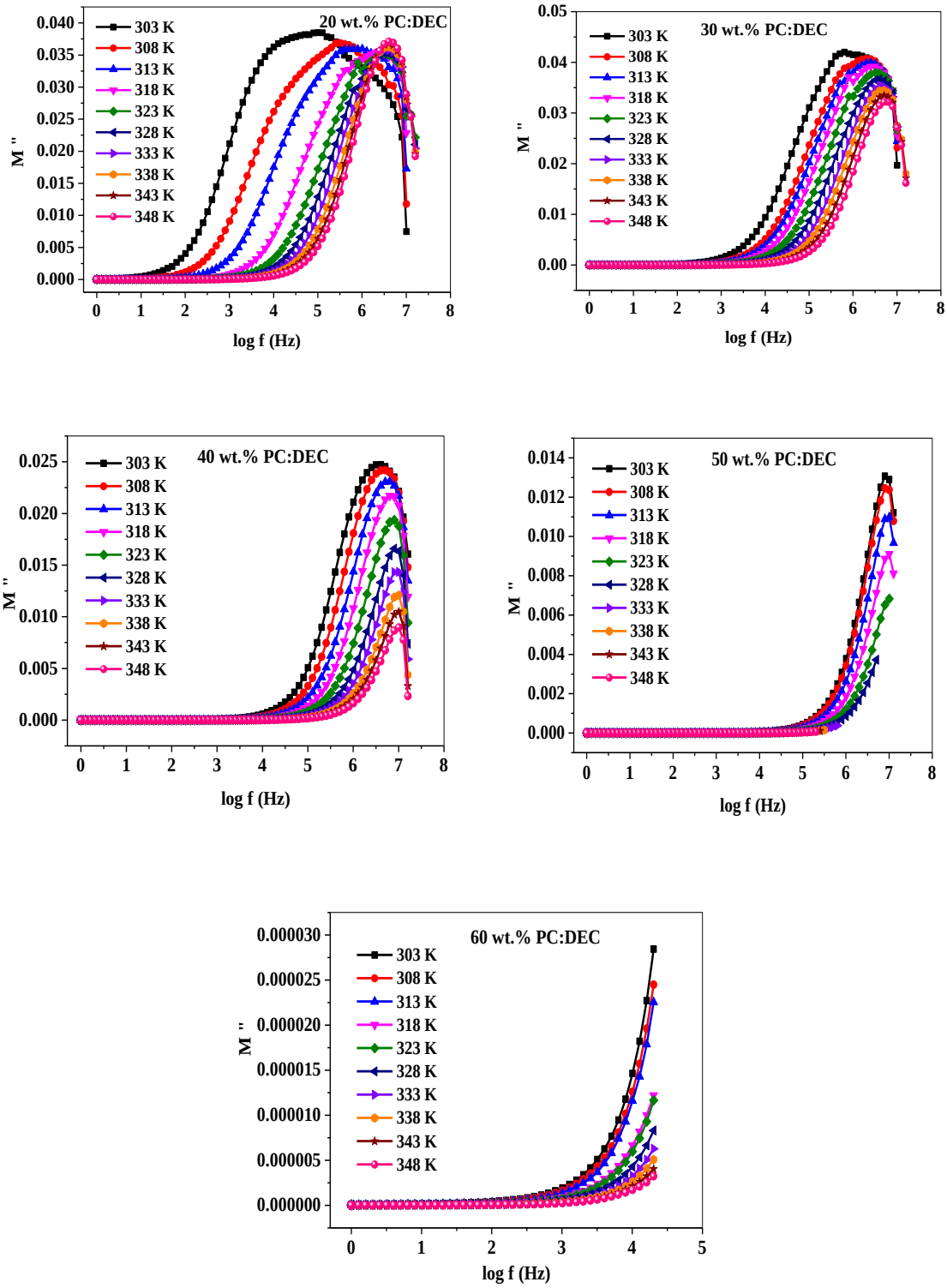

Figure 5.58 Variations in the imaginary part of modulus (M′′) versus log f for different concentration of PC:DEC in the GPE system at different temperatures – Series (b).

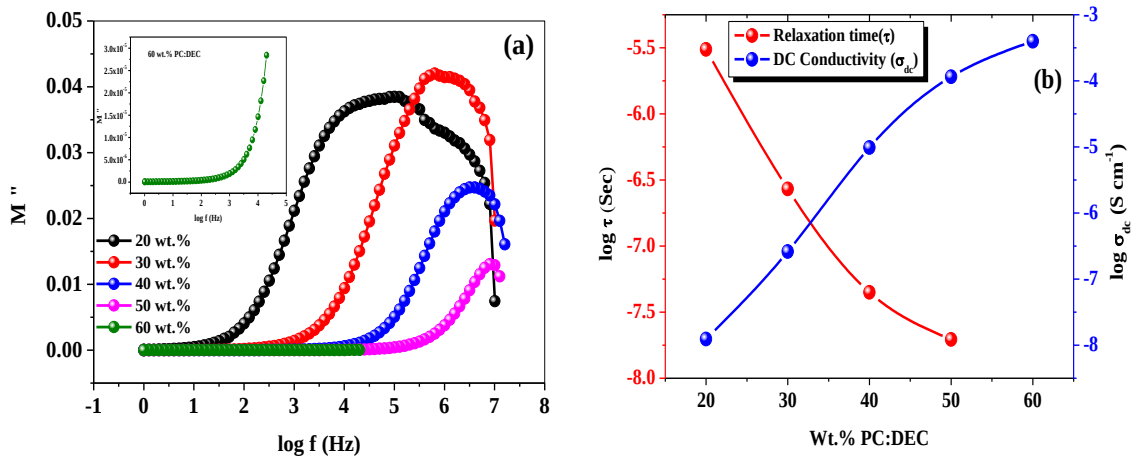

Figure 5.59 (a) M′′ versus log f for different concentrations of PC:DEC in the GPE system at 303 K (b) Variation of conductivity relaxation time and DC conductivity as a function of PC:DEC concentration at 303 K – Series (b).

Table 5.4 β exponent values of KWW function for different concentrations of PC:DEC in the GPE system at different temperatures – Series (b).

Temperature (K)	20 wt.%	30 wt.%	40 wt.%	50 wt.%	60 wt.%
303	0.06	0.25	0.38	0.79	1.05
308	0.13	0.30	0.46	0.80	1.06
313	0.16	0.32	0.56	0.86	1.10
318	0.24	0.33	0.66	-	-
323	0.30	0.36	0.77	-	-
328	0.36	0.40	0.91	-	-
333	0.40	0.42	1.00	-	-
338	0.45	0.53	1.10	-	-
343	0.50	0.59	1.17	-	-
348	0.51	0.64	1.24	-	-

Series (C): Further, the incorporation of Al_2O_3 nano-fillers in terms of modulus has been analyzed. Figure 5.60 shows the M″ versus log f for the nano-composite gel polymer electrolyte system containing different wt.% Al_2O_3 at temperature range 303 - 348 K. The similar behavior has been observed in the modulus spectra as discussed for the previous series. The long tail at low frequency is due to the large capacitance associated with the system. The high-frequency region is the bulk region of electrolytes where the conductivity relaxation phenomenon takes place. The peak at a particular frequency where long-range motion is constrained to caged motion called conductivity relaxation frequency is shifted

towards the higher frequency side as temperature increases[91]. This is because of the upsurge in the flexibility of the polymer chain segment wherein movement of the ion within the available site becomes faster and corresponds to decrease in relaxation time [92]. In another word, we can say that that the relaxation process is thermally activated, where the dominant process is the hopping of the charge carriers. At high temperatures > 328 K, the peak is not observed due to the high ionic conductivity of the system. Another feature of decreasing the height of the peak with a rise in temperature indicates that the bulk resistance of the system is decreasing. The broader and asymmetric nature of the peaks predict the present system are of non-Debye type. Verma et al.[93] also reported the similar behavior of modulus and non-Debye nature for the PEO based polymer electrolyte system with different amount TiO_2 nano-filler. To explore more on non-Debye nature, we have extracted β parameter from this M″ spectra according to Eq. 5.25 and tabulated in Table 5.5 which is departed away from the predicted value for the Debye nature.

Figure 5.61(a) depicts the M″ versus log f for the NCGPE with different concentrations of Al_2O_3 nanofiller at 303 K. On the variation of Al_2O_3 nanofiller in the GPE system, the position and height of the peak are varied. From the values of f_{max} corresponds to the peak M''_{max}, the relaxation time is calculated according to ωτ=1 and the log of relaxation time and log σ_{dc} values are plotted against different wt.% Al_2O_3 in Figure 5.61(b). On comparing the trend of relaxation time with conductivity, the relaxation time decreases whereas conductivity increases as Al_2O_3 nanofiller concentration are varied from 0.5 wt.% to 2 wt.%. This may be due to the provision of a facilitating path for the ionic transport and motion of the polymer segment due to undissociated salt. The decrease in the relaxation time on the addition of 3 wt.% Al_2O_3 could be explained on the basis of the ion aggregation or formation of ion-pair which hinders the motion of the ion. Again, a small increase in conductivity and simultaneous decrease in the relaxation time is observed for the NCGPE with 4 wt.% Al_2O_3 which can be explained by taking into account on percolation model and/or space charge model also well-known as the two-phase effect [94]. This is also explained in Chapter 2 in the section of "Theoretical models". Many reports show this type of behavior [93,95]. For higher conducting samples (NCGPE with 2 wt.% Al_2O_3), a shorter conductivity relaxation time has been observed.

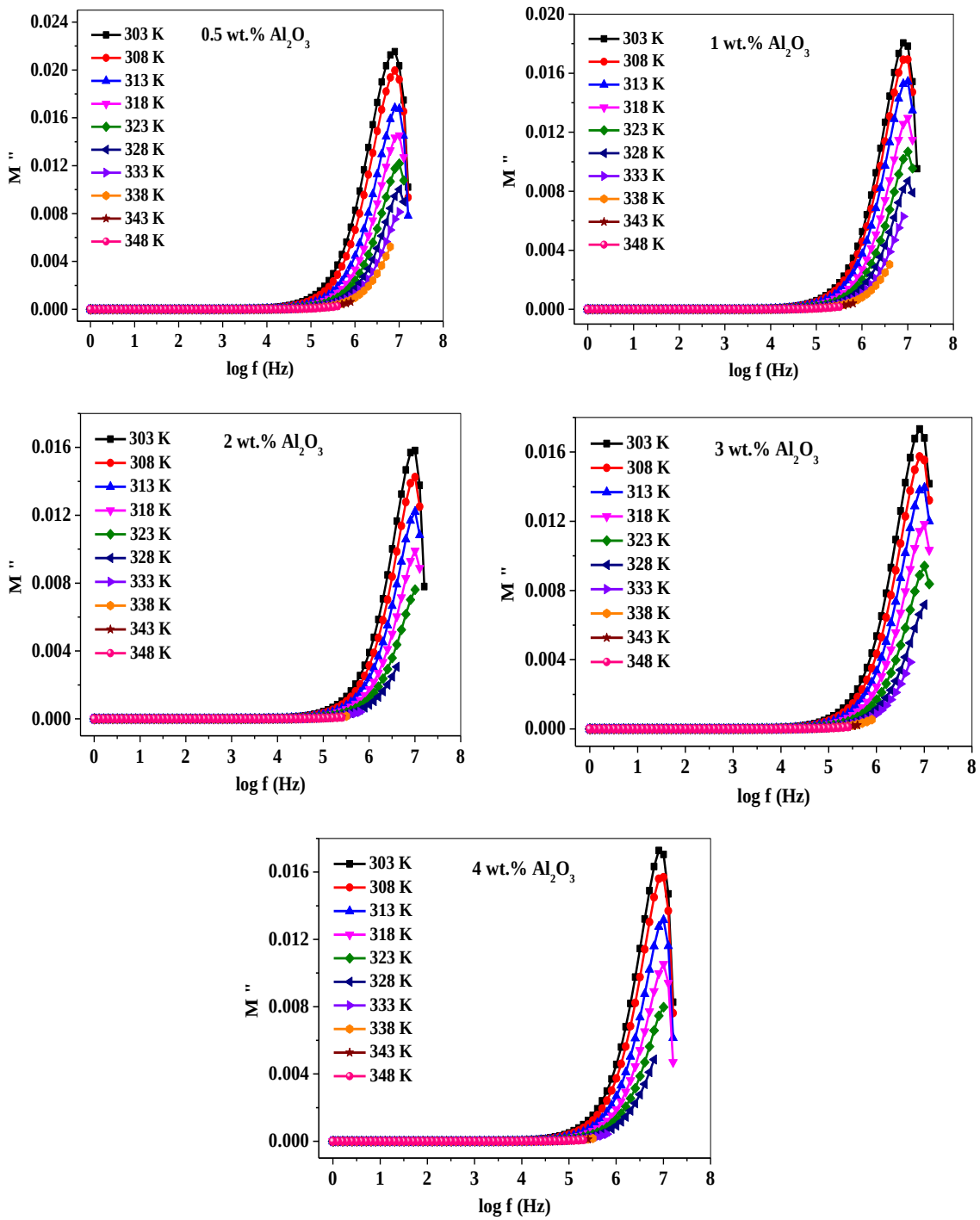

Figure 5.60 Variation in the imaginary part of modulus (M′′) versus log f for different concentrations of Al_2O_3 in the GPE system at different temperatures – Series (c).

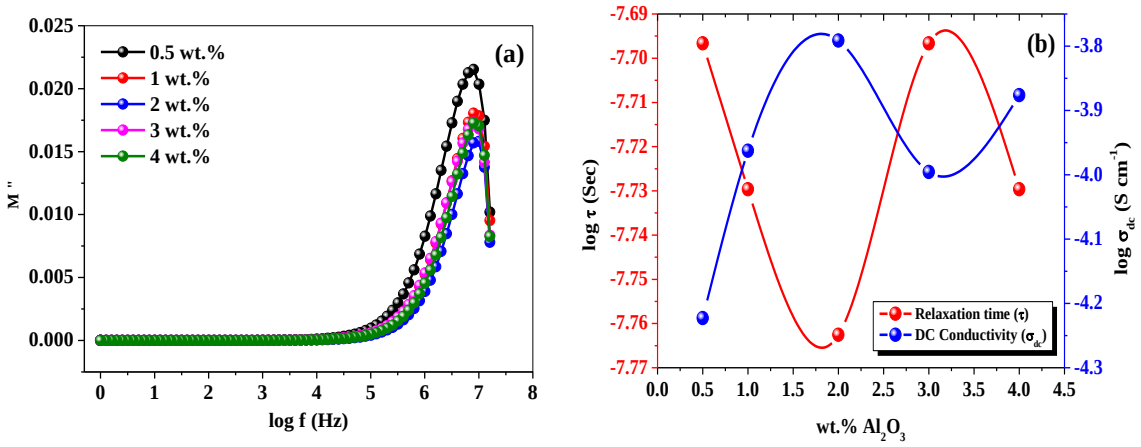

Figure 5.61 (a) M′′ versus log f for different concentrations of Al_2O_3 in the GPE system at 303 K (b) Variation of conductivity relaxation time and DC conductivity as a function of Al_2O_3 concentration at 303 K – Series (c).

Table 5.5 β exponent values of KWW function for different concentrations of Al_2O_3 in the GPE system at different temperatures – Series (c).

Temperature (K)	0.5 wt.%	1 wt.%	2 wt.%	3 wt.%	4 wt.%
303	0.82	0.87	0.95	0.77	0.86
308	0.83	0.88	0.95	0.79	0.89
313	0.86	0.92	0.99	0.85	0.93
318	0.87	0.97	1.02	0.89	0.97
323	0.93	1.01	1.04	0.92	1.02
328	0.98	1.03	1.19	0.93	1.05
333	1.02	1.10	-	1.07	1.17
338	-	1.20	-	-	-
343	-	-	-	-	-
348	-	-	-	-	-

Spectroscopic Plots

Another approach to explore the Debye and non-Debye behavior of the polycrystalline materials, the spectroscopic plot (Z′′ and M′′ versus log f) is believed to be a convenient way. The spectroscopic plot, i.e., graphs of Z′′ and M′′ versus log f offers a convenient way of presenting the data as suggested by Grant et al. [96]. They reported the normalized modulus and impedance spectra for ideal solid electrolyte (single RC element

with single relaxation time ωRC=1) were completely supposable, which can be interpreted as ideal Debye Curve which is given by [96]

$$Z'' = R\frac{\omega RC}{1+(\omega RC)^2} \tag{5.26}$$

and

$$M'' = \frac{C_0}{C}\frac{\omega RC}{1+(\omega RC)^2} \tag{5.27}$$

But for real solid electrolyte, there is a wide range of distribution of relaxation time with the occurrence of peak maxima of Z′′ and M′′ at a different frequency having non-Debye nature wherein the peak of modulus and impedance no longer coincide. Hodge et al. [97] have discussed the impedance and modulus spectroscopy for the ideal and real polycrystalline solid electrolyte.

Series (a): The plot of Z′′ and M′′ versus log f for the sample containing different wt.% of $LiClO_4$ at 308 K is shown in Figure 5.62. The maxima of Z′′ and M′′ do not coincide at the same frequency. The peak of Z′′ is at the lower frequency side, whereas the peak of M′′ is at higher frequency side having broadened nature indicating the wide distribution of relaxation times which confirms non-Debye nature.

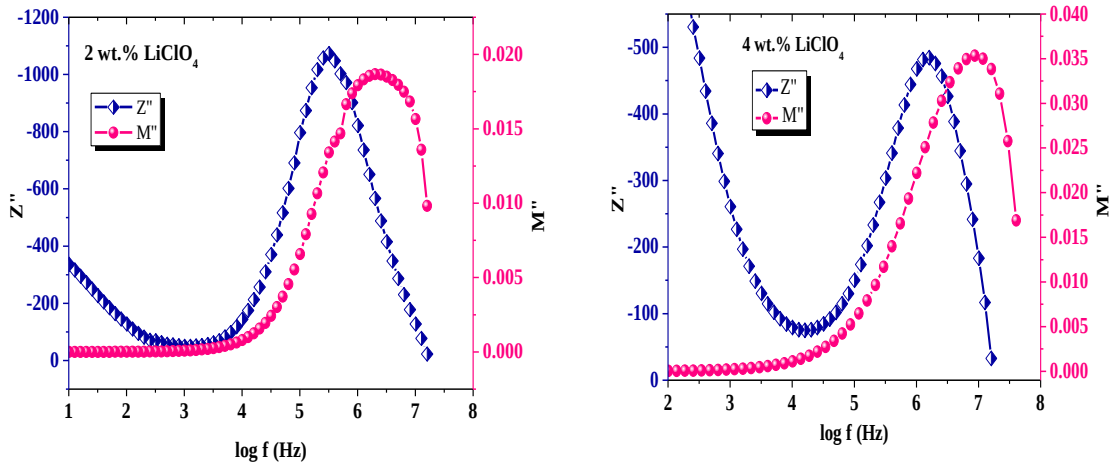

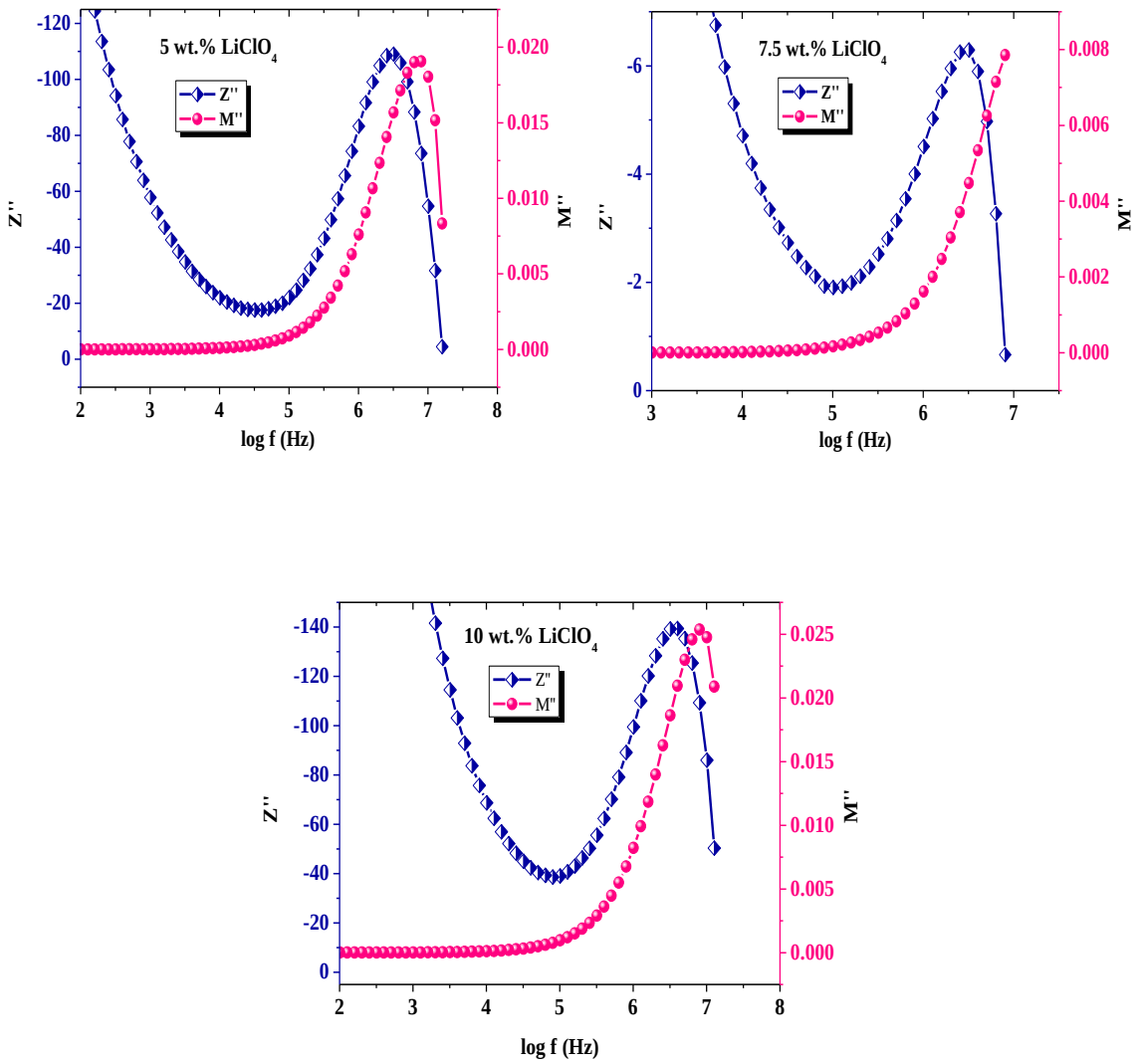

Figure 5.62 Spectroscopic plot (Z′′ and M′′ versus log f) for different concentrations of $LiClO_4$ salt in the GPE system at 308 K – Series (a).

Series (b): Similarly, Figure 5.63 shows the spectroscopic plot for the gel polymer electrolyte system with different concentrations of PC: DEC at 313 K. It can be seen from the figure the peak occurring in Z′′ and M′′ data is not supposable. The peak of Z′′ and M′′ occurring at different frequencies revealed that the system is non-Debye which has wide distributions of relaxation time. Similar behavior of non-Debye nature has been revealed for the PEO-PMMA based polymer electrolyte system by Sharma et al. [98]

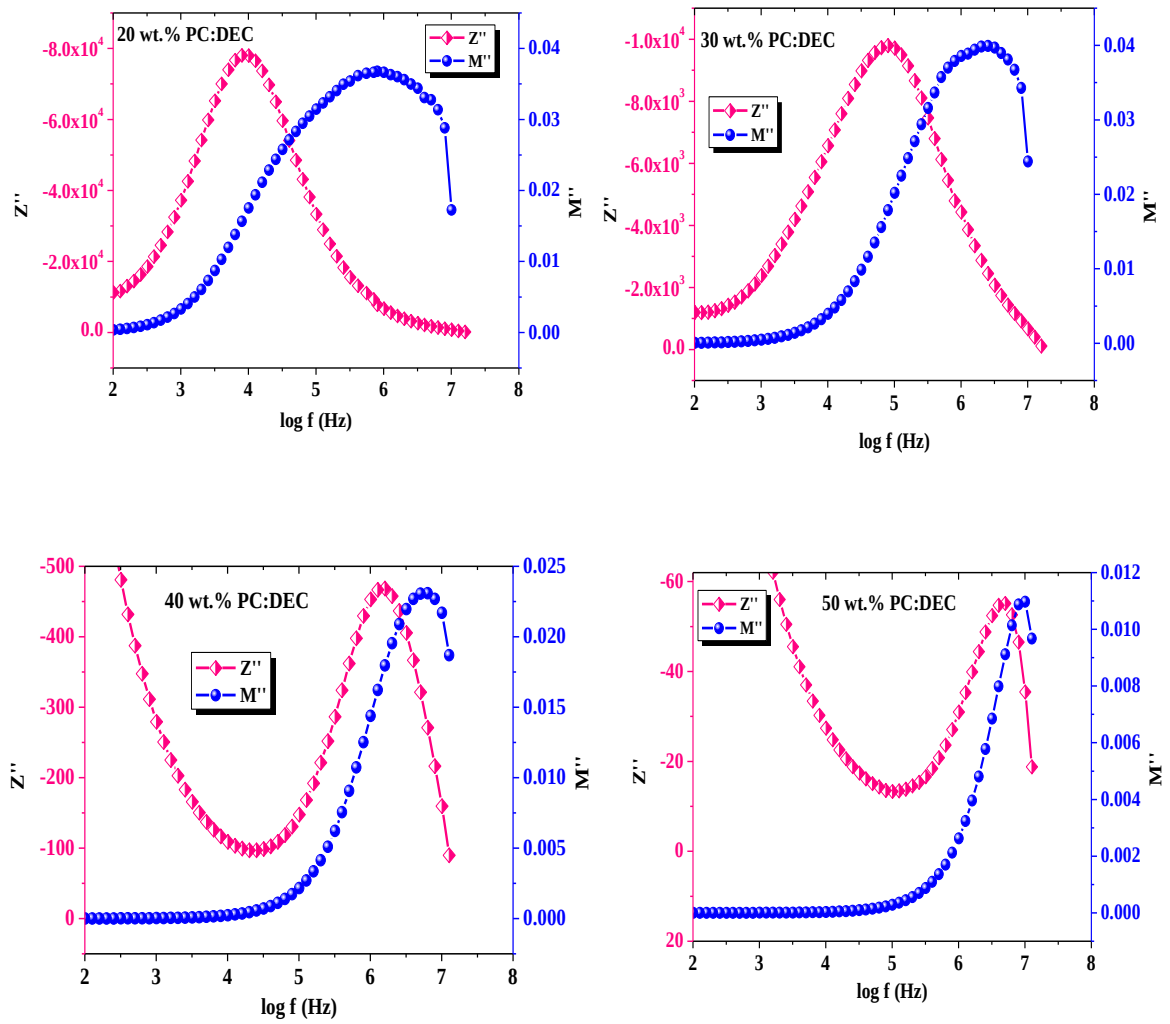

Figure 5.63 Spectroscopic plot (Z′′ and M′′ versus log f) for different concentrations of PC:DEC in the GPE system at 313 K – Series (b).

Series (C): The spectroscopic plot (i.e. Z″ and M″ versus log f) of nanocomposite gel polymer electrolyte with different concentrations of Al_2O_3 at 308 K is shown in Figure 5.64. The peak of Z″ and M″ occurring at different frequencies indicates the non-Debye nature of the present nanocomposite gel polymer electrolyte. Apart from it, the asymmetric nature and broader nature than Debye peak point out to have a wider distribution of relaxation time i.e. non-Debye nature. Similar behavior has been observed for all the samples.

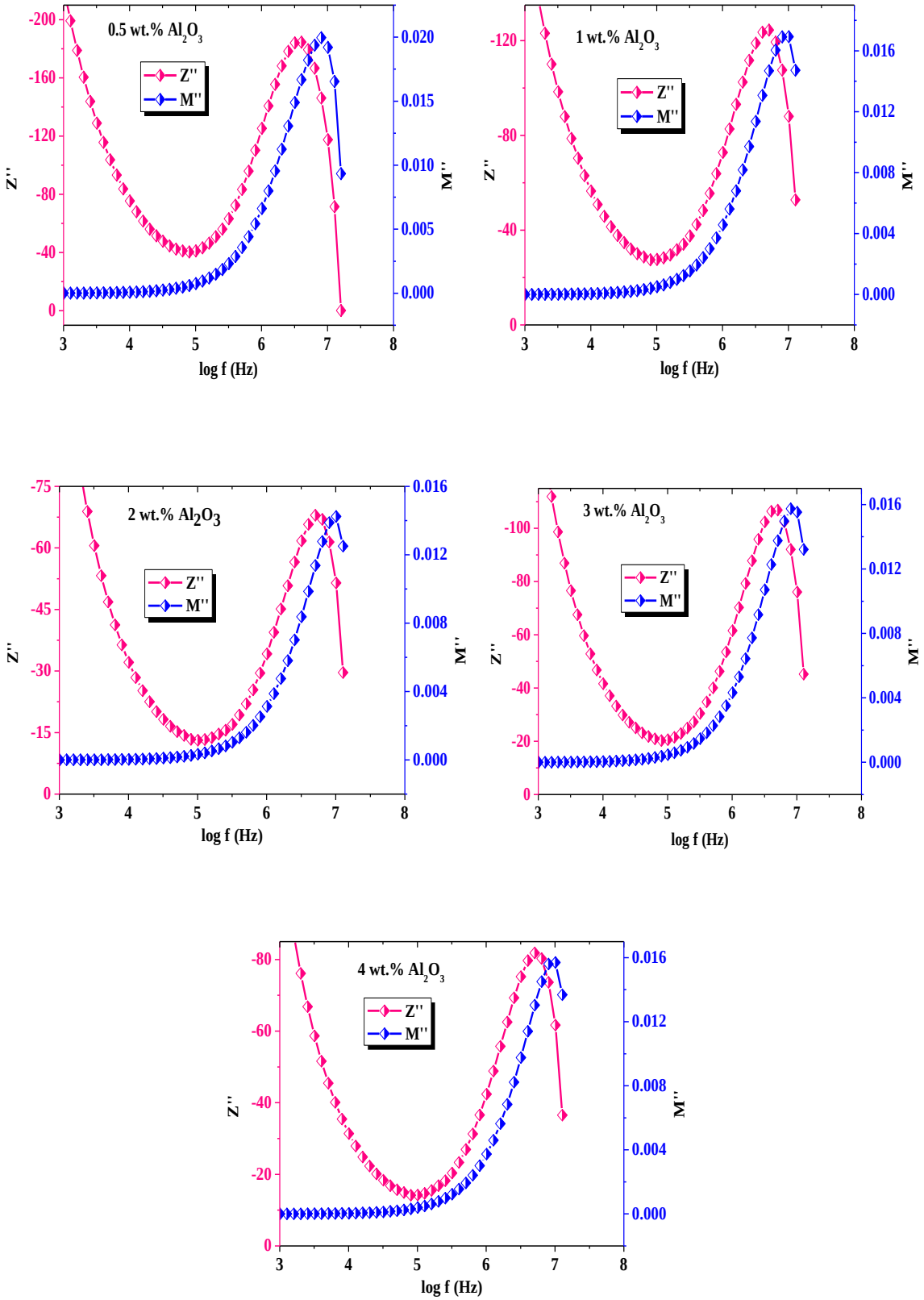

Figure 5.64 Spectroscopic plot (Z′′ and M′′ versus log f) for different concentrations of Al_2O_3 in the GPE system 308 K – Series (c).

Scaling of Modulus

The scaling is also known as the "Time-temperature superposition principle" is explored to obtain a comprehensive depiction of the role of temperature on an ion conduction mechanism. It provides an insight into the temperature dependence of the relaxation dynamics. As seen in this section, with an increase in temperature, the peak corresponds to conductivity relaxation shifts towards the higher frequency side. The purpose of the scaling is to examine whether the mechanism of conduction is temperature-dependent or independent. The scaled data have a tendency to collapse onto a single master curve if it is temperature independent mechanism.

Ghosh's scaling method is adopted to scale the imaginary part of modulus in which the x-axis is scaled by frequency corresponds to a peak value and Y-axis is scaled by M''_{max} value i.e. peak maximum value. The scaling function can be defined as

$$\frac{M''}{M''_{max}} = F\left(\frac{f}{f_{max}}\right) \tag{5.28}$$

Series (a): Figure 5.65 represent scaled spectra of M″ for GPE having 4 wt.% and 5 wt.% $LiClO_4$ at different temperatures. The normalized plots show a single relaxation peak i.e. merging of M″ at different temperatures. The time-temperature superposition attributes temperature-independent relaxation behavior.

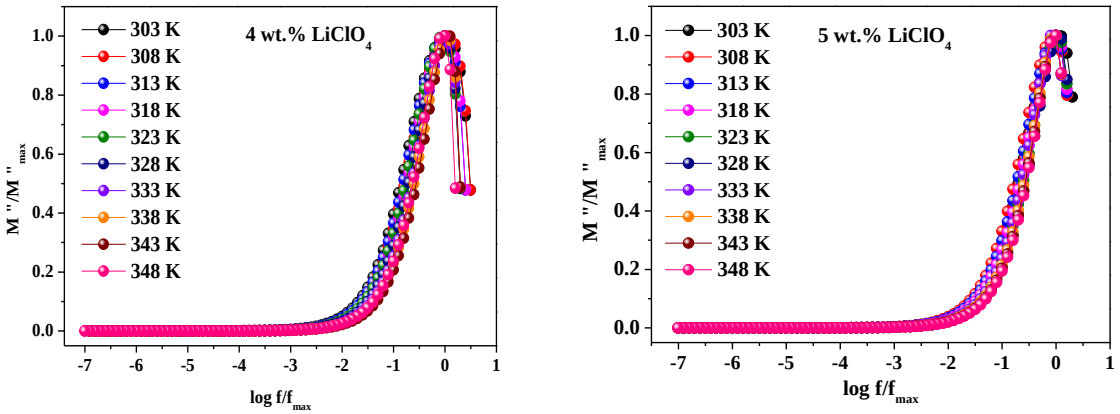

Figure 5.65 Scaled M″ spectra for GPE with 4 wt.% and 5 wt.% $LiClO_4$ at different temperatures – Series (a).

Series (b): Next in the plasticizer variation GPE system, the scaled spectra for the GPE system with 40 wt.% and 50 wt.% PC:DEC is plotted in Figure 5.66. Nearby overlapped

data has been observed for the GPE with 40 wt.% and perfect overlapping of M″ spectra is seen which indicates the relaxation processes of Li^+ ion conduction in the present system is independent of temperature.

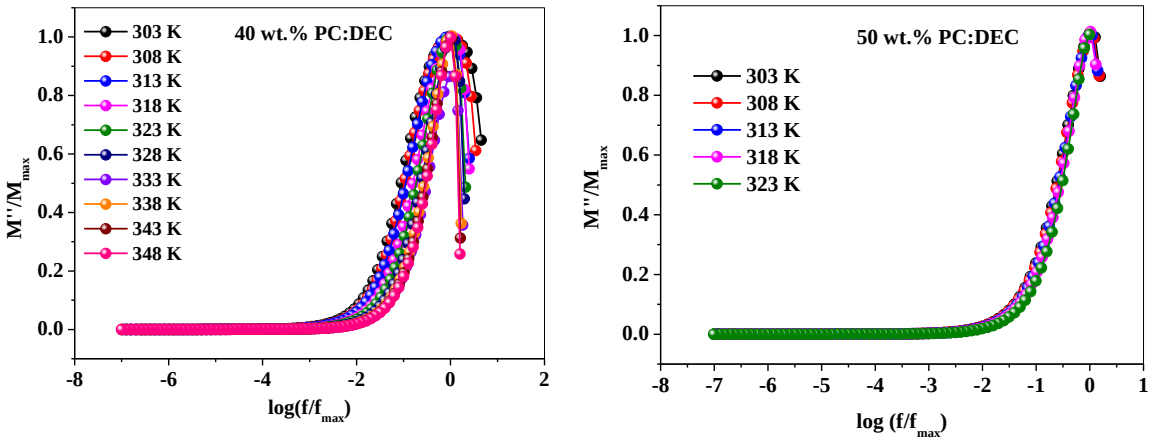

Figure 5.66 Scaled M″ spectra for GPE containing 40 wt.% and 50 wt.% PC:DEC at different temperatures – Series (b).

Series (c): The scaling of the nano-composite gel polymer electrolyte system containing 0.5 wt.% Al_2O_3 and 3 wt.% Al_2O_3 is shown in Figure 5.67. The scaling behavior shows that the modulus spectra superimposed to each other making a master curve for all isotherm which indicates the conductivity relaxation process is temperature independent.

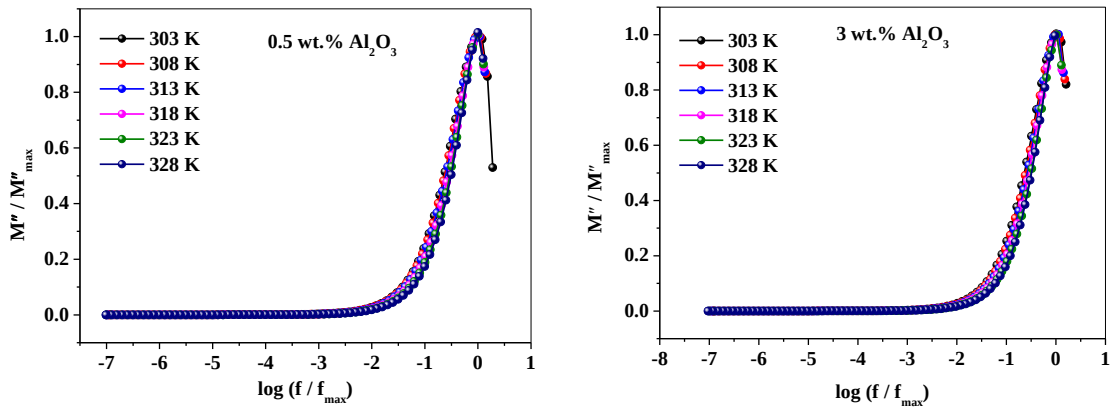

Figure 5.67 Scaled M″ spectra for NCGPE containing 0.5 wt.% and 3 wt.% Al_2O_3 at different temperatures – Series (c).

References

[1] D. Hellio and M. Djabourov, "Physically and Chemically Crosslinked Gelatin Gels," *Macromol. Symp.*, vol. 241, no. 1, pp. 23–27, Jul. 2006, doi: 10.1002/masy.200650904.

[2] D. Saikia, Y. W. Chen-Yang, Y. T. Chen, Y. K. Li, and S. I. Lin, "Investigation of ionic conductivity of composite gel polymer electrolyte membranes based on P(VDF-HFP), $LiClO_4$ and silica aerogel for lithium ion battery," *Desalination*, vol. 234, no. 1, pp. 24–32, 2008, doi: https://doi.org/10.1016/j.desal.2007.09.066.

[3] A. Manuel Stephan, "Review on gel polymer electrolytes for lithium batteries," *Eur. Polym. J.*, vol. 42, no. 1, pp. 21–42, Jan. 2006, doi: 10.1016/J.EURPOLYMJ.2005.09.017.

[4] K. S. Ngai, S. Ramesh, K. Ramesh, and J. C. Juan, "A review of polymer electrolytes: fundamental, approaches and applications," *Ionics (Kiel).*, vol. 22, no. 8, pp. 1259–1279, 2016, doi: 10.1007/s11581-016-1756-4.

[5] S. B. Aziz, "Li^+ ion conduction mechanism in poly (ε-caprolactone)-based polymer electrolyte," *Iran. Polym. J.*, vol. 22, no. 12, pp. 877–883, 2013, doi: 10.1007/s13726-013-0186-7.

[6] K. Gohel and D. K. Kanchan, "Ionic conductivity and relaxation studies in PVDF-HFP:PMMA-based gel polymer blend electrolyte with $LiClO_4$ salt," *J. Adv. Dielectr.*, vol. 08, no. 01, p. 1850005, Feb. 2018, doi: 10.1142/S2010135X18500054.

[7] R. J. Sengwa and S. Choudhary, "Dielectric properties and fluctuating relaxation processes of poly(methyl methacrylate) based polymeric nanocomposite electrolytes," *J. Phys. Chem. Solids*, vol. 75, no. 6, pp. 765–774, 2014, doi: https://doi.org/10.1016/j.jpcs.2014.02.008.

[8] S. Ramesh, K. H. Leen, K. Kumutha, and A. K. Arof, "FTIR studies of PVC/PMMA blend based polymer electrolytes," *Spectrochim. Acta Part A Mol. Biomol. Spectrosc.*, vol. 66, no. 4, pp. 1237–1242, 2007, doi: https://doi.org/10.1016/j.saa.2006.06.012.

[9] S. Ramesh, S.-C. Lu, and E. Morris, "Towards magnesium ion conducting poly(vinylidenefluoride-hexafluoropropylene)-based solid polymer electrolytes with great prospects: Ionic conductivity and dielectric behaviours," *J. Taiwan Inst. Chem. Eng.*, vol. 43, no. 5, pp. 806–812, 2012, doi: https://doi.org/10.1016/j.jtice.2012.04.004.

[10] C.-W. Liew, S. Ramesh, K. Ramesh, and A. K. Arof, "Preparation and characterization of lithium ion conducting ionic liquid-based biodegradable corn starch polymer electrolytes," *J. Solid State Electrochem.*, vol. 16, no. 5, pp. 1869–1875, 2012, doi: 10.1007/s10008-012-1651-5.

[11] S. Ramesh and L. C. Wen, "Investigation on the effects of addition of SiO_2 nanoparticles on ionic conductivity, FTIR, and thermal properties of nanocomposite PMMA–$LiCF_3SO_3$–SiO_2," *Ionics (Kiel).*, vol. 16, no. 3, pp. 255–262, 2010, doi: 10.1007/s11581-009-0388-3.

[12] Z. Wen, T. Itoh, T. Uno, M. Kubo, and O. Yamamoto, "Thermal, electrical, and mechanical properties of composite polymer electrolytes based on cross-linked poly(ethylene oxide-co-propylene oxide) and ceramic filler," *Solid State Ionics*, vol. 160, no. 1, pp. 141–148, 2003, doi: https://doi.org/10.1016/S0167-2738(03)00129-2.

[13] S. Rajendran, O. Mahendran, and R. Kannan, "Ionic conductivity studies in composite solid polymer electrolytes based on methylmethacrylate," *J. Phys. Chem. Solids*, vol. 63, no. 2, pp. 303–307, 2002, doi: https://doi.org/10.1016/S0022-3697(01)00144-5.

[14] S. H. Chung *et al.*, "Enhancement of ion transport in polymer electrolytes by addition of nanoscale inorganic oxides," *J. Power Sources*, vol. 97–98, pp. 644–648, 2001, doi: https://doi.org/10.1016/S0378-7753(01)00748-0.

[15] kok hau Teoh, R. T subramaniam, and A. K. Arof, "Investigation on the effect of nanosilica towards corn starch–lithium perchlorate-based polymer electrolytes," *J. Solid State Electrochem.*, vol. 16, Oct. 2012, doi: 10.1007/s10008-012-1741-4.

[16] J. H. Kim, M.-S. Kang, Y. J. Kim, J. Won, N.-G. Park, and Y. S. Kang, "Dye-sensitized nanocrystalline solar cells based on composite polymer electrolytes containing fumed silica nanoparticles," *Chem. Commun.*, no. 14, pp. 1662–1663, 2004, doi: 10.1039/B405215C.

[17] K. Vignarooban, M. A. K. L. Dissanayake, I. Albinsson, and B.-E. Mellander, "Effect of TiO_2 nano-filler and EC plasticizer on electrical and thermal properties of poly(ethylene oxide) (PEO) based solid polymer electrolytes," *Solid State Ionics*, vol. 266, pp. 25–28, 2014, doi: https://doi.org/10.1016/j.ssi.2014.08.002.

[18] S. Das and A. Ghosh, "Charge Carrier Relaxation in Different Plasticized PEO/PVDF-HFP Blend Solid Polymer Electrolytes," *J. Phys. Chem. B*, vol. 121, no. 21, pp. 5422–5432, Jun. 2017, doi: 10.1021/acs.jpcb.7b02277.

[19] L. N. Sim, S. R. Majid, and A. K. Arof, "Characteristics of PEMA/PVdF-HFP blend polymeric gel films incorporated with lithium triflate salt in electrochromic device," *Solid State Ionics*, vol. 209–210, pp. 15–23, 2012, doi: https://doi.org/10.1016/j.ssi.2011.11.035.

[20] X. Flora, M. Ulaganathan, and S. Rajendran, "Role of Different Plasticizers in Li-Ion Conducting Poly(Acrylonitrile)-Poly(Methyl Methacrylate) Hybrid Polymer Electrolyte," *Int. J. Polym. Mater.*, vol. 62, pp. 737–742, Jun. 2013, doi: 10.1080/00914037.2013.769235.

[21] I. Jayasekara, M. Poyner, and D. Teeters, "Investigation of a nanoconfined, ceramic composite, solid polymer electrolyte," *Electrochim. Acta*, vol. 247, pp. 1147–1154, 2017, doi: https://doi.org/10.1016/j.electacta.2017.06.129.

[22] F. Croce, L. Persi, B. Scrosati, F. Serraino-Fiory, E. Plichta, and M. A. Hendrickson, "Role of the ceramic fillers in enhancing the transport properties of composite polymer electrolytes," *Electrochim. Acta*, vol. 46, no. 16, pp. 2457–2461, 2001, doi: https://doi.org/10.1016/S0013-4686(01)00458-3.

[23] Y.-J. Wang and D. Kim, "Crystallinity, morphology, mechanical properties and conductivity study of in situ formed PVdF/$LiClO_4$/TiO_2 nanocomposite polymer electrolytes," *Electrochim. Acta*, vol. 52, no. 9, pp. 3181–3189, 2007, doi: https://doi.org/10.1016/j.electacta.2006.09.070.

[24] A. S. Aricò, P. Bruce, B. Scrosati, J.-M. Tarascon, and W. van Schalkwijk, "Nanostructured materials for advanced energy conversion and storage devices," *Nat. Mater.*, vol. 4, no. 5, pp. 366–377, 2005, doi: 10.1038/nmat1368.

[25] T. Itoh, Y. Miyamura, Y. Ichikawa, T. Uno, M. Kubo, and O. Yamamoto, "Composite polymer electrolytes of poly(ethylene oxide)/$BaTiO_3$/Li salt with hyperbranched polymer," *J. Power Sources*, vol. 119–121, pp. 403–408, 2003, doi: https://doi.org/10.1016/S0378-7753(03)00261-1.

[26] A. Arya, M. Sadiq, and A. L. Sharma, "Salt concentration and temperature dependent dielectric properties of blend solid polymer electrolyte complexed with $NaPF_6$," *Mater. Today Proc.*, vol. 12, pp. 554–564, 2019, doi: https://doi.org/10.1016/j.matpr.2019.03.098.

[27] S. Summerfield and P. N. Butcher, "Universal behaviour of AC hopping conductivity in

disordered systems," *J. Non. Cryst. Solids*, vol. 77–78, pp. 135–138, 1985, doi: https://doi.org/10.1016/0022-3093(85)90627-1.

[28] T. Malkow, "Immittance Data Validation by Kramers-Kronig Relations – Derivation and Implications," *ChemElectroChem*, vol. 4, no. 11, pp. 2777–2782, Nov. 2017, doi: 10.1002/celc.201700630.

[29] S. Cruz-Manzo, R. Chen, and P. Greenwood, "Evaluate the Validity of Electrochemical Impedance Measurements of Polymer Electrolyte Fuel Cells using a Computational Algorithm based on Fast Fourier Transform," *Insights Anal. Electrochem.*, vol. 1, Oct. 2015.

[30] B. A. Boukamp, "A Linear Kronig-Kramers Transform Test for Immittance Data Validation," *J. Electrochem. Soc.*, vol. 142, no. 6, p. 1885, 1995, doi: 10.1149/1.2044210.

[31] P. Prabakaran and R. P. Manimuthu, "Enhancement of the electrochemical properties with the effect of alkali metal systems on PEO/PVdF-HFP complex polymer electrolytes," *Ionics (Kiel).*, vol. 22, no. 6, pp. 827–839, 2016, doi: 10.1007/s11581-015-1618-5.

[32] T. M. W. J. Bandara, M. A. K. L. Dissanayake, I. Albinsson, and B.-E. Mellander, "Mobile charge carrier concentration and mobility of a polymer electrolyte containing PEO and Pr4N+I− using electrical and dielectric measurements," *Solid State Ionics*, vol. 189, no. 1, pp. 63–68, 2011, doi: https://doi.org/10.1016/j.ssi.2011.03.004.

[33] K. S. Ngai, S. Ramesh, K. Ramesh, and J. C. Juan, "Electrical, dielectric and electrochemical characterization of novel poly(acrylic acid)-based polymer electrolytes complexed with lithium tetrafluoroborate," *Chem. Phys. Lett.*, vol. 692, pp. 19–27, 2018, doi: https://doi.org/10.1016/j.cplett.2017.11.042.

[34] S. Rajendran, V. S. Bama, and M. R. Prabhu, "Effect of lithium salt concentration in PVAc/PMMA-based gel polymer electrolytes," *Ionics (Kiel).*, vol. 16, no. 1, pp. 27–32, 2010, doi: 10.1007/s11581-009-0329-1.

[35] K. Karuppasamy *et al.*, "Ionic liquid incorporated nanocomposite polymer electrolytes for rechargeable lithium ion battery: A way to achieve improved electrochemical and interfacial properties," *J. Ind. Eng. Chem.*, vol. 40, pp. 168–176, 2016, doi: https://doi.org/10.1016/j.jiec.2016.06.020.

[36] W. Cong, R. Miao, F. Miao, and B. Tao, "Electrodeposition manganese oxide on Ni foam loaded graphene for high-performance supercapacitor," *Mater. Res. Express*, vol. 6, no. 11, p. 115525, 2019, doi: 10.1088/2053-1591/ab49e9.

[37] M. S. Jayswal, D. K. Kanchan, P. Sharma, and M. Pant, "The effect of PbI_2 on electrical conduction in Ag2O-V_2O_5-B_2O_3 superionic glass system," *Solid State Ionics*, vol. 186, no. 1, pp. 7–13, Mar. 2011, doi: 10.1016/J.SSI.2011.01.016.

[38] L. N. Patro and K. Hariharan, "AC conductivity and scaling studies of polycrystalline SnF_2," *Mater. Chem. Phys.*, vol. 116, no. 1, pp. 81–87, 2009, doi: https://doi.org/10.1016/j.matchemphys.2009.02.056.

[39] O. Mahendran and S. Rajendran, "Ionic conductivity studies in PMMA/PVdF polymer blend electrolyte with lithium salts," *Ionics (Kiel).*, vol. 9, no. 3, pp. 282–288, 2003, doi: 10.1007/BF02375980.

[40] P. Sharma, D. K. Kanchan, and N. Gondaliya, "Effect of ethylene carbonate concentration on structural and electrical properties of PEO–PMMA polymer blends," *Ionics (Kiel).*, vol. 19, no. 5, pp. 777–785, 2013, doi: 10.1007/s11581-012-0797-6.

[41] M. R. Johan, O. H. Shy, S. Ibrahim, S. M. Mohd Yassin, and T. Y. Hui, "Effects of Al_2O_3

nanofiller and EC plasticizer on the ionic conductivity enhancement of solid PEO–$LiCF_3SO_3$ solid polymer electrolyte," *Solid State Ionics*, vol. 196, no. 1, pp. 41–47, 2011, doi: https://doi.org/10.1016/j.ssi.2011.06.001.

[42] R. T subramaniam and K. Bing, "Conductivity, Mechanical and Thermal Studies on Poly(methyl methacrylate)-Based Polymer Electrolytes Complexed with Lithium Tetraborate and Propylene Carbonate," *J. Mater. Eng. Perform.*, vol. 21, pp. 89–94, Jan. 2012, doi: 10.1007/s11665-010-9807-x.

[43] C. Capiglia, P. Mustarelli, E. Quartarone, C. Tomasi, and A. Magistris, "Effects of nanoscale SiO_2 on the thermal and transport properties of solvent-free, poly(ethylene oxide) (PEO)-based polymer electrolytes," *Solid State Ionics*, vol. 118, no. 1–2, pp. 73–79, Mar. 1999, doi: 10.1016/S0167-2738(98)00457-3.

[44] R. Prasanth, N. Shubha, H. H. Hng, and M. Srinivasan, "Effect of nano-clay on ionic conductivity and electrochemical properties of poly(vinylidene fluoride) based nanocomposite porous polymer membranes and their application as polymer electrolyte in lithium ion batteries," *Eur. Polym. J.*, vol. 49, no. 2, pp. 307–318, 2013, doi: https://doi.org/10.1016/j.eurpolymj.2012.10.033.

[45] A. Arya, M. Sadiq, and A. L. Sharma, "Effect of variation of different nanofillers on structural, electrical, dielectric, and transport properties of blend polymer nanocomposites," *Ionics (Kiel).*, vol. 24, no. 8, pp. 2295–2319, 2018, doi: 10.1007/s11581-017-2364-7.

[46] M. A. Ratner, P. Johansson, and D. F. Shriver, "Polymer Electrolytes: Ionic Transport Mechanisms and Relaxation Coupling," *MRS Bull.*, vol. 25, no. 3, pp. 31–37, 2000, doi: DOI: 10.1557/mrs2000.16.

[47] M. Hema, S. Selvasekarapandian, H. Nithya, A. Sakunthala, and D. Arunkumar, "Structural and ionic conductivity studies on proton conducting polymer electrolyte based on polyvinyl alcohol," *Ionics (Kiel).*, vol. 15, no. 4, pp. 487–491, 2009, doi: 10.1007/s11581-008-0254-8.

[48] Z. Li, G. Su, X. Wang, and D. Gao, "Micro-porous P(VDF-HFP)-based polymer electrolyte filled with Al_2O_3 nanoparticles," *Solid State Ionics*, vol. 176, no. 23, pp. 1903–1908, 2005, doi: https://doi.org/10.1016/j.ssi.2005.05.006.

[49] S. D. Druger, M. A. Ratner, and A. Nitzan, "Generalized hopping model for frequency-dependent transport in a dynamically disordered medium, with applications to polymer solid electrolytes," *Phys. Rev. B*, vol. 31, no. 6, pp. 3939–3947, Mar. 1985, doi: 10.1103/PhysRevB.31.3939.

[50] C. Pan, Q. Feng, L. Wang, Q. Zhang, and M. Chao, "Morphology and conductivity of in-situ PEO-$LiClO_4$-TiO_2 composite polymer electrolyte," *J. Cent. South Univ. Technol.*, vol. 14, no. 3, pp. 348–352, 2007, doi: 10.1007/s11771-007-0069-1.

[51] V. PROVENZANO, L. P. BOESCH, V. VOLTERRA, C. T. MOYNIHAN, and P. B. MACEDO, "Electrical Relaxation in $Na_2O{\cdot}3SiO_2$ Glass," *J. Am. Ceram. Soc.*, vol. 55, no. 10, pp. 492–496, Oct. 1972, doi: 10.1111/j.1151-2916.1972.tb13413.x.

[52] Z. Osman, M. I. Mohd Ghazali, L. Othman, and K. B. Md Isa, "AC ionic conductivity and DC polarization method of lithium ion transport in PMMA–$LiBF_4$ gel polymer electrolytes," *Results Phys.*, vol. 2, pp. 1–4, Jan. 2012, doi: 10.1016/J.RINP.2011.12.001.

[53] N. Shukla, A. Thakur, A. Shukla, and D. Marx, "Ion Conduction Mechanism in Solid Polymer Electrolyte: An Applicability of Almond-West Formalism," *Int. J. Electrochem. Sci.*, vol. 9, p. 7644, Dec. 2014.

[54] S. Das and A. Ghosh, "Effect of plasticizers on ionic conductivity and dielectric relaxation of PEO-$LiClO_4$ polymer electrolyte," *Electrochim. Acta*, vol. 171, pp. 59–65, 2015, doi: https://doi.org/10.1016/j.electacta.2015.04.178.

[55] S. Ke, H. Huang, L. Ren, and Y. Wang, "Nearly constant dielectric loss behavior in poly(3-hydroxybutyrate-co-3-hydroxyvalerate) biodegradable polyester," *J. Appl. Phys.*, vol. 105, no. 9, p. 96103, May 2009, doi: 10.1063/1.3125271.

[56] A. K. Jonscher, *Dielectric relaxation in solids*. London: Chelsea Dielectrics Press, 1983.

[57] A. Papathanassiou, I. Sakellis, and J. Grammatikakis, "Universal frequency-dependent ac conductivity of conducting polymer networks," *Appl. Phys. Lett.*, vol. 91, Jun. 2008, doi: 10.1063/1.2779255.

[58] M. Kumar, "Ion Dynamic Studies of Few Sodium and Ammonium salt Containing Polymer Electrolyte Systems," Banaras Hindu University,Varanasi, 2014.

[59] D. P. Almond, A. R. West, and R. J. Grant, "Temperature dependence of the a.c. conductivity of Naβ-alumina," *Solid State Commun.*, vol. 44, no. 8, pp. 1277–1280, 1982, doi: https://doi.org/10.1016/0038-1098(82)91103-6.

[60] D. P. Almond and A. R. West, "Mobile ion concentrations in solid electrolytes from an analysis of a.c. conductivity," *Solid State Ionics*, vol. 9–10, pp. 277–282, 1983, doi: https://doi.org/10.1016/0167-2738(83)90247-3.

[61] D. P. Almond and A. R. West, "Impedance and modulus spectroscopy of 'real' dispersive conductors," *Solid State Ionics*, vol. 11, no. 1, pp. 57–64, 1983, doi: https://doi.org/10.1016/0167-2738(83)90063-2.

[62] M. Jayswal, "Transport Properties Of PbI_2 Doped Silver Oxysalt Based Amorphous Solid Electrolytes," The Maharaja Sayajirao University Of Baroda, 2014.

[63] S. R. S. and H. M. A. Shujahadeen B. Aziz, Omed Gh. Abdullah, "Electrical and Dielectric Properties of Copper Ion Conducting Solid Polymer Electrolytes Based on Chitosan: CBH Model for Ion Transport Mechanism," *Int. J. Electrochem. Sci.*, vol. 13, pp. 3812–3826, 2018, doi: 10.20964/2018.04.10.

[64] N. Tripathi, A. Shukla, A. K. Thakur, and D. T. Marx, "Dielectric Modulus and Conductivity Scaling Approach to the Analysis of Ion Transport in Solid Polymer Electrolytes," *Polym. Eng. Sci.*, vol. 60, no. 2, pp. 297–305, Feb. 2020, doi: 10.1002/pen.25283.

[65] A. Arya and A. Sharma, "Structural, Electrical Properties and Dielectric Relaxation in Na^+ Ion Conducting Solid Polymer Electrolyte," *J. PhysicsCondensed Matter*, vol. 30, p. 165402, Mar. 2018, doi: 10.1088/1361-648X/aab466.

[66] T. M. W. J. Bandara *et al.*, "Binary counter ion effects and dielectric behavior of iodide ion conducting gel-polymer electrolytes for high-efficiency quasi-solid-state solar cells," *Phys. Chem. Chem. Phys.*, vol. 22, no. 22, pp. 12532–12543, 2020, doi: 10.1039/D0CP01547D.

[67] S. Summerfield, "Universal low-frequency behaviour in the a.c. hopping conductivity of disordered systems," *Philos. Mag. B*, vol. 52, no. 1, pp. 9–22, Jul. 1985, doi: 10.1080/13642818508243162.

[68] B. Roling, A. Happe, K. Funke, and M. D. Ingram, "Carrier Concentrations and Relaxation Spectroscopy: New Information from Scaling Properties of Conductivity Spectra in Ionically Conducting Glasses," *Phys. Rev. Lett.*, vol. 78, no. 11, pp. 2160–2163, Mar. 1997, doi: 10.1103/PhysRevLett.78.2160.

[69] D. L. Sidebottom, "Universal Approach for Scaling the ac Conductivity in Ionic Glasses," *Phys. Rev. Lett.*, vol. 82, no. 18, pp. 3653–3656, May 1999, doi: 10.1103/PhysRevLett.82.3653.

[70] A. Ghosh and A. Pan, "Scaling of the Conductivity Spectra in Ionic Glasses: Dependence on the Structure," *Phys. Rev. Lett.*, vol. 84, no. 10, pp. 2188–2190, Mar. 2000, doi: 10.1103/PhysRevLett.84.2188.

[71] P. Pal and A. Ghosh, "Dynamics and relaxation of charge carriers in poly(methylmethacrylate)-lithium salt based polymer electrolytes plasticized with ethylene carbonate," *J. Appl. Phys.*, vol. 120, no. 4, p. 45108, Jul. 2016, doi: 10.1063/1.4959985.

[72] S. Das and A. Ghosh, "Ionic relaxation in PEO/PVDF-HFP-$LiClO_4$ blend polymer electrolytes: dependence on salt concentration," *J. Phys. D. Appl. Phys.*, vol. 49, no. 23, p. 235601, 2016, doi: 10.1088/0022-3727/49/23/235601.

[73] S. K. Chaurasia *et al.*, "Studies on structural, thermal and AC conductivity scaling of PEO-LiPF6 polymer electrolyte with added ionic liquid [BMIMPF6]," *AIP Adv.*, vol. 5, no. 7, p. 77178, Jul. 2015, doi: 10.1063/1.4927768.

[74] J. C. Dyre and T. B. Schrøder, "Universality of ac conduction in disordered solids," *Rev. Mod. Phys.*, vol. 72, no. 3, pp. 873–892, Jul. 2000, doi: 10.1103/RevModPhys.72.873.

[75] S. Ibrahim, S. M. Mohd Yasin, N. M. Nee, R. Ahmad, and M. R. Johan, "Conductivity and dielectric behaviour of PEO-based solid nanocomposite polymer electrolytes," *Solid State Commun.*, vol. 152, no. 5, pp. 426–434, 2012, doi: https://doi.org/10.1016/j.ssc.2011.11.037.

[76] M. Kumar, T. Tiwari, and N. Srivastava, "Electrical transport behaviour of bio-polymer electrolyte system: Potato starch+ammonium iodide," *Carbohydr. Polym.*, vol. 88, no. 1, pp. 54–60, 2012, doi: https://doi.org/10.1016/j.carbpol.2011.11.059.

[77] P. Bhargav, B. Sarada, A. Sharma, and V. Rao, "Electrical Conduction and Dielectric Relaxation Phenomena of PVA Based Polymer Electrolyte Films," *J. Macromol. Sci.*, vol. Part A: Pu, pp. 131–137, Feb. 2010, doi: 10.1080/10601320903458564.

[78] H. J. Woo, S. R. Majid, and A. K. Arof, "Dielectric properties and morphology of polymer electrolyte based on poly(ε-caprolactone) and ammonium thiocyanate," *Mater. Chem. Phys.*, vol. 134, no. 2, pp. 755–761, 2012, doi: https://doi.org/10.1016/j.matchemphys.2012.03.064.

[79] V. K. Thakur, D. Vennerberg, S. A. Madbouly, and M. R. Kessler, "Bio-inspired green surface functionalization of PMMA for multifunctional capacitors," *RSC Adv.*, vol. 4, no. 13, pp. 6677–6684, 2014, doi: 10.1039/C3RA46592F.

[80] K. Gohel, D. Kanchan, H. Machhi, S. Soni, and C. Maheshwaran, "Gel polymer electrolyte based on PVDF-HFP:PMMA incorporated with propylene carbonate (PC) and diethyl carbonate (DEC) plasticizers : electrical, morphology, structural and electrochemical properties," *Mater. Res. Express*, 2020, doi: 10.1088/2053-1591/ab6c06.

[81] S. Suthanthiraraj and M. Johnsi, "Nanocomposite polymer electrolytes," *Ionics (Kiel).*, vol. 23, pp. 1–12, Dec. 2016, doi: 10.1007/s11581-016-1924-6.

[82] A. Dey, S. Karan, and S.K.De, "Effect of nanoadditives on ionic conductivity of solid polymer electrolyte," *Indian J Pure Appl Phys*, vol. 51, pp. 281–288, 2013.

[83] M. Hema and P. Tamilselvi, "Lithium ion conducting PVA:PVdF polymer electrolytes doped with nano SiO_2 and TiO_2 filler," *J. Phys. Chem. Solids*, vol. 96–97, pp. 42–48, 2016, doi: https://doi.org/10.1016/j.jpcs.2016.04.008.

[84] M. PB, M. CT, and R. BOSE, "The role of ionic diffusion in polarisation in vitreous ionic conductors," *Phys. Chem. Glas.*, vol. 13, pp. 171–179, 1972.

[85] A. Langar, N. Sdiri, H. Elhouichet, and M. Ferid, "Structure and electrical characterization of ZnO-Ag phosphate glasses," *Results Phys.*, vol. 7, pp. 1022–1029, 2017, doi: https://doi.org/10.1016/j.rinp.2017.02.028.

[86] S. Nasri, A. Oueslati, I. Chaabane, and M. Gargouri, "AC conductivity, electric modulus analysis and electrical conduction mechanism of $RbFeP_2O_7$ ceramic compound," *Ceram. Int.*, vol. 42, no. 12, pp. 14041–14048, 2016, doi: https://doi.org/10.1016/j.ceramint.2016.06.011.

[87] D. N. Vasoya, P. Jha, K. Saija, S. Dolia, K. Zankat, and K. Modi, "Electric Modulus, Scaling and Modeling of Dielectric Properties for Mn^{2+}-Si^{4+} Co-substituted Mn-Zn Ferrites," *J. Electron. Mater.*, vol. 45, Dec. 2015, doi: 10.1007/s11664-015-4224-4.

[88] P. Sharma, D. K. Kanchan, N. Gondaliya, M. Pant, and M. S. Jayswal, "Conductivity relaxation in Ag^+ ion conducting PEO–PMMA–PEG polymer blends," *Ionics (Kiel).*, vol. 19, no. 2, pp. 301–307, 2013, doi: 10.1007/s11581-012-0738-4.

[89] M. Ravi, S. Bhavani, K. Kiran Kumar, and V. V. R. Narasimaha Rao, "Investigations on electrical properties of PVP:KIO_4 polymer electrolyte films," *Solid State Sci.*, vol. 19, pp. 85–93, 2013, doi: https://doi.org/10.1016/j.solidstatesciences.2013.02.006.

[90] K. L. Ngai, A. K. Jonscher, and C. T. White, "On the origin of the universal dielectric response in condensed matter," *Nature*, vol. 277, no. 5693, pp. 185–189, 1979, doi: 10.1038/277185a0.

[91] S. B. Aziz, "Influence of silver ion reduction on electrical modulus parameters of solid polymer electrolyte based on chitosan-silver triflate electrolyte membrane," *eXPRESS Polym. Lett.*, vol. 4, pp. 300–310, Apr. 2010, doi: 10.3144/expresspolymlett.2010.38.

[92] A. Dutta, T. P. Sinha, P. Jena, and S. Adak, "Ac conductivity and dielectric relaxation in ionically conducting soda–lime–silicate glasses," *J. Non. Cryst. Solids*, vol. 354, no. 33, pp. 3952–3957, 2008, doi: https://doi.org/10.1016/j.jnoncrysol.2008.05.028.

[93] M. L. Verma and H. D. Sahu, "Study on ionic conductivity and dielectric properties of PEO-based solid nanocomposite polymer electrolytes," *Ionics (Kiel).*, vol. 23, no. 9, pp. 2339–2350, 2017, doi: 10.1007/s11581-017-2063-4.

[94] N. Lakshmi and S. Chandra, "Proton Conducting Composites of Heteropolyacid Hydrates (Phosphomolybdic and Phosphotungstic Acids) Dispersed with Insulating Al_2O_3," *Phys. status solidi*, vol. 186, no. 3, pp. 383–399, Aug. 2001, doi: https://doi.org/10.1002/1521-396X(200108)186:3<383::AID-PSSA383>3.0.CO;2-9.

[95] R. Agrawal and R. K. Gupta, "Superionic Solids: Composite Electrolyte Phase - An Overview," *J. Mater. Sci.*, vol. 34, pp. 1131–1162, Mar. 1999, doi: 10.1023/A:1004598902146.

[96] R. J. Grant, M. D. Ingram, and A. R. West, "An investigation of β-alumina electrolytes by electric modulus spectroscopy," *Electrochim. Acta*, vol. 22, no. 7, pp. 729–734, 1977, doi: https://doi.org/10.1016/0013-4686(77)80027-3.

[97] I. M. Hodge, M. D. Ingram, and A. R. West, "Impedance and modulus spectroscopy of polycrystalline solid electrolytes," *J. Electroanal. Chem. Interfacial Electrochem.*, vol. 74, no. 2, pp. 125–143, 1976, doi: https://doi.org/10.1016/S0022-0728(76)80229-X.

[98] P. Sharma, "Study of conduction mechanism in PEO-PMMA polymer blend nano-composite electrolytes," The M.S.University of Baroda, Vadodara.